UNIVERSITÀ DEGLI STUDI DI PADOVA

DIPARTIMENTO DI SCIENZE FARMACEUTICHE

SCUOLA DI DOTTORATO IN SCIENZE MOLECOLARI

INDIRIZZO SCIENZE FARMACEUTICHE

CICLO XXIV

TESI DI DOTTORATO

Designing adenosine receptors antagonists using an *in silico* approach

Direttore della Scuola: Prof. MAURIZIO CASARIN

Supervisore: Prof. STEFANO MORO

Dottoranda: SILVIA PAOLETTA

31 GENNAIO 2012

Abstract

The neuromodulator adenosine affects a wide variety of physiopathological processes through activation of four receptors, classified as A_1, A_{2A}, A_{2B}, and A_3 subtypes. Adenosine receptors (ARs) belong to family A of G protein-coupled receptors (GPCRs) and are ubiquitously expressed in the human body. Activation or blockade of ARs is responsible for a wide range of effects in numerous organ systems; and therefore the regulation of ARs can have many potential therapeutic applications.

The main objective of this project has been the investigation of the *in silico* molecular pharmacology of adenosine receptors and, in particular, of the human A_{2A} and A_3 adenosine receptors to guide the discovery and the structural refinement of new potent and selective AR antagonists.

Relevant potential therapeutic indications of human A_{2A}AR antagonists are neurodegenerative diseases, such as Parkinson's and Alzheimer's, restless legs syndrome, depression and addiction. On the other hand, antagonists for the human A_3AR subtype have been tested as therapeutic agents for asthma and chronic obstructive pulmonary disease (COPD), glaucoma, stroke, cardiac hypoxia and cerebral ischemia; but, unfortunately, there are currently no human A_3AR antagonists in clinical phases.

The recently published crystal structures of the human A_{2A} adenosine receptor (hA_{2A}AR) provide detailed three-dimensional information useful to support homology modeling studies and receptor-based drug design approaches. Structural models can be used to describe the interatomic interactions between ligand and receptor, and how the binding information is transmitted through the receptor. In particular, the 2.6 Å crystallographic structure of the hA_{2A}AR in complex with the potent and selective antagonist ZM241385 was used as template to build a homology model of the hA_3AR.

The hA_3AR three-dimensional model was constructed and refined using a conventional template-based homology modeling approach. This model was used to probe specific ligand-receptor interactions, also considering site-directed mutagenesis analysis, in order to guide docking of ligands into the receptor binding pocket.

In order to validate the molecular docking protocols for the adenosine receptors family, the hA_{2A}AR crystal structure was used to perform in parallel molecular docking studies using different docking software (such as GOLD,

Glide, MOE-Dock, and PLANTS). In particular, the antagonist ZM241385 was re-docked to the $hA_{2A}AR$ binding site, using different docking algorithms and scoring functions. Then RMSD values between predicted and crystallographic poses of ZM241385 were calculated to select the docking protocol able to better reproduce this molecular system and to be used in the following molecular docking studies.

Subsequently, molecular docking studies of different ARs antagonists were performed at the hA_3AR model and at the $hA_{2A}AR$ crystal structure, enabling the exploration of the potential effects of chemical modifications of these compounds, and thus facilitating the lead optimization process. Docking simulations were useful for the pharmacological characterization in terms of structure-activity relationships of several new series of adenosine receptor antagonists, and for the selection of novel potential antagonist candidates.

Different series of new compounds belonging to known adenosine antagonists classes, including triazolo-triazines and pyrazolo-triazolo-pyrimidines, have been analyzed and modified with the aim to modulate their affinity towards different adenosine receptor subtypes, to increase their solubility, or to overcome their metabolic instability. Moreover, several compounds with simplified scaffolds have been proposed as new adenosine receptor antagonists; such as pyrazolo-pyrimidinones, phthalazinones and triazolo-pyrimidines.

Finally, the knowledge gained through the docking studies led to the identification of structural features of antagonist compounds important for the interaction with the hA_3AR and was applied to the design of fluorescent ligands for this subtype, of particular interest as pharmacological probes.

In conclusion, the integration of *in silico* studies with synthetic work and pharmacological tests resulted to be a good strategy for the development of new compounds as adenosine receptors antagonists and led to a better understanding at the molecular level of this class of GPCRs.

Riassunto

L'adenosina è un neuromodulatore che regola molti processi fisiopatologici attraverso l'attivazione di quattro diversi recettori accoppiati a proteine G (GPCRs), classificati come sottotipi A_1, A_{2A}, A_{2B} e A_3. I recettori adenosinici sono ubiquitari nell'organismo umano e la loro attivazione è responsabile di numerosi effetti in diversi organi. Proprio per questo motivo la regolazione dell'attività di questi recettori può avere interessanti applicazioni terapeutiche.

Il principale obiettivo di questo progetto è stato l'analisi *in silico* a livello molecolare dei recettori adenosinici, ed in particolare dei recettori adenosinici umani A_{2A} e A_3, per guidare la scoperta e l'ottimizzazione strutturale di nuovi antagonisti adenosinici potenti e selettivi.

Le più rilevanti indicazioni terapeutiche degli antagonisti del recettore adenosinico umano A_{2A} sono rappresentate da malattie neurodegenerative, quali Alzheimer e Parkinson, depressione e dipendenza. Antagonisti del recettore adenosinico A_3 sono stati testati, invece, come agenti terapeutici per il trattamento di asma e broncopneumopatia cronica ostruttiva, glaucoma, infarto, ipossia cardiaca e ischemia cerebrale; tuttavia, ad oggi, non sono presenti in fase clinica antagonisti di questo recettore.

Le strutture cristallografiche del recettore adenosinico umano A_{2A}, recentemente pubblicate, forniscono dettagliate informazioni strutturali utili per supportare studi di homology modeling e approcci di drug design di tipo structure-based. Infatti, i modelli strutturali possono essere molto utili per descrivere le interazioni interatomiche tra ligando e recettore.

In particolare, la struttura cristallografica del recettore adenosinico umano A_{2A}, in complesso con l'antagonista potente e selettivo ZM241385, è stata utilizzata come templato per la costruzione di un modello per omologia del recettore adenosinico umano A_3.

Il modello tridimensionale del recettore A_3 umano è stato costruito e perfezionato utilizzando un convenzionale approccio di homology modeling. In seguito, il modello è stato utilizzato per esplorare specifiche interazioni ligando-recettore, anche grazie all'analisi dei dati di mutagenesi sito-specifica disponibili, con lo scopo di guidare studi di docking di ligandi all'interno della cavità recettoriale.

Inoltre, con l'intento di selezionare il protocollo di docking molecolare

più adatto per la famiglia dei recettori adenosinici, la struttura cristallografica del recettore adenosinico A_{2A} è stata utilizzata per effettuare simulazioni di docking con diversi softwares in parallelo (GOLD, Glide, MOE-dock, PLANTS).

In particolare, l'antagonista ZM241385 è stato riposizionato all'interno della cavità di legame del recettore A_{2A} attraverso l'utilizzo di diversi algoritmi di ricerca e diverse funzioni di scoring. Successivamente, le conformazioni ottenute dal docking sono state confrontate con la pose cristallografica di ZM241385 per selezionare il protocollo di docking che fosse in grado di riprodurre al meglio questo sistema molecolare e che potesse quindi essere usato per i successivi studi di docking.

Sono stati quindi effettuati studi di docking molecolare di vari antagonisti adenosinici sul modello del recettore A_3 e sulla struttura cristallografica del recettore A_{2A}, in modo da ricavare informazioni che potessero facilitare il processo di ottimizzazione dei composti. Le simulazioni di docking sono state utili per la caratterizzazione farmacologica, in termini di relazione struttura-affinità, di numerose serie di antagonisti adenosinici e per la selezione di nuovi potenziali candidati antagonisti di questi recettori.

Sono stati infatti analizzati numerosi nuovi composti appartenenti a classi note di antagonisti adenosinici, tra cui composti triazolotriazinici e pirazolotriazolopirimidinici, in modo da suggerire modifiche strutturali in grado di modularne l'affinità nei confronti dei vari sottotipi recettoriali adenosinici, di aumentarne la solubilità o di superarne i punti di instabilità metabolica. Diversi derivati con strutture semplificate, come per esempio composti pirazolopirimidinonici, ftalazinonici e triazolotriazinici, sono stati inoltre proposti come nuovi composti con attività antagonista nei confronti dei recettori adenosinici.

Le informazioni ricavate grazie agli studi di docking hanno permesso l'identificazione di caratteristiche strutturali degli antagonisti adenosinici fondamentali per l'interazione con questi recettori. Queste informazioni sono state quindi applicate alla progettazione di derivati fluorescenti per il recettore adenosinico A_3, che risultano particolarmente interessanti per il loro potenziale utilizzo in saggi farmacologici.

In conclusione, quindi, questo studio sui recettori adenosinici dimostra come l'integrazione di metodologie computazionali con il lavoro sintetico e farmacologico risulta essere una strategia efficace per lo sviluppo di nuovi ligandi dei recettori adenosinici, a potenziale interesse terapeutico, e per il chiarimento di importanti aspetti strutturali riguardanti questa famiglia recettoriale e più in generale tutti i GPCRs.

List of Papers

1. Cheong SL, Dolzhenko AV, Paoletta S, Lee EP, Kachler S, Federico S, Klotz KN, Dolzhenko AV, Spalluto G, Moro S, Pastorin G.

   Does the combination of optimal substitutions at the C(2)-, N(5)- and N(8)-positions of the pyrazolo-triazolo-pyrimidine scaffold guarantee selective modulation of the human A(3) adenosine receptors? *Bioorg. Med. Chem.* **2011**, 19(20):6120-34.

2. Poli D, Catarzi D, Colotta V, Varano F, Filacchioni G, Daniele S, Trincavelli L, Martini C, Paoletta S, Moro S.

   The identification of the 2-phenylphthalazin-1(2H)-one scaffold as a new decorable core skeleton for the design of potent and selective human A3 adenosine receptor antagonists. *J. Med. Chem.* **2011**, 54(7):2102-2113.

3. Federico S, Paoletta S, Cheong SL, Pastorin G, Cacciari B, Stragliotto S, Klotz KN, Siegel J, Gao ZG, Jacobson KA, Moro S, Spalluto G.

   Synthesis and Biological Evaluation of a New Series of 1,2,4-Triazolo[1,5-a]-1,3,5-triazines as Human A(2A) Adenosine Receptor Antagonists with Improved Water Solubility. *J. Med. Chem.* **2011**, 54(3):877-889.

4. Paoletta S, Federico S, Spalluto P, Moro S.

   Receptor-driven identification of novel human A3 adenosine receptor antagonists as potential therapeutic agents. *Methods Enzymol.* **2010**, 485:225-244.

5. Cheong SL, Dolzhenko A, Kachler S, Paoletta S, Federico S, Cacciari B, Dolzhenko A, Klotz KN, Moro S, Spalluto G, Pastorin G.

   The Significance of 2-Furyl Ring Substitution with a 2-(para-substituted) Aryl Group in a New Series of Pyrazolo-triazolo-pyrimidines as Potent and Highly Selective hA(3) Adenosine Receptors Antagonists: New Insights into Structure-Affinity Relationship and Receptor-Antagonist Recognition. *J. Med. Chem.* **2010**, 53(8):3361-3375.

6. Pastorin G, Federico S, Paoletta S, Corradino M, Cateni F, Cacciari B, Klotz KN, Gao ZG, Jacobson KA, Spalluto G, Moro S.

   Synthesis and pharmacological characterization of a new series of 5,7-disubstituted-[1,2,4]triazolo[1,5-a][1,3,5]triazine derivatives as adenosine receptor antagonists: A preliminary inspection of ligand-receptor recognition process. *Bioorg. Med. Chem.* **2010**, 18(7):2524-2536.

7. Lenzi O, Colotta V, Catarzi D, Varano F, Poli D, Filacchioni G, Varani K, Vincenzi F, Borea PA, Paoletta S, Morizzo E, Moro S.

   2-Phenylpyrazolo[4,3-d]pyrimidin-7-one as a new scaffold to obtain potent and selective human A3 adenosine receptor antagonists: new insights into the receptor-antagonist recognition. *J. Med. Chem.* **2009**, 52(23):7640-7652.

Contents

List of Figures

List of Tables

List of Abbreviations

AC	Adenylyl cyclase
ARs	Adenosine receptors
cAMP	Cyclic adenosine monophosphate
CNS	Central nervous system
EL	Extracellular loop
FCM	Flow cytometry
FP	Fluorescence polarization
G protein	Guanine nucleotide-binding protein
GPCRs	G protein-coupled receptors
hA_1AR	Human A_1 adenosine receptor
$hA_{2A}AR$	Human A_{2A} adenosine receptor
$hA_{2B}AR$	Human A_{2B} adenosine receptor
hA_3AR	Human A_3 adenosine receptor
I%	Percentage of inhibition
IC_{50}	Half maximal inhibitory concentration
IL	Intracellular loop
K_i	Dissociation constant
NMR	Nuclear magnetic resonance
PBD	Protein Data Bank
PHTZ	Phthalazin-1(2H)-one
PQ	Pyrazolo-quinolinone
PTP	Pyrazolo-triazolo-pyrimidine
QZ	Quinazoline
RMSD	Root mean square deviation
SAR	Structure-activity relationship
TM	Transmembrane
TQ	Triazolo-quinazoline
TQX	Triazolo-quinoxalinone

Chapter 1

Introduction

Contents

1.1 G protein-coupled receptors

The family of G protein-coupled receptors (GPCRs), also known as seven-transmembrane (7TM) receptors, is the largest and most important group of signal transduction transmembrane proteins. GPCRs represent a very efficient signaling system used by cell to transmit information from the extracellular side to the intracellular side. [1] These receptors play a crucial role in many physiological processes through the interaction with a wide number of bioactive molecules, including ions, lipids, aminoacids, peptides, proteins and small organic molecules. Physiological processes regulated by the activation of GPCRs are, for instance, the transmission of the light and of odorant signal, the mediation of neurotransmission and hormonal action, the cell growth and the immune defense. [2]

The GPCRs mediated signal transduction process starts with the binding of the agonist to the receptor that promotes conformational changes in the intracellular domains of the receptor resulting in the activation of a guanine nucleotide-binding protein (G protein). G proteins are heterotrimeric structures, made up of an α subunit, with both catalytic activity and signaling function, and a $\beta\gamma$ heterodimeric subunit complex, which targets the

G-protein to the appropriate membrane receptor and also interacts with downstream effectors. [3] A G protein is considered to be in an "inactive" state when its α subunit is bound to GDP and associated with its respective $\beta\gamma$ subunit. Therefore, after the agonist binds to the receptor the α subunit of the G protein catalyzes the GDP-GTP exchange and this promotes the dissociation of the $\beta\gamma$ subunit. Subsequently, the free GTP-α and $\beta\gamma$ subunits can transfer the signal to their intracellular effectors, such as enzymes and ions channels. [4]

The signaling pattern mediated by GPCRs can be generated bypassing the G protein intervention. In fact, it is generally accepted that GPCRs can form homodimers or heterodimers that play a role in G protein independent signaling, although the exact mechanism is not entirely elucidated. It is still unclear the relevance of this oligomerization process in various tissues and its pharmacological implications. [5, 6, 7] G protein-coupled receptors signaling pathways are described in Figure 1.1. [8]

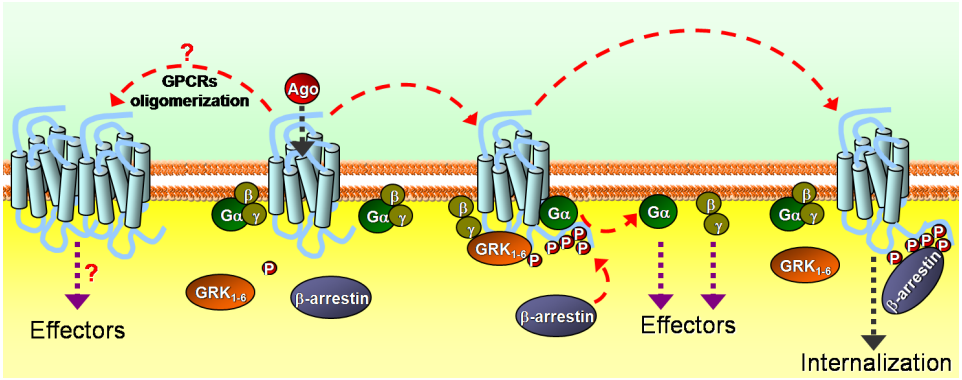

Figure 1.1: G protein-coupled receptors signaling pathways. From the inactive to the active GPCR and to the internalization of the phosphorylated GPCR; and possible GPCR oligomerization. Abbreviations: Ago, agonist; GRK, G protein-coupled receptor kinase; P, phosphate moiety; Gα, β, γ, G protein subunits.

All GPCRs possess highly conserved structural features even though the sequence identity among them is low. In particular, these receptors have in common a central domain consisting of seven transmembrane helices (from TM1 to TM7), connected by three intracellular (IL1, IL2 and IL3) and three extracellular (EL1, EL2 and EL3) loops, an extracellular N-terminal domain and an intracellular C-terminal domain. The seven transmembrane helices are the most conserved regions of GPCRs, while their intra- and extracellular regions (N-term, C-term and loops) greatly differ in terms of length and function and therefore provide very specific properties to each receptor.

The human genome encodes thousands of G protein-coupled receptors; among these, about 350 are receptors for endogenous ligands, while about 150

have unknown functions. [9, 10] According to sequence similarities, GPCRs have been clustered in different families: family A or rhodopsin-like class, family B or secretin class, family C or metabotropic glutamate and pheromone class, family D or fungal pheromone class, family E or cAMP receptors class, family F or frizzeled/smoothened class. [11, 12, 13] Among these, family A is the largest and the currently most studied.

Family A GPCRs show specific common fingerprints even though the sequence similarity is not very high. In particular, identifying motifs defined by highly conserved residues in this class are for instance the DRY motif at the cytoplasmic end of TM3 and two highly conserved cysteine residues, one in TM3 and one in EL2, that form a disulfide bridge. Moreover, each TM helix contains at least one highly conserved residue. These residues are used as references for the Ballesteros and Weinstein amino acids numbering system. Following this scheme, every residue of the TM regions is identified by two numbers: the first refers to the TM helix, the second refers to the amino acid position relative to the reference residue of that helix. The number 50 has been arbitrarily assigned to each reference residue: Asn1.50, Asp2.50, Arg3.50, Trp4.50, Pro5.50, Pro6.50 and Pro7.50. [14]

As above described, the activation of native GPCRs is usually initiated by the agonist binding; however GPCRs can achieve the active state independently of agonists and become constitutively active. These constitutively active GPCRs can be involved in the pathogenesis of many diseases. [15] Moreover, dysregulation of GPCRs has been found to be associated to a large number of human disease. [16, 17]

It has been estimated that GPCRs constitute the target of about half of the drugs in clinical use today. Therefore, studies aimed at a better understanding of GPCRs at a molecular level are of great interest in medicinal chemistry.

1.2 Adenosine receptors

The neuromodulator adenosine affects a wide variety of physiopathological processes through activation of four family A GPCRs, classified as A_1, A_{2A}, A_{2B}, and A_3 subtypes. [18, 19] These receptors are ubiquitously expressed in the human body and many cells express several adenosine receptor subtypes, although in different densities.

Adenosine receptors (ARs) are coupled to different kind of G proteins that can modulate various second messenger systems. In particular, activation of adenosine receptors can induce inhibition (A_1AR and A_3AR) or activation (A_{2A}AR and A_{2B}AR) of the adenylate cyclase. Even though the modulation of adenylyl cyclase activity could be considered the principal signal mediated by these receptors other second messenger signaling pathways can be associated with stimulation of ARs (see Figure 1.2).

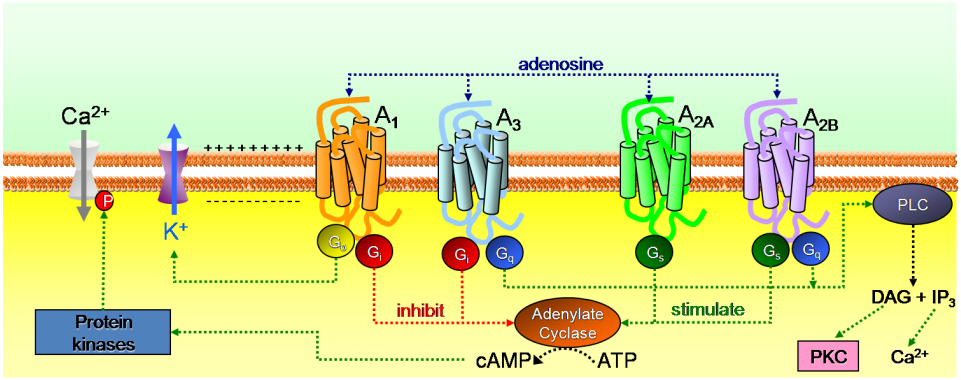

Figure 1.2: Signal transduction pathways associated with the activation of the four human adenosine receptors. Abbreviations: ATP, adenosine triphosphate; cAMP, cyclic adenosine monophosphate; PKC, protein kinase C; PLC, phospholipase C; DAG, diacylglycerol; IP_3, inositol (1,4,5)-trisphosphate; P, phosphate moiety; G_i, G_s, G_q, G_o, different families of G proteins.

Activation or blockade of ARs is responsible for a wide range of effects in numerous organ systems; and therefore the regulation of ARs can have many potential therapeutic applications.

The physio-pathological roles of ARs and their clinical potential have been exhaustively reviewed. [20, 21, 22] Due to the potential therapeutic applications of ARs ligands, in recent years, a large variety of adenosine receptors agonists and antagonists has been synthesized and has helped the pharmacological characterization of this family of G protein-coupled receptors. [23]

In particular, in this study we have taken in consideration the A_{2A} and A_3 subtypes and their potential antagonists.

1.2.1 A_{2A} adenosine receptor

The human A_{2A} adenosine receptor (A_{2A}AR) has been mapped on chromosome 22 and it is composed of 409 amino acids [24]; its size is larger than the other human adenosine receptors (hA_1AR 326 residues, hA_{2B}AR 328 residues, and hA_3AR 318 residues) because of its carboxyl-terminal tail, which is much longer than those ones of the other AR subtypes.

The A_{2A} adenosine receptor has been found in both the periphery and the central nervous system (CNS) and it is abundant in basal ganglia, T lymphocytes, vasculature and platelets.

In the peripheral system the A_{2A}AR is mainly coupled with G_s proteins, while in the striatum with G_{olf} proteins. Both of these two G proteins increase adenylyl cyclase activity and therefore the intracellular concentration

of cyclic adenosine monophosphate (cAMP). [18] The cAMP generation lead to the activation of protein kinase A, which can activate various receptors, ion channels, phosphodiesterases and cAMP responsive element binding protein (CREB) that is critical for many neuronal functions.

Neurons that express the A_{2A}AR also express dopamine D_2 receptors and one of the role of dopamine is to suppress the A_{2A}AR signaling. This interaction have interesting implication for the treatment of patologies related to an abnormal function of dopamine neurons, such as schizophrenia and Parkinson's disease.

Moreover, in the brain, the A_{2A} receptor subtype can form various functional heteromers with other G-protein coupled receptors. In particular, heterodimers consisting of receptors for adenosine A_1/A_{2A}, dopamine D_2/A_{2A} and D_3/A_{2A}, glutamate mGluR5/A_{2A} and cannabinoid CB_1/A_{2A} have all been observed, as well as $CB_1/A_{2A}/D_2$ heterotrimers.

In the central nervous system A_{2A}AR plays a role in neuroprotection and is implicated in several patologies such as Parkinson's disease, Huntington's disease, Alzheimer's disease.

A_{2A}AR activation is protective against ischemic reperfusion injury in mice, probably due to its actions on lymphocytes. [21] A_{2A}AR is found in several immune cells and its activation inhibits early and late events occuring during an immune response.

Therefore, A_{2A}AR ligands have been studied for various therapeutic applications; in particular its agonists have been explored as anti-inflammatory drugs while its antagonists for neurodegenerative diseases, e.g., Parkinson's disease.

1.2.2 A_3 adenosine receptor

The A_3 adenosine receptor (A_3AR) is the last member of the adenosine receptors family to have been cloned. [21] Considering receptor distribution, the highest levels of human A_3AR mRNA have been found in lung and liver. [25] However, A_3ARs have been detected in various tissues including testis, lung, kidney, placenta, heart, brain, spleen, liver, uterus, bladder, jejunum, aorta, proximal colon and eyes. [25]

The A_3AR has been mapped on human chromosome 1 and consists of 318 amino acid residues. Differently to other adenosine receptors, the C-terminal region presents multiple serine and threonine residues, which may serve as potential sites of phosphorylation that are important for receptor desensitization upon agonist application. [25]

Species differences for A_3 receptors are larger than for other AR subtypes, particularly between rodent and human receptors (only 74% sequence identity between rat and human A_3 sequences). The low identity reflects in different affinity values of ligands for rat versus human A_3 receptors, making more difficult the use of rat models for *in vivo* studies.

The firstly identified second-messenger systems associated with A_3AR activation have been adenylyl cyclase (AC), which is inhibited via $G_{i2,3}$ coupling, and phospholipase C (PLC), which is stimulated via $G_{q/11}$ coupling. [26] In addition, other intracellular pathways have been described as being linked with A_3AR activation, as summarized in Figure 1.3.

The A_3AR positively modulates phospolipase D, [27] ATP-sensitive potassium channels, inositol triphosphate, and intracellular calcium. [28, 29] Activation of this receptor subtype leads to modulation of mitogen-activated protein kinases (MAPK), such as the extracellular signal-regulated kinase (ERK) 1/2 and the stress-activated protein kinase p38. [30]

A_3AR signaling is involved in several physio-pathological processes, but what is known about its role it is still unclear.

The A_3AR regulation of the cell cycle may induce cell protection or cell death, depending on the degree of receptor activation, the cell type and the toxic insult. [31, 32] As a consequence of this dual effect, both A_3 receptor agonists and antagonists might be effective therapeutics in cancer. [33] Moreover, A_3AR have been demonstrated to be over-expressed in some tumor cell lines, thus suggesting this receptor as a potential target in cancer therapy. [21, 25]

In the brain and in other tissues, such as kidney, lung, and eye, activation of the A_3AR may induce both pro- and antisurvival effects, determining either protection or damage, depending on the situation. [31]

The role of A_3AR in inflammatory diseases is also currently controversial, and both anti- and pro-inflammatory effects have been attributed to its activation depending on the investigated model. One of the first therapeutic applications that was hypothesized for A_3AR antagonists was the treatment of asthma. In fact, it was reported that in rodents, A_3AR activation was responsible for mast cell degranulation. [21, 25]

Activation of A_3AR leads to the regulation of chloride channels in non-pigmented ciliary epithelial cells, suggesting that A_3AR agonists would increase aqueous humor secretion and thereby intraocular pressure in vivo, whilst A_3AR antagonists may represent a specific approach for treating ocular hypertension. [21, 25]

Another important topic in the area of A_3AR-targeted therapy is the protective role of this adenosine receptor subtype in cardiac ischemia. To date, several studies have pointed to the evidence that the A_3AR is a key player in adenosine-induced cardioprotection during and following ischemia-reperfusion.

Thus, even though it is clear that the A_3AR is involved in many disease pathways, much remains to be clarified about its role. Therefore, the search for new selective A_3AR ligands, either agonists or antagonists, continues to be attractive.

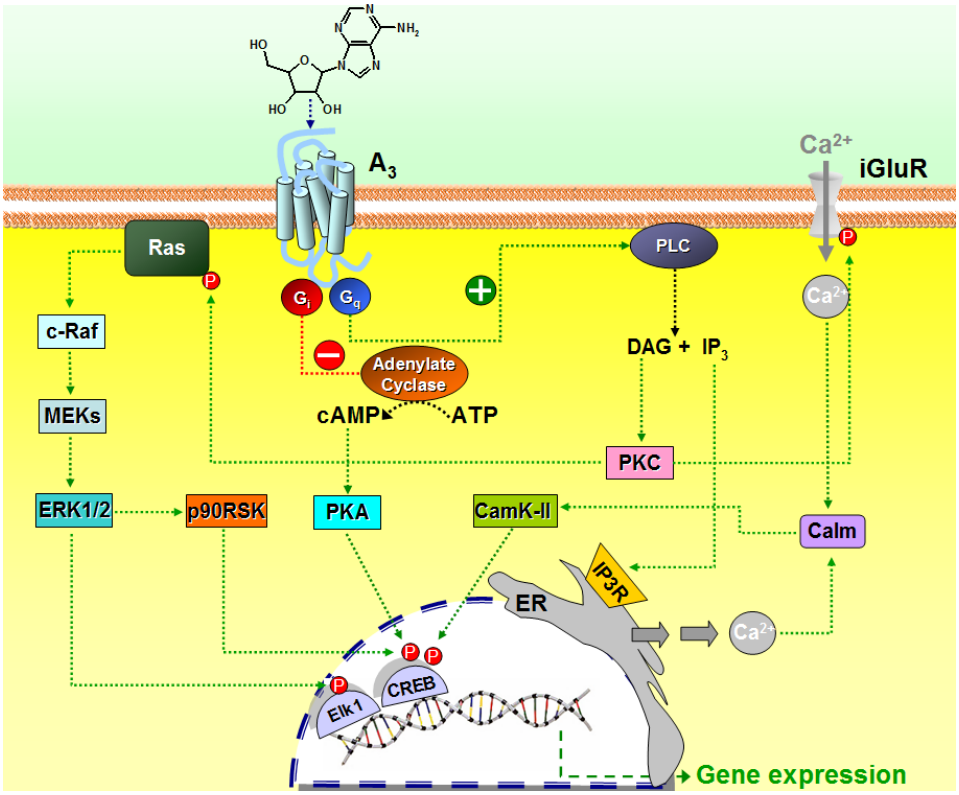

Figure 1.3: Signal transduction pathways associated with the activation of the human A_3 adenosine receptor. Abbreviations: ATP, adenosine triphosphate; Calm: calmodulin; CamK-II: Ca2+/calmodulin-dependent protein kinase; cAMP, cyclic adenosine monophosphate; c-Raf: RAF proto-oncogene serine/threonine-protein kinase; CREB: cAMP response element-binding; DAG, diacylglycerol; ERK: extracellular signal-regulated kinase; G_i, G_i family of G proteins; G_q, G_q family of G proteins; iGluR: ionotropic glutamate receptors; IP_3, inositol (1,4,5)-trisphosphate; MEK: mitogen-activated protein kinase/extracellular signal-regulated kinase kinase; P, phosphate moiety; PKA, protein kinase A; PKC, protein kinase C; PLC, phospholipase C.

1.3 Adenosine receptors antagonists

Many efforts have been made in medicinal chemistry for the development of selective agonists and antagonists for each of the four AR subtypes. The availability of selective ligands helped the research on therapeutic applications of modulating the ARs and provided some clinical candidates. [22]

Of particular interest for this study is the exploration of synthetic adenosine antagonists for potential therapeutic applications.

Historically, prototypical ARs antagonists were alkylxanthine derivatives. Natural xanthines, such as caffeine and theofilline, behave as weak and non selective antagonists for adenosine receptors.

Nowadays, many newer and highly selective ARs antagonists have been developed; they are more chemically diverse than xanthines and contain non-purine heterocyclic core structures. [22]

1.3.1 A_{2A} adenosine receptor antagonists

Relevant potential therapeutic indications of A_{2A}AR antagonists are neurodegenerative diseases, such as Parkinson's and Alzheimer's, restless legs syndrome, depression and addiction. [22] Several selective A_{2A}AR antagonists have been evaluated in clinical trials for the treatment of Parkinson's disease. In Figure 1.4 some representative A_{2A}AR antagonists, with their binding affinities, are reported.

The first A_{2A}-selective antagonists were developed modifying the xanthine nucleus at the 8-position with alkenes (notably styryl groups) and the 8-styrylxanthine istradefylline (**1**, KW6002) was one of the first A_{2A}AR antagonists reported.

The substitution of the xanthine core with various heterocyclic ring systems has led to some compounds with very high affinity and selectivity toward the A_{2A} subtype. The triazoloquinazoline CGS15943 (**2**) was one of the early example of a heterocyclic structure showing A_{2A}AR antagonist activity but with only slight selectivity. Subsequent refinement of the triazoloquinazoline core by addition of a third ring or alteration of the pattern of N inclusion in the heterocyclic system greatly improved the A_{2A}AR selectivity.

Examples of highly potent A_{2A}AR antagonists of later generation are the triazolotriazine ZM241385 (**3**), the triazolopyrimidine vipadenant (**4**), and the pyrazolotriazolopyrimidine SCH442416 (**5**). Another pyrazolotriazolopyrimidine compound with a very good affinity and selectivity profile at the hA_{2A}AR is preladenant (**6**) that is undergoing clinical trials for the treatment of Parkinson's disease.

Examples of further non-xanthine A_{2A}AR antagonists, which are being clinically evaluated, are the adenine derivative ST-1535 (**7**) and the benzothiazole derivative SYN-115 (**8**).

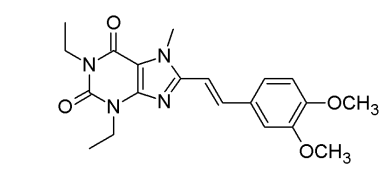

Istradefylline (KW6002), **1**

hA_1 = 841 nM
hA_{2A} = 12 nM
hA_{2B} > 10,000 nM
hA_3 = 4470 nM

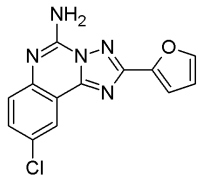

CGS15943, **2**

hA_1 = 3.5 nM
hA_{2A} = 1.2 nM
hA_{2B} = 32.4 nM
hA_3 = 35 nM

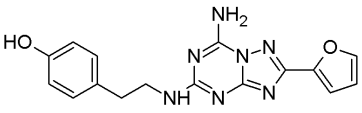

ZM241385, **3**

hA_1 = 774 nM
hA_{2A} = 1.6 nM
hA_{2B} = 75 nM
hA_3 = 743 nM

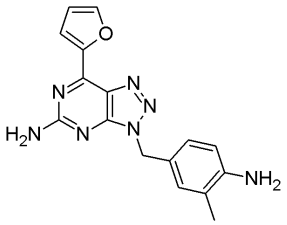

Vipadenant (BIIO14, V2006), **4**

hA_1 = 68 nM
hA_{2A} = 1.3 nM
hA_{2B} = 63 nM
hA_3 = 1005 nM

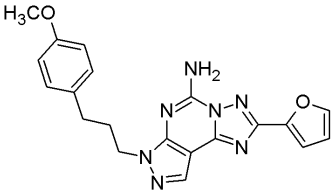

SCH-442416, **5**

hA_1 = 1110 nM
hA_{2A} = 4.1 nM
hA_{2B} > 10,000 nM
hA_3 > 10,000 nM

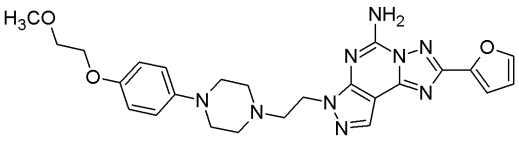

Preladenant (SCH-420814), **6**

hA_1 > 1000 nM
hA_{2A} = 0.9 nM
hA_{2B} > 1000 nM
hA_3 > 1000 nM

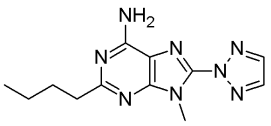

ST-1535, **7**

hA_1 = 71.8 nM
hA_{2A} = 6.6 nM
hA_{2B} = 352.3 nM
hA_3 > 1000 nM

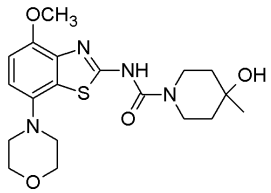

SYN-115, **8**

Figure 1.4: Structures and binding affinities of known hA_{2A} adenosine receptor antagonists.

1.3.2 A_3 adenosine receptor antagonists

In light of the plethora of biological effects attributed to A_3AR, substantial efforts in medicinal chemistry have been directed towards developing potent and selective antagonists for the human A_3AR subtype. [21, 23, 34] In fact, a number of molecules are in biological testing as therapeutic agents for asthma and chronic obstructive pulmonary disease (COPD), glaucoma, stroke, cardiac hypoxia and cerebral ischemia; [21, 25] but, unfortunately, there are currently no A_3AR antagonists in clinical phases.

A large amount of human A_3 adenosine receptor antagonists posses polyheterocyclic nucleus, which can be classified in six families of derivatives: i) Flavonoids; ii) 1,4-dihydropyridines and pyridines; iii) Triazoloquinazolines; iv) Isoquinolines and quinazolines; v) Pyrazolo-triazolo-pirimidines, vi) various. In Figure 1.5 are summarized some representative members of different families of A_3AR antagonists, which have been extensively reviewed. [21, 34, 23, 35]

Xanthines, that are considered the natural antagonists for adenosine receptors, show in general very low affinity for the A_3 adenosine receptor subtype (high micromolar range). Nevertheless, recent SAR studies on these compounds indicated that a cyclization between the 7- and 8- or 3- and 4- positions led to A_3 adenosine receptor antagonists, such as 2-phenylimidazopurin-5-one PSB-10 (**9**). Other classes of extended xanthine structures have been reported as A_3 adenosine receptor antagonists such as triazolopurines (**10**) which proved to be potent and selective human A_3 adenosine receptor antagonists.

Optimization of flavonoid nucleus, through a classical structure-activity relationship study led to MRS 1067 (**11**), the most potent and selective compound of this series at the hA_3AR subtype.

A very similar approach was utilized for studying dihydropiridines which are typically antagonists of the L-type calcium channel, but a combination of substitutions on the 1,4-dihydropyridine skeleton led to MRS1334 (**12**) which proved to be the most potent derivative of this series. Simultaneously the same authors studied the affinity of the pyridines, derived from the oxidation of the corresponding 1,4-dihydropiridines, obtaining MRS1523 (**13**), which showed quite good affinity at the human A_3 adenosine receptor but could be considered the first derivative which possessed discrete affinity for the rat A_3 adenosine subtype.

Acylation at the 5-position of the triazoloquinazoline derivative CGS 15943 (9-chloro-2-(2-furanyl)-[1,2,4]triazolo[1,5-*c*]quinazoline-5-amine), a classic unselective adenosine receptor antagonist, led to the discovery of MRS1220 (**14**) a highly potent and quite selective hA_3 adenosine receptor antagonist. In a screening program of compounds, quinazoline derivatives, such as VUF5574 (**15**), showed good affinity at human A_3 adenosine receptor while resulted to be uneffective at A_1 and A_{2A} receptor subtypes. Further library

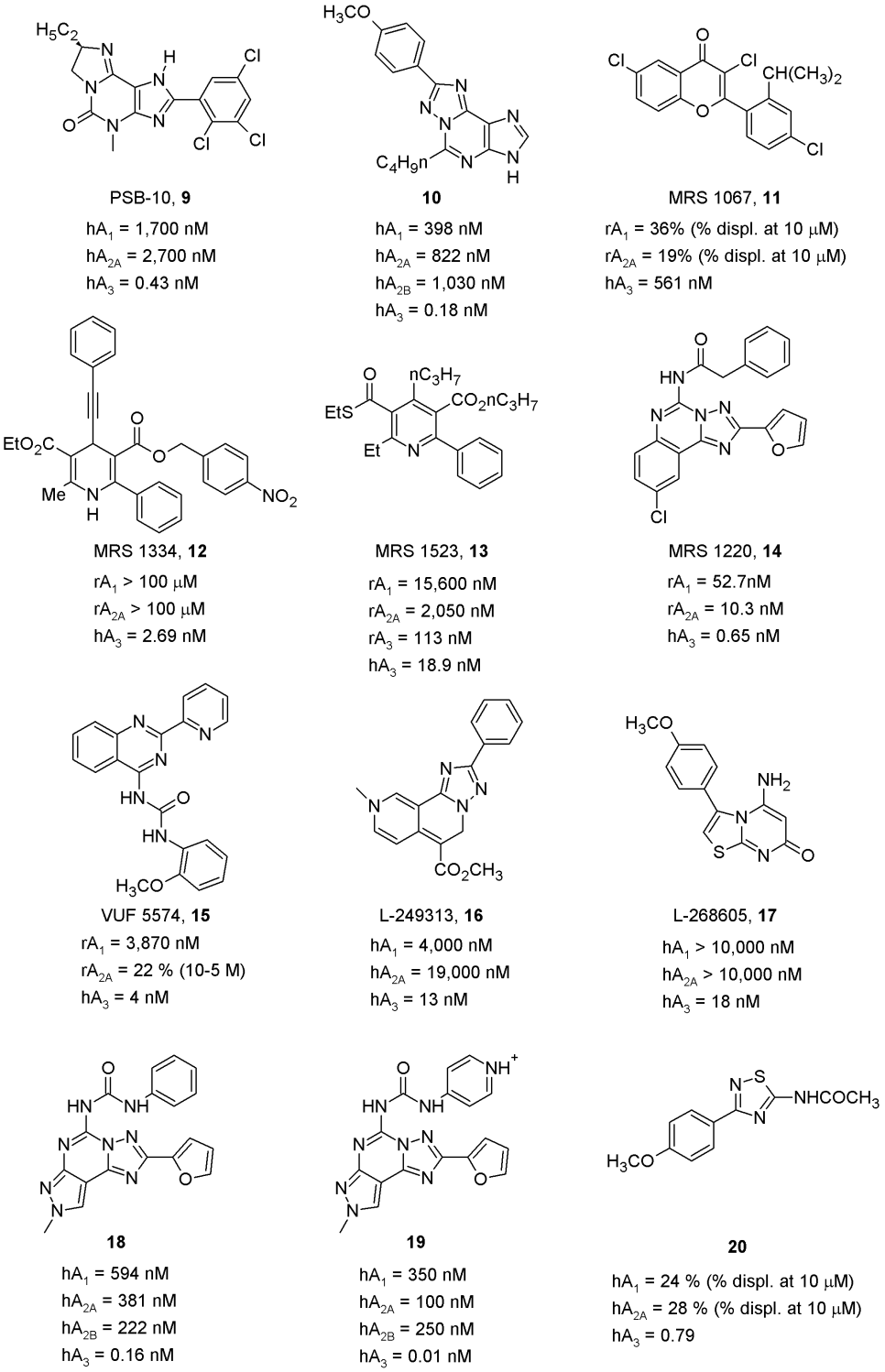

Figure 1.5: Structures and binding affinities of known hA_3 adenosine receptor antagonists.

screenings led to novel heterocyclic A_3 antagonists which shown quite good affinity, such as L-249313 (**16**) and L-268605 (**17**).

The best results in terms of potency and selectivity at the human A_3AR were obtained with the pyrazolo-triazolo-pyrimidines derivatives. In particular, introduction at the N^5 position of a phenyl carbamoyl moiety and a methyl group at the N^8 pyrazole nitrogen led to compound **18** which can be considered one of the most potent and selective human A_3 adenosine receptor antagonists ever reported. Interestingly, the bioisosteric substitution of the phenyl ring with a piridinium salt led to a completely water soluble (15 mM) derivative **19** and with an increased affinity and selectivity for the hA_3 adenosine receptor.

Other derivatives structurally related to this family have been reported, in particular the triazolo-quinoxalines. In this class several compounds have been synthesized as antagonists for the different adenosine receptor subtypes. [21, 34, 23]

Structural simplified A_3 adenosine receptor antagonists have been reported and in particular bicyclic scaffolds were investigated. Some simplified compounds, such as the thiadiazole (derivative **20**) seem to be promising agent considering the very simple synthetic preparation and their low hydrophobic propensities. [23]

Finally, it should be underlined that all the reported compounds showed significant potency and selectivity at the human A_3 adenosine receptor in human model, thus limiting studies *in vivo*. This aspect has been partially avoided working on the adenosine core. In fact, adenosine derivatives are considered receptor agonists for the presence of the ribose moiety, but the introduction of extended substituents at the 8 position or the constraint of the ribose ring led to quite potent A_3AR antagonist also in rat model. [36]

Chapter 2

Materials and methods

Contents

For the development of this project several computational tools have been applied to the study of proteins, other molecules and their interactions to predict some of their behaviors.

In this section the computational methodologies used are described along with the structural and sequence information necessary for the development of this project.

2.1 Amino acid sequences

Nowadays, wide information about protein sequences are available and stored in databases. Amino acid sequences used in this study were downloaded from the Universal Protein Resource (UniProt) database, that contains more than 500000 protein entries. [37]

In this project, sequences of adenosine receptors and other GPCRs were analyzed and compared. In particular, UniProt identifiers of the considered human adenosine receptors sequences are: P30542 for hA_1AR, P29274 for $hA_{2A}AR$, P29275 for $hA_{2B}AR$, and P33765 for hA_3AR.

2.2 Crystallographic structures

Three-dimensional structural information about proteins and nucleic acids are collected in the Protein Data Bank (PDB). [38] Today, more than 78000 3D structures, solved mainly with the use of X-ray crystallography or nuclear magnetic resonance (NMR), are available in the PDB.

However, despite the enormous biomedical relevance of GPCRs, high resolution structural information on their active and inactive states is still poor. In fact, being GPCRs integral membrane proteins, they are not easy to crystallize and hence to characterize through X-ray diffraction.

Rhodopsin had represented for many years the only 3D structural information available for GPCRs and rhodopsin-based homology modeling had been the most widely used approach to obtain three dimensional models of GPCRs. In fact, rhodopsin is highly abundant from natural sources and structurally stabilized by the covalently bound ligand 11-*cis*-retinal, which mantains the receptor in a dark-adapted, non-signaling conformation. In contrast, all other GPCRs are activated by diffusible ligands and are expressed at relatively low levels in native tissues. These receptors are structurally more flexible and some of them are prone to instability. [39]

The first highly resolved structure of rhodopsin was published by Palczewski and collaborators in 2000. [40] This 2.8 resolution structure of bovine rhodopsin (PDB ID: 1F88) showed all major structural features of GPCRs as predicted from years of biochemical, biophysical and bioinformatics studies.

Subsequently, crystallographic structures of other GPCRs have been reported such as the human β2-adrenergic receptor in 2007 [41, 42] and the turkey β1-adrenergic receptor in 2008. [43]

Of particular interest for the adenosine receptors field has been the pubblication in 2008 of the crystal structure of the human A_{2A} adenosine receptor (PDB ID: 3EML) [44] in complex with a high-affinity subtype-selective antagonist, 4-(2-(7-amino-2-(furan-2-yl)-[1,2,4]triazolo[2,3-*a*][1,3,5]triazin-5-ylamino)ethyl)phenol, ZM241385 (compound **3** in Figure 1.4).

Interestingly, to crystallize the 2.60 Å resolution structure was applied the T4L fusion strategy, where most of the third cytoplasmic loop was replaced with lysozyme and the C-term tail was truncated from AlA317 to Ser412.

This crystal structure presents three features different from previously reported GPCR structures.

First of all, the EL2 is considerably different from $\beta1/\beta2$-adrenergic receptors and bovine/squid rhodopsins; in fact it lacks any clearly secondary structural element and possesses three disulfide linkages, one with TM3 (Cys77-Cys166), that is conserved among most of the members of family A GPCRs, and two with EL1 (Cys71-Cys159 and Cys74-Cys146) that are unique to the A_{2A} adenosine receptor. Moreover, the crystallographic structure of hA_{2A}AR shows a disulfide bond between Cys259 and Cys262 in the EL3 of the receptor. The presence of all these bridges contributes to the

formation of a disulfide bond network that forms a rigid, open structure exposing the ligand binding cavity to solvent, possibly allowing free access for small molecule ligands. [44]

Secondly, ZM241385 is perpendicular to the membrane plane, co-linear with TM7 and it interacts with both EL2 and EL3. The ligand position is significantly different from the position of retinal and amine ligands of adrenergic receptors.

Finally, even though the helical arrangement is similar to other GPCRs, the binding pocket of the A_{2A} adenosine receptor is shifted closer to TM6 and TM7 and less interactions are allowed with TM3 and TM5. [44] This means that even though GPCRs share a common topology, ligands may bind in a different fashion and interact with different positions of the receptor.

Recently, crystallographic structures of other different GPCRs have been published including human dopamine D_3 receptor, [45] human chemokine receptor CXCR4 [46] and human histamine H1 receptor. [47]

Moreover, in 2011 other three-dimensional structures of human A_{2A}AR, in complex with agonists or antagonists, have been solved: A_{2A}AR-T4L bound to the agonist UK-432097 (PDB ID: 3QAK), [48] thermostabilized A_{2A}AR bound to its endogenous agonist adenosine and the synthetic agonist NECA (PDB IDs: 3PWH, 3REY, 3RFM), [49] thermostabilized A_{2A}AR in complex with ZM241385 and the xanthines XAC and caffeine (PDB IDs: 2YDO, 2YDV). [50]

2.3 Computational Methodologies

All modeling studies were carried out on a 20 CPU (Intel Core2 Quad CPU 2.40 GHz) Linux cluster.

Homology modeling, energy calculation, and analyses of docking poses were performed using the Molecular Operating Environment suite (MOE, version 2010.10). [51]

The software package MOPAC (version 7), [52] implemented in the MOE suite, was utilized for all quantum mechanical calculations.

Docking simulations were performed using MOE-Dock, [51] GOLD, [53] Glide, [54] and PLANTS. [55]

2.4 Molecular Mechanics

The field of molecular modeling is composed of several interlinked activities, including molecular graphics, computational chemistry and statistical modeling, where the common component is the computer.

One of the approaches to molecular modeling is based on the molecular mechanics formalism. In this formalism each atom is treated as a mass proportional to its atomic mass and each bond is treated as an analog of a

mechanical spring, which has a force constant associated with it. The atoms are classified as atom-types that describe the atom features. The molecular mechanics approach assumes that the potential energy of a molecular system is made up of contributions derived from each atom and and each bond in the system and is expressed by an equation called force field. Molecular mechanics can be used to study small molecules as well as large biological systems.

2.4.1 Empirical Force Fields

The force field is an equation expressing the potential energy of a molecular system in a given conformation as a sum of individual energy terms. The calculation sums the energy resulting from all interactions among all atoms, both bonded and non-bonded.

$$E_{total} = E_{bonded} + E_{non-bondend}$$

The bonded term considers the energy attributable to all the bonding interactions, so this term refers to the stretching or compressing of the bonds, to the bending of the bond angles and to the torsional (twisting) distortions of the dihedral angles.

The non-bonded component considers the energy attributable to the non-bonding interactions, such as Van der Waals steric interactions and electrostatic or charge interactions. The importance of the non-bonded terms in the energy expression is strongly dependent on the distance between the interaction atoms.

$$E_{bonded} = E_{bond} + E_{angle} + E_{dihedral}$$

$$E_{non-bondend} = E_{electrostatic} + E_{vanderWaals}$$

Some terms are more influential than others in their contributions to the overall energy of the system. The exact functional form of the potential function, or force field, depends on the particular simulation program being used. Some additional terms (e.g., H-bonding interactions) are often included in the equation.

The force fields mainly used in this study have been AMBER99, [56] parameterized for proteins and nucleic acids, and MMFF94x, [57] parameterized for gas phase small organic molecules in medicinal chemistry.

2.5 Homology modeling

The structure-based drug design requires the structural information of receptors and ligands. The 3D structure of a protein target can be taken from the PDB, that contains protein structures determined by X-ray crystallography or nuclear magnetic resonance (NMR) spectroscopy. On the other hand,

the initial structure of a protein target can also be constructed by homology modeling based on both sequence and structural information from known families of proteins.

The homology modeling approach is the method of choice to predict the structure of a protein, starting from the sequence of that protein and based on the available 3D structure of an homologous protein. This computational approach is based on the notion that the primary structure of proteins is less conserved, through evolution, than the higher level structures, namely secondary, tertiary and quaternary.

Therefore, using this technique, an amino acid sequence (target protein) can be modeled on the structure of a second protein (template), which possesses the same folding. Based on the sequence alignment of the two proteins, the pairs of residues are spatially matched with the generation of the new coordinates for the target structure. Thus, the quality of the sequences alignment which determines the residues pairs is of primary importance. Usually, conserved regions, like secondary structure elements or patterns of residues implicated in the protein function, are identified in the structure of the template. Later, the alignment is optimized to match these conserved regions.

It has to be noted that when the alignment reveals one ore more long gaps, underlining structural variations between the two proteins, the generation of the new structure requires particular care. When new loops have to be built, meaning that the target sequence have non-correspondent stretches in the template, coordinates can be either assigned randomly and energy minimized or taken from experimentally known ones of other structures. The reliability of these additional loops depends on their length and the distance between the template extremities. The longer is the insertion, compared to the three-dimensional gap, the less reliable is the result. [58, 59]

Finally, the out-coming homology model can be structurally refined using different protocols such as energy minimization or simulated annealing. Finally, the resulting structure has to be checked for stereochemical quality, considering ϕ and ψ angles distribution (Ramachandran plot), bond lengths, angles etc, and also for its ability in explaining known biochemical data.

In fact, homology models are theoretical structures whose reliability has to be checked. In order to evaluate the goodness of a model, the accordance with available experimental data (mainly mutagenesis and ligand activity data) and the predictive ability of the model can be considered. Therefore, a "structural" validation can be performed through the inspection of the position of all the residues revealed by mutagenesis studies to play an important role in ligand binding. On the other hand, a "functional" validation is the ability of the model to predict the activity of known ligands, to suggest the design of new ones and to identify residues important for the interaction with ligands.

2.5.1 Human A_3AR homology model

On the basis of the assumption that GPCRs share similar TM boundaries and overall topology, a homology model of the hA_3 adenosine receptor was constructed using as template the recently published crystal structure of the hA_{2A} receptor in complex with ZM241385 (PDB ID: 3EML). [44] The model was built using the homology modeling protocol implemented in the MOE suite. [51]

As previouly underlined, the first important step in the homology modeling protocol is related to sequence alignment. For GPCRs, the alignment is guided by the most conserved residues in each TM helix (at least one highly conserved residue). These peculiar residues are used as reference for the Ballesteros and Weinstein nomenclature system: every amino acid of TM regions is identified by a number that refers to the transmembrane segment of the GPCR, followed by a number that refers to the position relative to the reference residue in that helix, that has arbitrarily the number 50 (Asn1.50, Asp2.50, Arg3.50, Trp4.50, Pro5.50, Pro6.50 and Pro7.50 in TM1-7, respectively). [14]

Therefore, as first step, the amino acid sequences of TM helices of the hA_3 receptor were aligned with those of the template crystal structure, guided by the highly conserved amino acid residues, including the DRY motif (Asp3.49, Arg3.50, and Tyr3.51) and three proline residues (Pro4.60, Pro6.50, and Pro7.50) in the TM segments of GPCRs.

The same boundaries were applied for the TM helices of the hA_3 receptor as they were identified from the 3D structure of the hA_{2A}AR, the coordinates of which were used to construct the seven TM helices for the hA_3 receptor.

The loop domains were constructed by the loop search method implemented in MOE on the basis of the structure of compatible fragments found in the Protein Data Bank. In particular, loops are modeled first in random order. For each loop, a contact energy function analyzes the list of candidates collected in the segment searching stage, taking into account all atoms already modeled and any atom specified by the user as belonging to the model environment. These energies are then used to make a Boltzmann-weighted choice from the candidates, the coordinates of which are then copied to the model.

Missing side chains were modeled using a library of rotamers generated by systematic clustering of the Protein Data Bank data, using the same procedure. Side chains belonging to residues, whose backbone coordinates were copied from a template, are modeled first, followed by side chains of modeled loops. Outgaps and their side chains are modeled last.

Special caution has to be given to EL2 because amino acids of this loop could be involved in direct interactions with the ligands. A driving force to the peculiar fold of the EL2 might be the presence of a disulfide bridge between cysteines in TM3 and EL2. Since this covalent link is conserved in

all the adenosine receptors, the EL2 was modeled using a constrained geometry around the EL2-TM3 disulfide bridge. The constraints were applied before the construction of the homology model, in particular during the sequences alignment. The cysteine residues, involved in the disulfide bridge in the hA_{2A} receptor, were selected to be constrained with the corresponding cysteines in the hA_3 receptor sequence. In particular, Cys166 (EL2) and Cys77 (3.25) of the hA_{2A} receptor were constrained, respectively, with Cys166 (EL2) and Cys83 (3.25) of the hA_3 receptor. During the alignment, MOE-Align attempts to minimize the number of constraint violations. Then, after running the homology modeling, the presence of the conserved disulfide bridge in the model was manually checked.

After the heavy atoms were modeled, all hydrogen atoms were added and were then minimized with MOE using the AMBER99 force field. [56] The minimizations were carried out by the 1000 steps of steepest descent followed by conjugate gradient minimization until the rms gradient of the potential energy was less than 0.1 kcal mol^{-1} $Å^{-1}$. We used the Protonate 3D methodology, part of the MOE suite, for protonation state assignment by selecting a protonation state for each chemical group that minimizes the total free energy of the system (taking titration into account). [60]

Protein stereochemistry evaluation of the resulted model was then performed by several tools implemented in the MOE suite, such as Ramachandran plot, bond lengths, bond angles and dihedrals reports, rotamer strain energy report and clash contacts report. [51]

Finally, to check the reliability of the model, its accordance with available mutagenesis data was considered and molecular docking studies of AR antagonists were performed.

2.6 Molecular docking

The core step of protein-based drug design is docking and scoring. Docking is the process that place a ligand molecule into the binding site of a receptor protein and then optimize the relative orientation and conformation of the ligand to interact with the protein. Then each pose is scored by a proper scoring function.

Therefore, the main aim of molecular docking is trying to predict the 3D structure of the complex between a ligand and a protein. To do this a docking program needs two components: the search algorithm and the scoring function. In the molecular docking process, the search space (the set of all possible solutions to a problem) consists of all possible orientations and conformations of the protein paired with the ligand. Because it is impossible to explore the search space exhaustively, is important to use of search algorithms for sampling the search space. Then for each protein-ligand pose, the scoring function predicts the strength of the interaction between the two

molecules (binding affinity). In other terms, the scoring function takes a pose as input and returns a number indicating the probability that the pose represents a favourable binding interaction.

Obviously, reproducing the conformational space accessible to a macromolecule is a very difficult task and requires unavoidable approximation. Docking procedures can thus be classified into three categories depending on their degree of approximation:

- Rigid body docking: This is a highly simplistic model that regards both the ligand and the protein as two rigid solid bodies.
- Semi-flexible docking: This model is asymmetric; one of the molecules, usually the smaller ligand, is considered flexible, while the protein is regarded as rigid.
- Flexible docking: Both molecules are considered flexible, although clearly the extent of flexibility of either (or of both) is necessarily limited, or simplified.

Since ligands are much smaller than macromolecules, ligand flexibility is computationally easier to handle and thus today it is standard in docking protocols. The ideal docking method would allow both ligand and receptor to explore their conformational degree of freedom. However, such calculations are computationally very demanding and most of the methods only consider the conformational space of the ligand while the receptor is invariably assumed to be rigid.

As previously said, the success of a docking program depends on two components: the search algorithm and the scoring function.

The search algorithm is used to generate ligand conformations inside the protein binding pocket. Algorithms can be grouped into deterministic and stochastic approaches. Deterministic algorithms are reproducible, whereas stochastic algorithms include a random factor and are thus not fully reproducible. A brief description of the different docking algorithms used in this study is here reported:

Genetic Algorithm: This algorithm is a computer program that mimics the process of evolution by manipulating a collection of data structures called chromosomes. Each of these chromosomes encodes a possible solution to the problem to be solved. In case of docking, each chromosome encodes a possible ligand-receptor complex conformation and to each of them is assigned a fitness score on the basis of the relative quality of that solution in terms of protein-ligand interactions.

Starting from an initial, randomly generated, parent population of chromosomes, the genetic algorithm repeatedly applies two major genetic operators, crossover and mutation, resulting in children chromosomes that replace the least-fit members of the population. The

crossover operator requires two parent chromosomes and combining their features generates two children. The mutation operator requires one parent and introducing random perturbations produce one child. The parent chromosomes are randomly selected from the existing population with a bias towards the best, thus introducing an evolutionary pressure into the algorithm. This emphasis on the survival of the best individuals ensures that, over time, the population should move toward an optimal solution, that is the correct binding mode.

The genetic algorithm is used by the software GOLD [53] and is available as search algorithm in MOE-Dock. [51]

Tabu search: This algorithm is characterized by the imposition of restrictions to enable the search process to explore otherwise difficult regions. These restrictions take the form of a tabu list that stores a number of previously visited solutions. By preventing the search to visit these regions, the exploration of new search space is encouraged. While the genetic algorithm usually converges quickly at the close proximity of a global minimum, it can be trapped in a local minimum. Using a tabu list helps in avoiding this drawback.

Tabu search is available as search algorithm in MOE-Dock. [51]

Simulated Annealing: It is a special molecular dynamics simulation, in which the system is cooled down at regular time intervals by decreasing the simulation temperature. The system thus gets trapped in the nearest local minimum conformation. Disadvantages of simulated annealing are that the result depends on the initial placement of the ligand and that the algorithm does not explore the solution space exhaustively.

Simulated annealing is available as search algorithm in MOE-Dock. [51]

Glide Algorithm: The Glide (Grid-based Ligand Docking with Energetics) [54] algorithm approximates a systematic search of positions, orientations and conformations of the ligand in the receptor binding site using a series of hierarchical filters. The shape and properties of the receptor are represented on a grid by several different set of fields that provide progressively more accurate scoring of the ligand pose. The fields are computed prior to docking. The binding site is defined by a rectangular box confining the translation of the mass center of the ligand. A set of initial ligand conformations is generated through exhaustive search of the torsional minima, and the conformers are clustered in a combinatorial fashion. Each cluster, characterized by a common conformation of the core and an exhaustive set of rotamer group conformations, is docked as a single object in the first stage. The search begins with a rough positioning and scoring phase that significantly

narrows the search space and reduces the number of poses to be further considered to a few hundred. In the following stage, the selected poses are minimized on pre-computed OPLS-AA van der Waals and electrostatic grids for the receptor. In the final stage the lowest-energy poses obtained are subjected to a Montecarlo procedure in which nearby torsional minima are examined, and the orientation of peripheral groups of the ligand is refined. These minimized poses are finally rescored.

Plants: The docking algorithm PLANTS (Protein-Ligand ANT System) is based on a class of stochastic optimization algorithms called ant colony optimization (ACO). ACO is inspired by the behavior of real ants finding a shortest path between their nest and a food source. The ants use indirect communication in the form of pheromone trails which mark paths between the nest and a food source. In the case of protein-ligand docking, an artificial ant colony is employed to find a minimum energy conformation of the ligand in the binding site. These ants are used to mimic the behavior of real ants and mark low energy ligand conformations with pheromone trails. The artificial pheromone trail information is modified in subsequent iterations to generate low energy conformations with a higher probability. [55]

Scoring function are fast approximate mathematical methods used to predict the strength of the non-covalent interaction between two molecules given the 3D structure of their complex and therefore their binding affinity. There are three general classes of scoring functions:

- Force field-based scoring functions based on the non-bonded terms of a classical molecular mechanics force field. Usually a Lennard-Jones potential describes van der Waals interactions and the Coulomb energy describes the electrostatic components of the interaction. A major disadvantage of these scoring functions lies in the fact that is unclear to what extend they can be applied to protein-ligand complexes not represented in the training set used for deriving the master equation. GoldScore and MOE Energy score are some examples.

- Empirical scoring functions based on counting the number of various types of interactions between the two binding partners. They use several terms describing properties known to be important in drug binding to construct a master equation for predicting binding affinity. Multilinear regression is used to optimize the coefficients to weight the computed terms using a training set of protein-ligand complexes for which both the binding data and the high resolution 3D crystal structures are known. ChemScore and Glidescore are some examples.

- Knowledge-based scoring functions based on statistical observations of intermolecular close contacts in large 3D databases which are used to

derive "potentials of mean force". This method is founded on the assumption that close intermolecular interactions between certain types of atoms or functional groups that occur more frequently than one would expect by a random distribution are likely to be energetically favorable and therefore contribute favorably to binding affinity.

Finally hybrid scoring functions have also been developed in which the terms from two or more of the above types of scoring functions are combined into one function.

2.6.1 Docking protocol selection

One of the main problem in computational chemistry is the ability to predict the binding mode and estimate the binding affinity for each ligand, given the structure of a protein and a list of potential small molecule ligands. The first step to solve this problem is the application of computational methods in trying to reproduce the bound conformation of a ligand in a high-resolution X-ray crystal structure; so that the most accurate molecular docking protocol for that system can be selected.

The release of the $hA_{2A}AR$ crystal structure provided not only important structural information about adenosine receptors, but also information about ligand binding. Therefore we used these information to test different molecular docking softwares and select the one that is able to better describe this molecular system, to be used then for the docking studies of ARs antagonists.

Four different programs have been used to calibrate our docking protocol: MOE-Dock, [51] GOLD, [53] Glide, [54] and PLANTS. [55]

In particular, ZM241385 was re-docked to the crystal structure of the $hA_{2A}AR$ (PDB code: 3EML) [44] with different docking algorithms and scoring functions (see Table 2.1). [61]

First of all, structures of protein and ligand were prepared using MOE. ZM241385 was built using the builder tool part of the MOE suite and was subjected to MMFF94x energy minimization until the rms of conjugate gradient was <0.05 kcal mol^{-1} Å^{-1}. The $hA_{2A}AR$ structure was prepared starting from the crystallographic structure and adding hydrogen atoms using the Protonate 3D methodology implemented in MOE.

Subsequently, ZM241385 was docked to the $hA_{2A}AR$ binding site with all the available docking softwares. Each docking was performed automatically to the binding site of the $hA_{2A}AR$ without any constraints and without the presence of water molecules. For all the different docking simulations, the center of the docking box or of the docking sphere was set in the same point (got from the experimental pose of ZM241385 inside the crystal structure of $hA_{2A}AR$) and the number of independent docking runs was set to 25.

Then, root mean square deviation (RMSD) values in Å between predicted and crystallographic poses of ZM241385 were calculated (see Table 2.1).

Docking Protocol	lowest RMSD (Å)	best pose RMSD (Å)	mean RMSD (Å)	no of poses with RMSD < 2.5 Å
MOE tabù search	1.61	3.35	5.65	4/25
MOE simulated annealing	2.17	4.36	6.47	1/25
MOE genetic algorithm	2.25	9.06	6.66	2/25
GOLD (goldscore)	0.63	1.95	1.2	25/25
GOLD (chemscore)	1.31	3.9	3.13	11/25
GOLD (asp)	0.61	4.96	1.5	23/25
GLIDE	0.79	2.71	6.82	7/25
PLANTS (chemplp)	0.93	1.98	6.96	3/25
PLANTS (plp)	0.84	1.93	6.7	6/25
PLANTS (plp95)	1.97	11.8	8.22	4/25

Table 2.1: Comparison of different docking protocols in reproducing the crystallographic pose of ZM241385 inside the $hA_{2A}AR$ binding pocket. In brackets different scoring functions for the same protocol are reported where available.

As shown in Table 2.1, for each docking result there is at least one pose in good agreement with the experimental binding mode (RMSD value < 2.5 Å). These poses with lowest RMSD value differ from the crystallographic pose of ZM241385 mainly for the position of the phenylethylamine chain, while the bicyclic triazolotriazine core is almost aligned. However, the mean RMSD value is quite high for the majority of the tested docking protocols except for GOLD. Docking performed with GOLD gives the lowest RMSD value, the lowest mean RMSD value and the highest number of poses with RMSD value < 2.5 Å. [61]

On the basis of these results, the software GOLD with the scoring function goldscore was selected to perform following docking studies of adenosine receptors antagonists. In Figure 2.1 the lowest RMSD pose and the best ranked pose of ZM241385 obtained with this protocol are displayed. From the comparison with the crystallographic pose of ZM241385, it is evident the good superimposition of the bicyclic triazolotriazine core that forms critical interactions with residues of the binding site. As expected, the position of the phenylethylamine chain in the two docking poses is different from the crystal, especially for the best ranked pose. In fact, this portion of the ligand does not form strong interactions with the binding site and is directed towards the extracellular environment; moreover, in an other crystal structure of the $hA_{2A}AR$ in complex with ZM241385 (PDB ID: 3PWH) [49] this chain is located in a different position and is directed towards TM1.

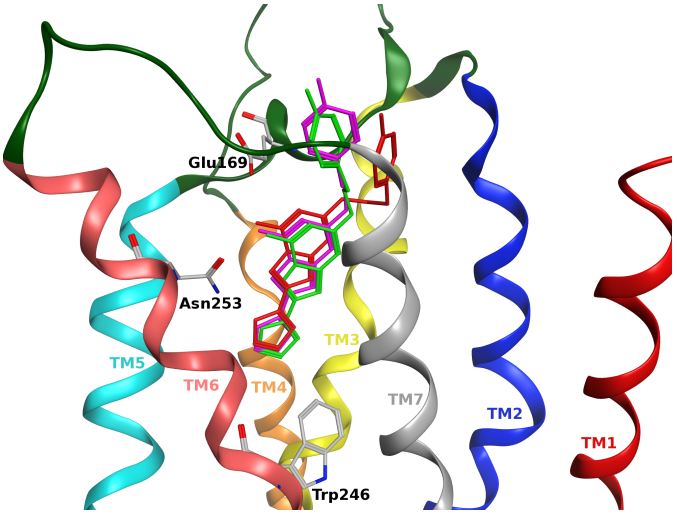

Figure 2.1: Comparison of crystallographic and docking poses of ZM241385 inside the $hA_{2A}AR$ binding pocket. Crystallographic pose of ZM241385 derived from 3EML crystal structure is shown in green; lowest RMSD pose of ZM241385 obtained with GOLD (goldscore) is shown in magenta; best ranked pose of ZM241385 obtained with GOLD (goldscore) is shown in red.

2.6.2 Molecular docking of adenosine receptors antagonists

In order to evaluate the binding modes of ARs antagonists and to rationalize their structure-affinity relationships and their selectivity profiles, molecular docking studies were performed at the previously built A_3AR model and at the $A_{2A}AR$ crystal structure (PDB ID: 3EML).

Ligand structures were built using the MOE-builder tool, part of the MOE suite, [51] and were subjected to MMFF94x energy minimization until the rms of conjugate gradient was <0.05 kcal mol^{-1} $Å^{-1}$. Charges were calculated using PM3/ESP methodology.

On the basis of the best docking protocol, previously selected, all antagonist structures were docked into the TM binding sites of the previously built hA_3AR model and of the $hA_{2A}AR$ crystal structure, by using the dock tool part of the GOLD suite. [53] Searching is conducted within a user-specified docking sphere, using the Genetic Algorithm protocol and the GoldScore scoring function. GOLD performs a user-specified number of independent docking runs (25 in our specific case) and writes the resulting conformations and their energies in a molecular database file.

The resulting docked complexes were subjected to MMFF94x energy minimization until the rms of the conjugate gradient was <0.1 kcal mol^{-1} $Å^{-1}$. Charges for the ligands were imported from the MOPAC output files using PM3/ESP methodology.

Prediction of the antagonist-receptor complex stability (in terms of corre-

sponding pKi value) and the quantitative analysis for nonbonded intermolecular interactions (H-bonds, transition metal, water bridges, hydrophobic, electrostatic) were calculated and visualized using several tools implemented in the MOE suite. [51]

To analyze in a more quantitative way the possible ligand- receptor recognition mechanism, the individual electrostatic (ΔE_{int}^{el}) and hydrophobic (ΔE_{int}^{hyd}) contributions to the interaction energy (ΔE_{int}) of each receptor residue have been calculated as implemented in the MOE suite. [51] To estimate the electrostatic contributions, atomic charges for the ligands were calculated using PM3/ESP methodology. Partial charges for protein amino acids were calculated on the basis of the AMBER99 force field. [56]

Chapter 3

Results and discussion

Contents

3.1 Human A_3AR homology model

The evolution of the field of computer-aided design of GPCR ligands, including A_3 agonists and antagonists, has depended on the availability of suitable molecular receptor templates. [23, 62]

Based on the assumption that GPCRs share similar overall topology, homology models of hA_3AR have been proposed by different groups. [62, 63, 8] In fact, all GPCRs have in common a central core domain consisting of seven transmembrane helices (TM1 to TM7) that are connected by three intracellular (IL1, IL2 and IL3) and three extracellular (EL1, EL2 and EL3) loops. Aside from sequence variation, GPCRs differ in the length and function of their N-terminal extracellular domain, their C-terminal intracellular domain

and their intra- and extracellular loops. Each of these domains provides very specific properties to these receptor proteins.

Homology models of the A_3AR have been helpful in providing structural hypothesis for the design of new ligands for this receptor. Many hA_3AR models, built using different templates, have been published describing the hypothetical interactions with known A_3AR ligands with different chemical scaffolds.

In 2008, the solved crystallographic structures of the hA_{2A}AR provided important structural information for the adenosine receptor family and for the contruction of hA_3AR models.

The availability and the selection of a suitable template structure is a critical step in the homology modeling process. Available GPCRs crystallographic structures are not so numerous and are summarized in section 2.2. The human A_{2A} adenosine receptor can be considered the best template for homology modeling of human A_3 adenosine receptor according to the percentages of identity of the aligned sequences (hA_3AR/hA_{2A}AR identity percentage $> 40\%$). The alignment, built following the most conserved residues in every helix, is displayed in Figure 3.1.

The identity percentage between the two AR subtypes is higher when considering only the transmembrane regions. However, there are some important differences between these two adenosine receptor subtypes that have to be considered while building homology models. [63] First of all, the sequence of hA_3AR consists of 318 amino acids, while the hA_{2A}AR sequence has 409 amino acids. The larger size of the hA_{2A}AR compared to the other human AR subtypes is related to its much longer carboxyl-terminal tail.

Moreover, loops constitute the most variable regions between different adenosine receptors. Among them, the second extracellular loop (EL2) is of great interest, while building homology models of GPCRs used for drug design, because of its possible role in ligand recognition process.

The crystallographic structure of hA_{2A}AR shows three disulfide bonds that involves EL2: one between Cys77 and Cys166, that is conserved among the members of family A of GPCRs and connects EL2 and TM3, and two between EL2 and EL1, that are unique to the hA_{2A}AR (Cys71-Cys159 and Cys74-Cys146). [44] This extensive disulfide bond network forms a rigid, open structure exposing the ligand binding cavity to solvent, possibly allowing free access for small molecule ligands.

In contrast, the sequences of hA_3AR present only one cysteine residue in the EL2 (Cys166) and this residue forms the disulfide bridge common to family A GPCRs with the respective cysteine of TM3 (Cys83). Then, no other disulfide bonds involving extracellular loops can be formed in the hA_3AR structure. [63]

So the presence of three disulfide links on EL2 is a peculiarity of human A_{2A}AR and the conformation of the hA_{2A}AR binding pocket is influenced by EL2 and is strictly dependent on these disulfide bonds; while, the confor-

Figure 3.1: Sequence alignment of hA_3AR and $hA_{2A}AR$. Conserved residues are identified by asterisks. In grey are highlighted the transmembrane regions, in red the highly conserved residues of family A GPCRs, and in yellow cysteines that forms disulfide bonds.

mation of EL2 and consequently of the binding pocket of the hA_3AR may be different from $hA_{2A}AR$.

Therefore, the use of the $A_{2A}AR$ as template for the homology modeling of other AR subtypes, and in particular of hA_3AR, is a powerful techniques but for some aspects is still imprecise. Especially, more efforts are necessary to elucidate the correct topological organization of the EL2 and its role in the recognition of both agonists and antagonists.

Keeping in mind these considerations, we built a homology model of the hA_3AR based on the crystal structure of the $hA_{2A}AR$ (PDB ID: 3EML), following the reported alignment and using the procedure detailed in section 2.5.1. As expected, the overall structure of the hA_3AR resulted to be really similar to the $hA_{2A}AR$ crystal structure with an RMSD between the alpha carbon atoms of 1.87 Å.

The high resolution three dimensional structure of human A_{2A} adenosine receptor elucidated the characteristic of this receptor subtype and clarified the role of the amino acids involved in antagonist binding. Next to the structural information provided by the crystallographic data, mutagenesis studies can help to identify the residues that are involved in ligand recognition.

It is interesting to compare the mutagenesis information available with the three dimensional information. Site-directed mutagenesis studies highlighted several residues important for antagonist binding at the A_{2A} adenosine receptor.

Mutagenesis studies have involved the TM3 domain and specifically the mutation of GlN^89 (3.37) with histidine or arginine. Experimentally the mutant clearly affects the antagonist binding. [64] At the same time, the investigation of EL2 revealed the important role of Glu169 and Glu151 whose mutations with alanine determine the loss of agonist and antagonist binding. [65]

Mutagenesis analysis of $A_{2A}AR$ anticipated the key role of TM5, TM6 and TM7 for agonist and antagonist interactions as successively confirmed by the $A_{2A}AR$ crystallographic structure. The substitution of Phe182 (5.43) with alanine determine the loss of agonist and antagonist binding. [66]

The important role of TM6 is supported by the fact that the mutations of His250 (6.52), Asn253 (6.55) and Phe257 (6.59) with alanine determine the loss of agonist and antagonist binding. [66] In the $A_{2A}AR$ crystal structure TM7 clearly plays a key role, accordingly to previously reported mutagenesis data; in fact the mutations of Ile274 (7.39), His278 (7.43) and Ser281 (7.46) with alanine determine the loss of agonist and antagonist binding. [66]

Therefore, many residues shown to be important for ligand binding in previously published mutagenesis studies, such as Glu169 (EL2), His250 (6.52), Asn253 (6.55) and Ile274 (7.39), were also shown to have important direct contacts with the bound ligand in the $A_{2A}AR$ crystal structure.

Very recently, some residues found to be important for the binding of ZM241385 in the crystal structure but for which no mutagenesis data has

been previously reported, namely Phe168 (5.29), Met177 (5.38), and Leu249 (6.51) were mutated. [67] The results of these mutagenesis studies confirm the critical role of Phe168(5.29) and Leu249(6.51) interactions with antagonists such as ZM241385 as observed in the crystal structure. In fact, the mutations of Phe168 (5.29) and Leu249 (6.51) with alanine lead to loss of antagonist binding while the mutation of Met177 (5.38) with alanine reduce the binding affinity of ZM241385. [67]

Moreover, considering a multiple sequence alignment of adenosine receptor subtypes, was noted that the lower trans-membrane part of the ZM241385-binding cavity, is highly conserved among adenosine subtypes, and the extracellular domains and upper part of the ZM241385 binding site are somewhat less conserved. [67] This observation suggests that the interactions that determine subtype selectivity reside in the more divergent "upper" region of the binding cavity.

Considering the human A_3AR, site-directed mutagenesis studies show an important role of TM3, TM5, TM6 and TM7 for interactions with both agonists and antagonists. [68, 69, 70, 71, 36, 72] The mutations of His95 (3.37), Met177 (5.38), Val178 (5.39), Ser271 (7.42), His272 (7.43) and Asn274 (7.45) with alanine determine a decrease of affinity of both agonists and antagonists in human A_3AR subtype. [68] The substitution of Asn250 (6.55) with alanine causes the loss of binding of agonists and antagonists. [71]

Antagonist binding is affected also by the substitutions of Thr94 (3.36), Lys152 (EL2), and Phe182 (5.43) with alanine. [68, 71] Finally, the mutation of Tpr243 (6.48), residue conserved among all four subtypes of adenosine receptors and a variety of other GPCRs, with alanine or phenylalanine determine a substantial decrease of antagonists affinity. [68, 71]

Therefore, as shown in Figure 3.2, the comparison of available mutagenesis data for amino acids affecting antagonist binding on hA_{2A} and hA_3 adenosine receptor subtypes shows that the binding pocket of hA_3 receptor can be slightly different from the one of hA_{2A} subtype. [35] More precisely, some residues whose site-directed mutagenesis affects antagonist binding at the hA_{2A} adenosine receptor, namely Phe168 (EL2), Leu249 (6.51) and Ile268 (7.39), are conserved at the corresponding positions in the hA_3 subtype. Therefore, although no mutagenesis data are available for these residues at the hA_3AR, they could be crucial for ligand binding also at this subtype.

Nevertheless, it can be noted that Glu169 (EL2), His250 (6.52) and Phe257 (6.59), whose mutation with alanine also affects antagonist binding at hA_{2A}AR are not present in the corresponding position of the hA_3 receptor, where these residues are replaced by Val169 (EL2), Ser247 (6.52) and Tyr254 (6.59) respectively. These particular amino acids could play a key role in determining the selectivity profile of adenosine antagonists. [35] In particular, the difference in position 169 of EL2 was supposed to influence not only the binding mode but also the entrance of ligands to the TM region of the receptors. [61]

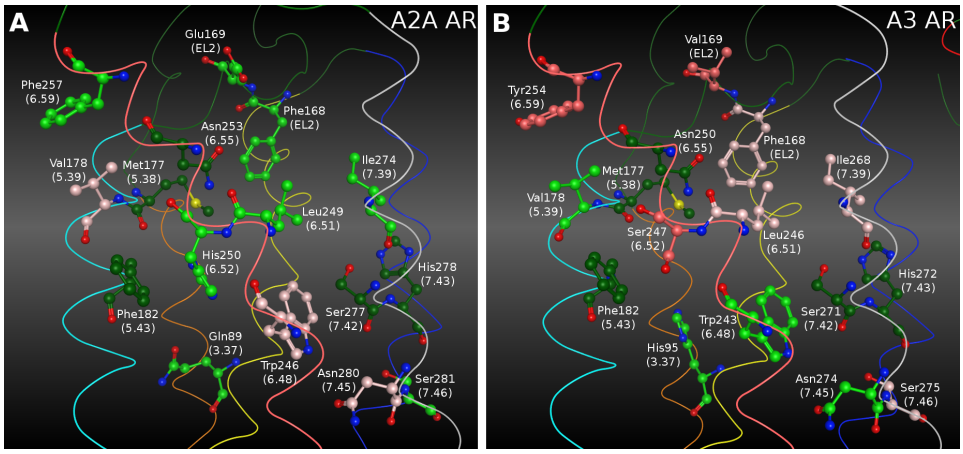

Figure 3.2: Comparison of available mutagenesis data for amino acids affecting antagonists binding on (A) hA_{2A} and (B) hA_3 adenosine receptor subtypes. Amino acids color legend: *light green*: mutagenesis data available for one subtype; *dark green*: mutagenesis data available for both subtypes; *light pink*: conserved residues whose mutagenesis data are available only for the other subtype; *dark pink*: not conserved residues whose mutagenesis data are available only for the other subtype.

In addition, the electrostatic potentials of amino acids present at the binding pocket entrance from the extracellular site are very different in the two receptors. In the hA_3AR model, the binding pocket gate is surrounded essentially by side chains of hydrophobic residues including Phe168 (EL2), Val169 (EL2), Ile253 (6.58), Val259 (EL3), Leu264 (7.35) (Figure 3.3, panel B). In the hA_{2A}AR crystal structure, there are ionic residues, such as Glu169 (EL2) and His264 (EL3) among the amino acids delimiting the binding site access (Figure 3.3, panel A). It was hypothesized that the presence of this charged gate may affect both the ligand orientation, while approaching the binding pocket, and its accommodation into the final TM binding cleft. [61]

All the structural and mutagenesis information, here described, resulted to be useful while considering the hA_3AR model for drug design approaches. In fact, the hA_3AR homology model built based on the hA_{2A}AR crystal structure has been used to rationalize the structure-activity relationship of new synthesized AR antagonists, analyzing their interactions inside the binding pocket and correlating them with their affinity and selectivity profile. The information obtained with these studies helped then the rational design of new ligands, as described in the following sections.

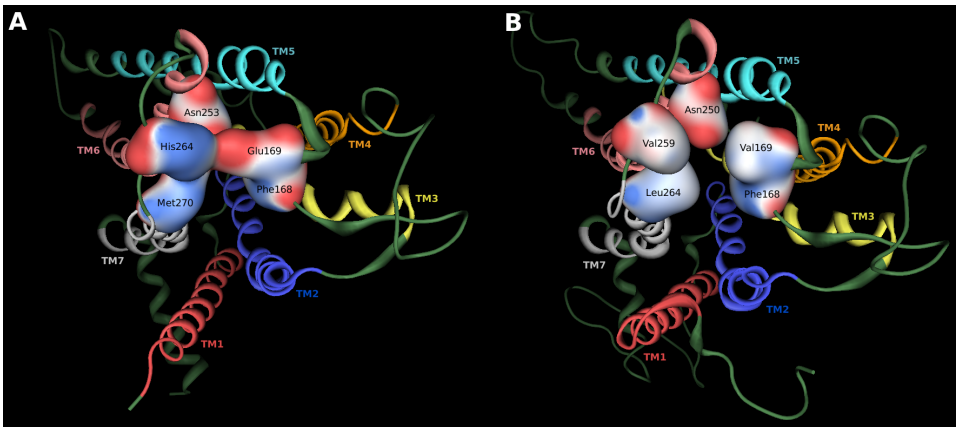

Figure 3.3: Access to the binding pocket of (A) $hA_{2A}AR$ and (B) hA_3AR. Receptors are viewed from the extracellular side. Gaussian surface of some important amino acids is displayed. Surface color shows a screened electrostatic potential (where scale parameters are as follows: red, -35 kcal/mol; white, 0 kcal/mol; blue, +35 kcal/mol).

3.2 Structure-based drug design approach

The discovery of new potent and selective adenosine receptors antagonists is important not only for their potential therapeutic applications but also because antagonists are preferred tools for the pharmacological characterization of receptors.

Starting from the actual knowledge about adenosine receptor ligands, a structure-based drug design approach has been applied to the development of new ARs antagonists.

In particular, the previously described hA_3AR model and the $hA_{2A}AR$ crystallographic structure have been used to rationalize the structure-affinity relationship profile of several classes of AR antagonists.

The molecular modeling work carried out during this project has been integrated with the work of synthetic and pharmacological groups.

In fact, all the compounds analyzed in this study have been synthesized thank to the collaboration of Prof. Spalluto group at the University of Trieste and Prof. Colotta group at the University of Firenze. Moreover, all the synthesized compounds have been tested to evaluate their binding affinity and potency towards the four adenosine receptor subtypes. Radioligands displacement tests and functional assays have been performed by several groups, including Dr. Jacobson group at NIH, Prof. Klotz group at the University of Würzburg and Prof Borea group at the University of Ferrara.

In general, binding affinities at the hA_1AR, $hA_{2A}AR$ and hA_3AR, expressed in dissociation constant values (K_i), were evaluated through the measurement of displacement of selective radioligands, which were previ-

ously bound to the receptors expressed at the cell surface. On the other hand, due to the lack of a suitable radioligand for the $hA_{2B}AR$ in binding assay, the potency of antagonists on the $hA_{2B}AR$, expressed in cells, was determined in adenylyl cyclase experiments through the measuring of the decrease of the cyclic adenosine monophosphate (cAMP) level.

A receptor-driven molecular modeling investigation has been performed in order to rationalize the results obtained from the pharmacological evaluation, in terms of both affinity at the hA_3AR and hA_3/hA_{2A} selectivity, so that the design of new AR antagonists can be guided. To that purpose, molecular docking simulations of all the newly synthesized derivatives were conducted on the previously described hA_3AR model and on the $hA_{2A}AR$ crystallographic structure.

Different drug design strategies can be applied to the optimization of existing ligands and to the development of new compounds, with improved properties. Figure 3.4 summarizes the various drug design approaches applied in the present study and described in the following sections. It has to be pointed out that each of the following sections refers to a published paper or to a manuscript in preparation, therefore compounds numbering in each section correspond to the numbering used in the paper.

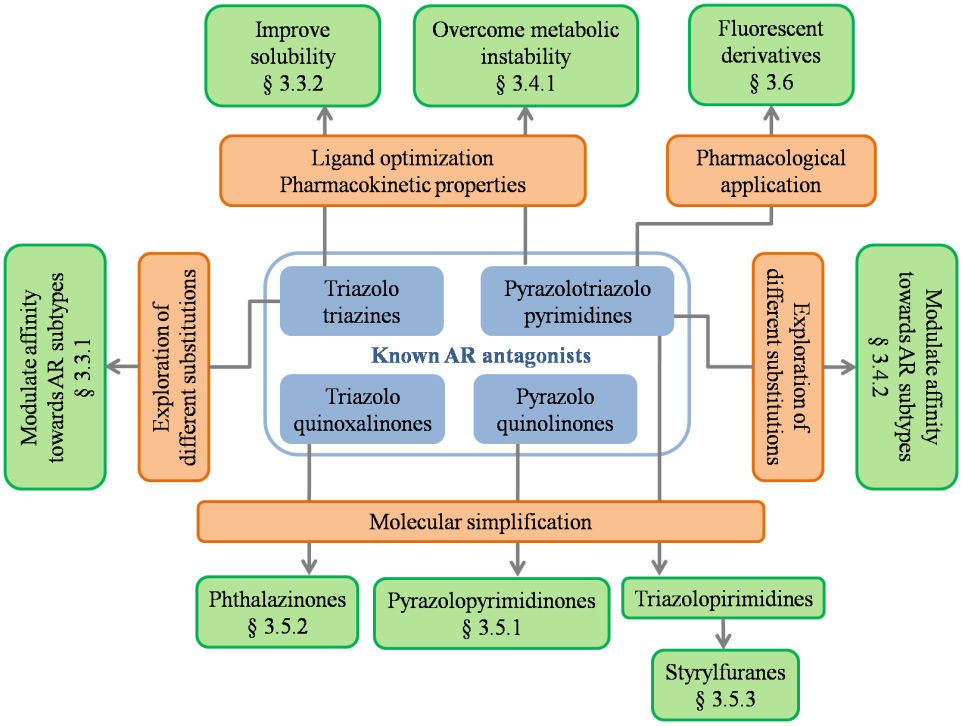

Figure 3.4: Structure-based drug design approaches applied for the development of new adenosine receptors antagonists.

Shortly, our study started from some classes of well known ARs antagonists such as triazolo-triazines, pyrazolo-triazolo-pyrimidines, triazolo-quinoxalinones and pyrazolo-quinolinones. All these scaffolds have been studied in recent years due to their antagonist activity against adenosine receptors. Therefore, in the present study different modifications of these compounds have been attempted in order to improve their pharmacokinetic and pharmacodynamic properties as well as to develop new compounds with different scaffolds.

In some cases, with the aim to modulate the affinity towards the AR subtypes and to develop more potent and selective antagonists, different substitution points on known scaffolds have been explored with the introduction of many substituents, such as for the triazolo-triazines (see section 3.3.1) [73] and the pyrazolo-triazolo-pyrimidines (see section 3.4.2). [74]

Another important aspect that has to be considered while developing potential drugs is the pharmacokinetic profile of the candidates. For this reason two different strategies have been adopted. On the one hand, the triazolo-triazine scaffold has been derivatized through the attachment of solubilizing group to enhance both aqueous solubility and physicochemical properties (see section 3.3.2). [75] While, on the other hand, the replacement of a furan ring with a substituted phenyl ring in the pyrazolo-triazolo-pyrimidine series allowed to overcome a point of metabolic instability while keeping a good pharmacological profile (see section 3.4.1). [76]

Many known AR antagonists possess complex heterocyclic structures that require difficult synthetic pathways with low yields. Therefore, molecular simplification approaches were applied to different AR antagonists scaffolds leading to more simple compounds with AR antagonist activity. In particular, pyrazolo-triazolo-pyrimidines were simplified to triazolo-pyrimidines and styril-furanes (see section 3.5.3); triazolo-quinoxalinones were simplified to phthalazinones (see section 3.5.2); [77] and pyrazolo-quinolinones were simplified to pyrazolo-pyrimidinones (see section 3.5.1). [61]

Finally, the pyrazolo-triazolo-pyrimidine scaffold was modified with the introduction of fluorophores in order to obtain fluorescent probes useful for the pharmacological characterization of adenosine receptors, such as *in vivo* localization, and as a safer and powerful alternative to radioligands in high throughput screenings (see section 3.6).

3.3 Triazolo-triazine derivatives

3.3.1 5,7-Disubstituted-triazolo-triazines

In the last 20 years intense medicinal chemical efforts led to the synthesis of a variety of AR agonists and antagonists for the pharmacological characterization of this family of G protein-coupled receptors. With respect to antagonists, several classes of heterocyclic derivatives have been reported as

AR antagonists with high levels of both affinity and selectivity. Among them, one of the most appealing bicyclic cores is represented by the triazolo-triazine nucleus, which led in the past to the discovery of ZM241385 (compound **3** in Figure 1.4) that could be considered as one of the most potent A_{2A}AR antagonists so far reported. [78, 79] In addition, ZM241385 also binds with good affinity at the human A_{2B}AR, and its tritiated form is suitable for use as a radioligand in binding studies at this receptor subtype. [80]

Taking into account previously reported triazolo-triazine compounds, we decided to better investigate the potential of modifying this nucleus at the C^5 and N^7 positions with the introduction of different substituents to obtain compounds **5-25**. [73] In particular, was previously seen that arylacetyl or arylcarbamoyl moieties at the N^7 position on the pyrazolo-triazolo-pyrimidine nucleus enhanced affinity at the A_{2B} and A_3ARs, respectively. [81, 82] Therefore similar substituents were inserted on the triazolo-triazine nucleus.

All the synthesized compounds have been fully characterized at the four ARs with the aim of better understand the structure-activity relationship (SAR) profile of this class of compounds and optimizing the substitution in order to modulate both AR affinity and selectivity.

Binding affinities at A_1, A_{2A} and A_3 adenosine receptors and IC_{50} at A_{2B}AR of all the newly synthesized 5,7-disubstituted- [1,2,4]triazolo[1,5-*a*][1,3,5]triazine (**5-25**) are reported in Table 3.1.

All the synthesized compounds showed affinities at the four ARs in the high nanomolar or micromolar range without significant levels of selectivity. The analysis of the data reported in Table 3.1, clearly indicates that in general, with the exception of compound **7**, compounds with a free amino group at the 7 position (**5** and **6**) showed good affinity at the A_{2A}AR (K_i range 18.3-96.5 nM) with quite significant levels of selectivity versus the other AR subtypes.

A significantly different selectivity profile could be noted when the amino group at the 7 position was substituted with an acyl group, and most importantly the affinities at the four AR subtypes seemed to be very sensitive to the substitution at both the 5 and 7 positions.

In particular, when a phenylacetyl moiety was introduced at the N^7 position (**9**, **15**, and **21**) the binding profiles of the derivatives were quite different with respect to the N^7-unsubstituted derivatives (**5**-**7**), and it was also significantly modified by the substitution at the 5 position. In fact, the presence of a methylthio (**9**) or phenoxy (**15**) group at the 5 position enhanced affinity at the A_{2A}AR (K_i range 136-429 nM), while the affinity at the other receptor subtypes was poor (K_i range 1-7 μM). In contrast, the presence of a dimethylamino group at the 5 position (**21**) reduced affinity (K_i range 1-7 μM) at all the ARs.

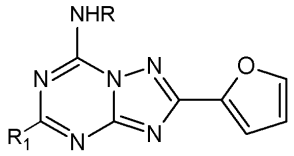

5-25

Compd	R_1	R	rA_1 (K_i, nM) or % displ. at 10 μM[a]	rA_{2A} (K_i, nM)[b]	hA_{2B} IC_{50} (nM)[c]	hA_3 (K_i, nM) or % displ. at 10 μM[d]
5	OPh	H	2,720 ± 680	18.3 ± 3.4	3,420 ± 200	489 ± 63
6	SCH_3	H	1730 ± 360	96.5 ± 36.1	14,900 ± 1,700	2580 ± 780
7	$N(CH_3)_2$	H	31,400 ± 8000	3800 ± 1230	33,700 ± 1,800	7270 ± 2230
8	SCH_3	$COCHPh_2$	557 ± 205	> 10,000	> 100,000	170 ± 45
9	SCH_3	$COCH_2Ph$	1420 ± 260	429 ± 38	> 100,000	4200 ± 950
10	SCH_3	$COCH_2$-Ph-4OCH_3	5000 ± 1170	1570 ± 660	42,400 ± 9,900	2100 ± 400
11	SCH_3	$CO(CH_2)4CH_3$	1520 ± 170	427 ± 96	> 100,000	24 ± 3%
12	SCH_3	CONHPh	10,000 ± 2900	1660 ± 1120	17,100 ± 2,700	414 ± 29
13	SCH_3	CONH-Ph-4CH_3	3440 ± 690	742 ± 194	16,800 ± 3,100	2200 ± 54
14	OPh	$COCHPh_2$	<10%	1880 ± 310	> 100,000	4400± 1150
15	OPh	$COCH_2Ph$	7260 ± 2820	136 ± 48	> 100,000	1020 ± 173
16	OPh	$COCH_2$4-OCH_3Ph	12 ± 2%	892 ± 252	> 100,000	5200± 1300
17	OPh	$CO(CH_2)4CH_3$	2900 ± 710	189 ± 26	> 100,000	2200± 470
18	OPh	CONHPh	17 ± 5%	38.9 ± 3.5	8,870 ± 1,680	633 ± 37
19	OPh	CONH-Ph-4CH_3	35 ± 5%	214 ± 72	20,000 ± 3,600	750 ± 130
20	$N(CH_3)_2$	$COCHPh_2$	951 ± 88	4090 ± 1360	> 100,000	473 ± 85
21	$N(CH_3)_2$	$COCH_2Ph$	6080 ± 1040	6700 ± 3200	> 100,000	1050 ± 466
22	$N(CH_3)_2$	$COCH_2$4-OCH_3Ph	8740 ± 590	10,300 ±1,300	> 100,000	2700 ± 345
23	$N(CH_3)_2$	$CO(CH_2)4CH_3$	1570 ± 380	> 10,000	> 100,000	2200 ± 370
24	$N(CH_3)_2$	CONHPh	3150 ± 550	580 ± 100	> 100,000	311 ± 122
25	$N(CH_3)_2$	CONH-Ph-4CH_3	2720 ± 830	2720 ± 2090	> 100,000	9600± 1200

[a] Displacement of specific [^{3}H]R-PIA binding (A_1) in rat brain membranes.
[b] Displacement of specific [^{3}H]CGS 21680 binding (A_{2A}) in rat striatal membranes.
[c] Measurement of adenylyl cyclase activity in CHO cells stably transfected with recombinant hA_{2B}AR, expressed as IC_{50} (lM).
[d] Displacement of specific [^{125}I]-I-AB-MECA binding at hA_3 receptors expressed in CHO cells. Data are expressed as K_i ± SEM in nM or as % of displacement at 10 μM (n = 3-6).

Table 3.1: Structures and binding profile of synthesized 5,7-disubstituted-triazolo-triazine compounds **5-25**.

When the phenylacetyl moiety at the N^7 was substituted at the *para* position with a methoxy group (**10**, **16**, and **22**), a general decrease of affinity versus all the ARs was observed in comparison to the unsubstituted derivatives (**9**, **15**, and **21**).

If a bulky arylacetyl moiety, such as diphenylacetyl, (**8**, **14**, and **20**) was introduced at the N^7 position, a completely different biological profile was evident. In fact, the presence of a bulky substituent at the N^7 position, combined with a methylthio (**8**) or dimethylamino (**20**) group at the 5 position, favored A_1 and A_3 ARs affinities (K_i range 170-950 nM). In contrast, the presence of a phenoxy group at the 5 position reduced affinity at all the ARs.

Different binding affinities were observed when an acyl chain was introduced at the N^7 position. In fact, a combination of an acyl chain at the N^7 position with a methylthio (**11**) or a phenoxy (**17**) groups at the 5 position afforded good affinity at the A_{2A}AR (K_i range 180-400 nM), while the affinities at the other AR subtypes were poor. However, the presence of a dimethylamino group at the 5 position (**23**) was detrimental to affinity at all the AR subtypes.

It was previously seen that the incorporation of an arylcarbamoyl moiety at the N^5 position of the pyrazolo-triazolo-pyrimidine nucleus enhanced hA_3AR affinity. In general, the affinity at the A_1AR was poor (K_i range from 3 μM to >10 μM) independent of the substitution at the 5 position (**12**, **13**, **18**, **19**, **24**, **25**). However, phenoxy (**18**, **19**) or dimethylamino (**24**) groups at the 5 position enhanced the affinity at the A_{2A} subtype (K_i range 39-580 nM).

Thus, most of these derivatives were nearly inactive at the hA_3AR, with the exception of compounds **12**, **18**, and **24**, which showed hA_3 affinity in the high nanomolar range (K_i range 311-633 nM) and were characterized by the presence of an unsubstituted phenylcarbamoyl moiety at the N^7 position, independently of the substitution at the N^5 position. The low affinity at the hA_3AR, was quite surprising considering that triazolo-triazine derivatives were simplified analogs of the pyrazolo-triazolo-pyrimidine antagonists of the hA_3AR. Nevertheless, a careful structural analysis of these two classes of compounds indicated that the dimethylamino group on the triazolo-triazine nucleus is not favored. In fact, the dimethylamino group seemed not to correspond to the N^8-methyl group of the PTP nucleus, but was similar to its N^7 pattern of substitution, which was extensively demonstrated to be inactive at the hA_3AR. [23, 83, 84]

Regarding the activity of this series at the hA_{2B}AR, most of these compounds were almost inactive at this receptor subtype. Only two compounds, bearing a phenoxy group at the 5 position (**5**, **18**), showed promising activity in the adenylyl cyclase assays at the A_{2B}AR, with an IC_{50} ranging from 3.4 to 8.8 μM. In particular, derivative **5**, which contained a free amino group at the 7 position, was the most potent at the hA_{2B}AR, and could represent a starting point for new non-xanthine hA_{2B}AR antagonists. Nevertheless,

the high affinity of this compound at the A_{2A}AR (K_i = 18.3 nM) clearly indicated that further investigation would be needed in order to delineate the activities at these two ARs.

A summary of the most relevant structure–activity features of the novel triazolo-triazine analogs has been reported in Figure 3.5.

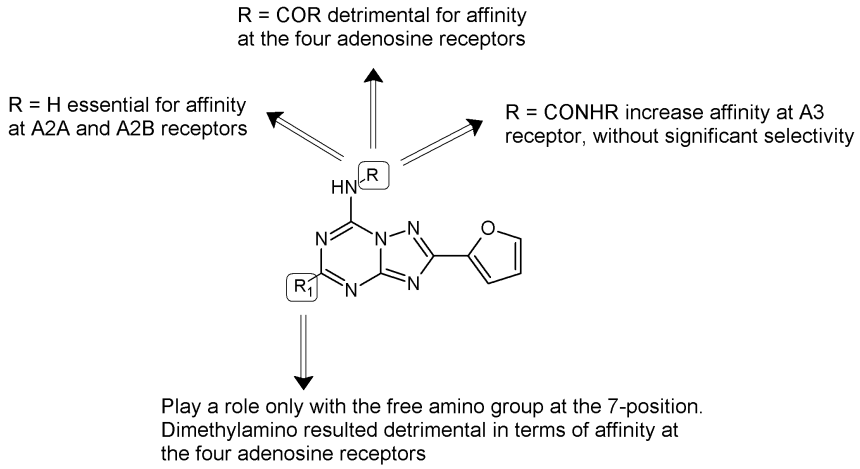

Figure 3.5: Summary of the most relevant SAR features of the novel 5,7-disubstituted-triazolo-triazine compounds.

From the data analysis it was very difficult to define a robust SAR profile of this new class of compounds. For this reason and with the aim to better understand these pharmacological results, docking studies of these derivatives have been performed in parallel at the A_{2A} and A_3 ARs. Therefore, we built models of the rA_{2A} and hA_3 receptors by homology modeling, using as template the crystal structure of hA_{2A} receptor (PDB code: 3EML).

Then, we performed docking studies to recognize the hypothetical binding motif of the newly synthesized 5,7-disubstituted-triazolo-triazine derivatives and we compared our docking results with the docking poses of the reference ligand ZM241385 at both receptors.

As shown in Figure 3.6, the binding mode of ZM241385 at the rA_{2A} receptor was similar to the crystallographic pose on the hA_{2A} receptor; this was consistent with the good binding affinity of ZM241385 at the two receptors. [85, 86] Consistently, all the residues belonging to the binding pocket are conserved in both receptors. From the analysis of docking of ZM241385 at the rA_{2A}AR, it appeared that the bicyclic triazolo-triazine core was anchored through an aromatic stacking interaction with Phe163 (EL2), an aliphatic hydrophobic interaction with Ile269 (7.39), and a hydrogen bonding interaction with Asn248 (6.55). The exocyclic amino group, linked to the bicyclic core of ZM241385, interacts with two polar residues, Asn248 (6.55) and Glu164 (EL2). The phenyl ring forms hydrophobic interactions with Pro262 (7.32)

and Met265 (7.35). The phenylethylamine substituent was directed towards the more solvent exposed extracellular region (EL2 and EL3) rather than towards the transmembrane domains of the receptor; while, the furan ring was located deep in the ligand binding cavity and directed towards TM5 and TM7; it forms hydrophobic interactions with the highly conserved Trp241 (6.48), an important residue in receptor activation, His245 (6.52) and Leu244 (6.51).

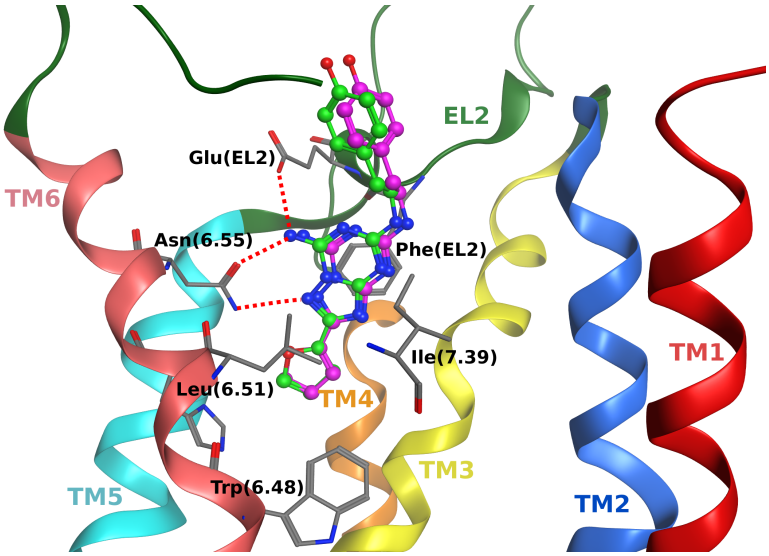

Figure 3.6: Structure superimposition of crystallographic pose of ZM241385 at the $hA_{2A}AR$ (in magenta) and docking pose of ZM241385 at the $rA_{2A}AR$(in green). Poses are viewed from the membrane side facing TM6, TM7, and TM1. The view of TM7 is partially omitted. Side chains of some amino acids important for ligand recognition and H-bonding interactions are highlighted. Hydrogen atoms are not displayed

The triazolo-triazine derivatives with a free amino group at the 7 position (**5**–**7**) showed a similar binding mode to ZM241385 inside the transmembrane region of the rA_{2A} receptor, as reported in Figure 3.7. In particular, the three H-bonding interactions with Asn248 (6.55) and Glu164 (EL2) were conserved.

Among these, compound **5** (K_i $rA_{2A}AR$ = 18.3 ± 3.4) was the most potent because the phenoxy group forms strong hydrophobic interactions with side chains of the following residues: Leu162 (EL2), Phe163 (EL2), Pro262 (7.32), Met265 (7.35), Tyr266 (7.36) and Ile269 (7.39).

The hydrogen bonding network with Asn248 (6.55) and Glu164 (EL2) seemed to be critical both for the recognition of these antagonist structures and for receptor selectivity versus hA_3. In particular, Glu164 (EL2) of rA_{2A} receptor subtype (Glu169 in hA_{2A}) was not present in the corresponding po-

sition of hA_3 receptor, where this amino acid was replaced by valine (Val169); in fact molecular docking results on hA_3 suggested that compounds **5**, **6** and **7** (Ki hA_3AR = 489 ± 63, 2580 ± 780, 7270 ± 2230, respectively) form only two (with Asn250) of the three hydrogen bonding interactions (data not shown).

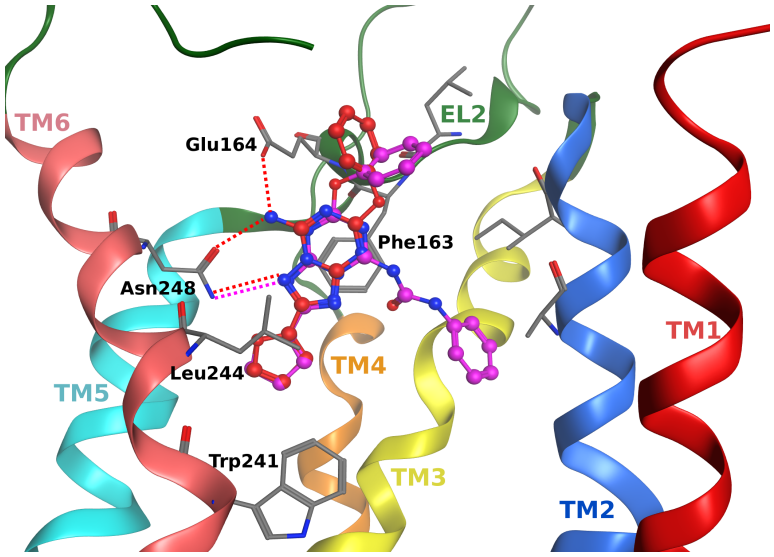

Figure 3.7: Structure superimposition of docked conformations of compound **5** (in red, K_i $rA_{2A}AR$ = 18.3 ± 3.4) and compound **18** (in magenta, K_i $rA_{2A}AR$ = 38.9 ± 3.5) inside the $rA_{2A}AR$ binding pocket. Poses are viewed from the membrane side facing TM6, TM7, and TM1. The view of TM7 is partially omitted. Side chains of some amino acids important for ligand recognition and H-bonding interactions are highlighted. Hydrogen atoms are not displayed.

Among other compounds (**8**–**25**) the most potent at the rA_{2A} receptor was derivative **18** (K_i $rA_{2A}AR$ = 38.9 ± 3.5). As shown in Figure 3.7, because of the presence of the phenylcarbamoyl moiety at N^7, the binding pose of compound **18** results to be quite different compared with the unsubstituted derivatives (ZM241385, **5**–**7**). In fact, the R substituent was directed towards TM2 and TM3 rather than towards TM5 and TM6 and was located in a hydrophobic pocket delimited by Ala56 (2.57), Ile57 (2.58), Phe59 (2.60), Ala60 (2.61), Ile63 (2.64), Phe77 (3.28), Ala78 (3.29), Phe80 (3.31) and Val81 (3.32). Nevertheless, compound **18** formed also the same hydrophobic interactions as compound **5** and ZM241385, but only one hydrogen bonding interaction with Asn248 (6.55). Moreover the bicyclic triazolo-triazine core of the disubstituted ligand was aligned with the same region of the other two compounds. At the hA_3 receptor, the presence of the less bulky side chain of Val169 (EL2) allowed the phenylcarbamoyl moiety of compound **18** to direct

towards TM5 and TM6 and so it lost the interactions with the residues of the hydrophobic pocket. Moreover, all the 5,7-disubstituted-triazolo-triazine derivatives were located deeper in the ligand binding cavity of hA_3; consequently they lost the π-π stacking interaction with Phe168 (EL2).

With respect to the R_1 moieties, the SAR at rA_{2A} was similar for compounds **8**–**25** and compounds **5**–**7**. It seemed that the presence of too bulky substituents at the N^7 position was not well tolerated because of unfavorable steric interactions.

To analyze in a more quantitative way the possible ligand–receptor recognition mechanism, the individual electrostatic and hydrophobic contributions to the interaction energy of each receptor residue has been calculated.

Analyzing the results of this study (collected in Figures 3.8 and 3.9) it was clear that, from the electrostatic point of view, two of the most critical residues affecting the affinity at ARs seem to be the asparagine 6.55 (Asn253 in hA_{2A}, Asn248 in rA_{2A} and Asn250 in hA_3) and the glutamic acid located within EL2 of both human and rat A_{2A} (Glu169 and Glu164, respectively) but mutated in valine in hA_3 (Val169). In particular, Asn 6.55 is responsible of two stabilizing interactions with ZM241385 in both human and rat A_{2A} and this is supported by the electrostatic contribution of around -13 kcal/mol to the whole interaction energy, in particular -9.5 kcal/mol in hA_{2A} and -17.9 kcal/mol in rA_{2A} (Figure 3.8).

In addition, the glutamic acid on EL2 can strongly interact through an additional hydrogen-bond with the exocyclic amino group of ZM241385 as supported by the stabilizing electrostatic contribution of around -13 kcal/mol to the whole interaction energy, in particular -9.0 kcal/mol in hA_{2A} and -17.6 kcal/mol in rA_{2A} (Figure 3.8). Consistently, this specific interaction is missing in hA_3.

Interestingly, compound **5** presents a very similar electrostatic energy contributions to ZM241385 supporting the hypothesis of a common TM binding motif. Conversely, compound **18** completely abolishes the capability to interact with both asparagine 6.55 and glutamic acid on EL2 due to the presence of phenylcarbamoyl moiety that forces the triazolo-triazine moiety to flip 180° (around its parallel TM axis) inside the TM binding cleft. However, the lack of these two stabilizing interactions seems to be balanced by the presence of several additional hydrophobic interactions as mapped in Figure 3.9. In fact, besides the three hydrophobic contributions mediated by the conserved phenylalanine on EL2 (Phe168 in hA_{2A}, Phe163 in rA_{2A} and Phe168 in hA_3), the leucine 6.51 (Leu249 in hA_{2A}, Leu244 in rA_{2A} and Leu246 in hA_3) and the tryptophan 6.48 (Trp246 in hA_{2A}, Trp241 in rA_{2A} and Trp243 in hA_3), the phenylcarbamoyl moiety at N^7 is surround by several hydrophobic side chains such as, for example for the rA_{2A}, Ala56 (2.57), Ile57 (2.58), Phe59 (2.60), Ala60 (2.61), Ile63 (2.64), Phe77 (3.28), Ala78 (3.29), Phe80 (3.31) and Val81 (3.32).

In conclusion, the docking studies of the new series of 5,7-disubstituted-

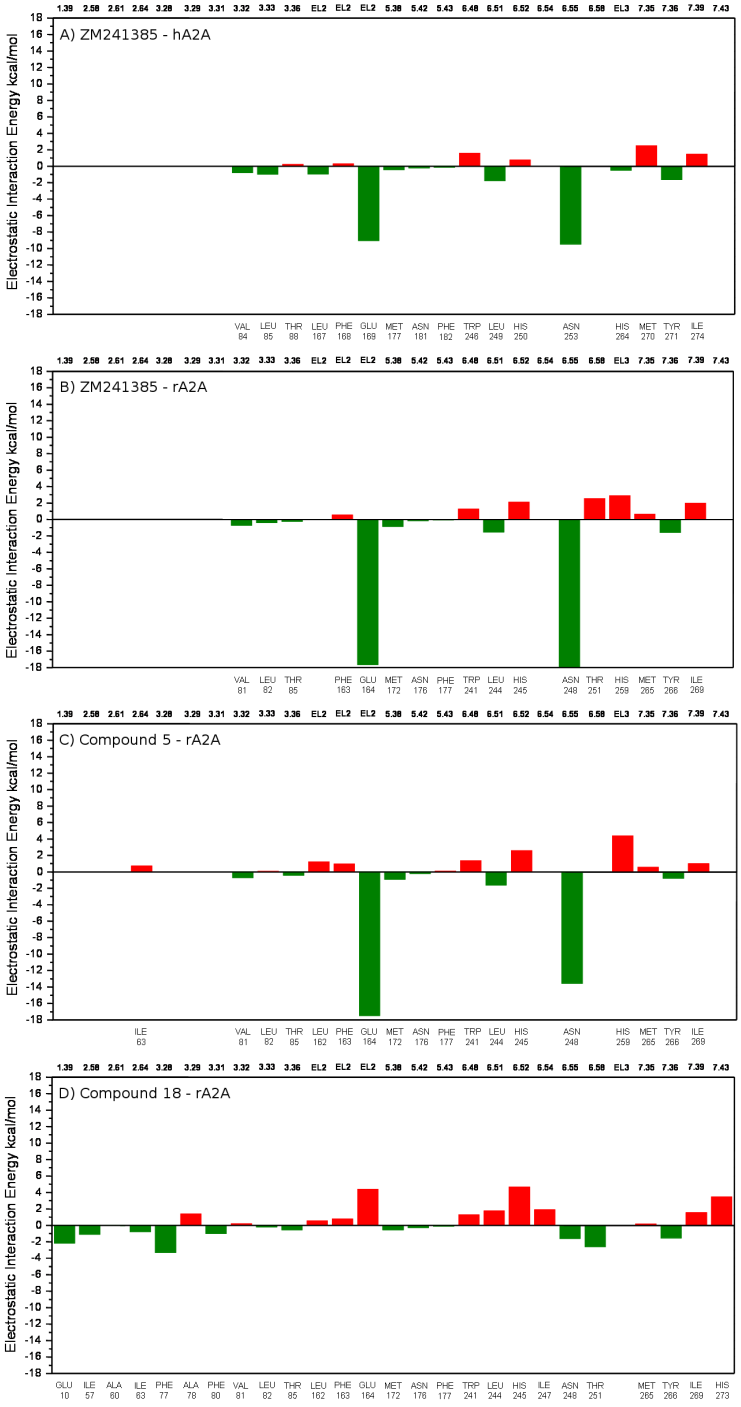

Figure 3.8: Electrostatic interaction energy (in kcal/mol) between the ligand and each single amino acid involved in ligand recognition calculated from: (A) crystallographic binding mode of ZM241385 inside the hA_{2A} receptor (PDB code: 3EML); (B) hypothetical binding mode of ZM241385 inside the rA_{2A} receptor obtained after docking simulations; (C) hypothetical binding mode of compound **5** inside the rA_{2A} receptor obtained after docking simulations; and (D) hypothetical binding mode of compound **18** inside the rA_{2A} receptor obtained after docking simulations.

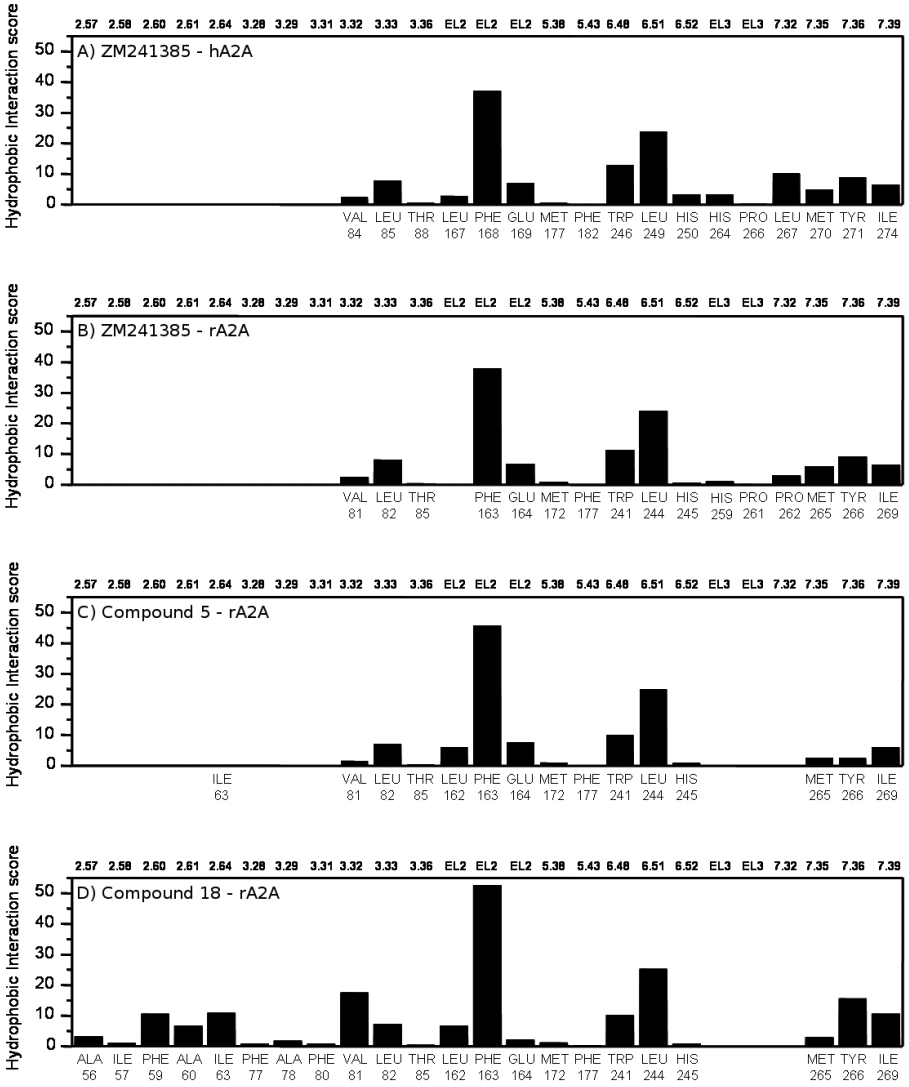

Figure 3.9: Hydrophobic interaction energy (in arbitrary hydrophobic unit) between the ligand and each single amino acid involved in ligand recognition calculated from: (A) crystallographic binding mode of ZM241385 inside the hA_{2A} receptor (PDB code: 3EML); (B) hypothetical binding mode of ZM241385 inside the rA_{2A} receptor obtained after docking simulations; (C) hypothetical binding mode of compound **5** inside the rA_{2A} receptor obtained after docking simulations; and (D) hypothetical binding mode of compound **18** inside the rA_{2A} receptor obtained after docking simulations.

[1,2,4]triazolo[1,5-*a*][1,3,5]triazine derivatives, permitted the formulation of very preliminary hypothesis, concerning the specific roles of a few crucial amino acids in affecting the molecular mechanism of both ligand-entering process and TM-recognition process for both A_{2A} and A_3 ARs. The $rA_{2A}AR$ and hA_3AR models, based on the recently published structure of the human A_{2A} receptor, provide a self-consistent framework that rationalizes the available SAR data.

3.3.2 Triazolo-triazines with improved water solubility

Most of the heterocyclic derivatives proposed as AR antagonists, suffered from limited aqueous solubility and difficulties in their synthetic preparation.

Considering the experimental observations derived from the previous study on the triazolo-triazine class, we decided to further investigate the potential of this nucleus, in particular, by exploring the C^5 position through the introduction of substituted amino or diamino functions (Figure 3.10), with the aim to modulate the activity at the A_{2A} and A_{2B} ARs and importantly to improve water solubility, which would otherwise limit their use as pharmacological tools.

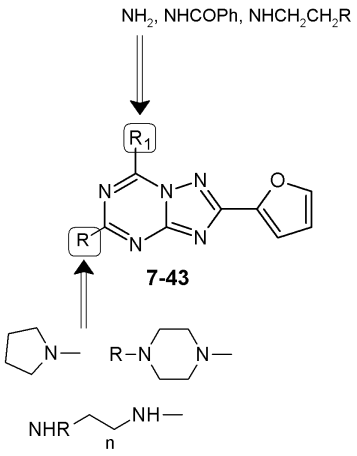

Figure 3.10: Designed and synthesized triazolo-triazine compounds **7-43**.

This new class of derivatives mainly contained a free amino group at the 7 position, but small substituents were introduced at this position in a few compounds. The synthesized analogues (**7-43**) have been evaluated for potency at all four hARs, and their receptor binding affinities or potency are reported in Table 3.2.

As clearly indicated in Table 3.2, all the analogues were in general nearly inactive at the hA_3AR independently of the substitution at the 5 and 7 positions, with the exception of compounds **10** and **29** having affinity in the range of 1 μM. A similar behavior, in contrast to expectations, could be

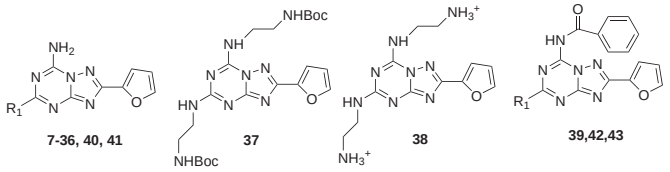

Compd	R_1	hA_1 % displ 10μM (or K_i, nM)[a]	hA_{2A} (K_i, nM)[b]	hA_{2B} IC_{50} (nM)[c]	hA_3 % displ 10μM (or K_i, nM)[d]
7	–N N–Boc	5400 ± 500	21 ± 4.5	>10,000	56.6 ± 1.3%
8	–N	1940 ± 70	59.1 ± 13.7	>30,000	75.0 ± 4.7%
9	–N NH_2^+	28.6 ± 6.0%	153 ± 32	>30,000	29.9 ± 0.4%
37	-	7.4 ± 4.5%	4360 ± 1670	>100,000	8490 ± 4810
10	$NH-(CH_2)_2NHBoc$	3730 ± 740	40.9 ± 5.7	>10,000	1490 ± 480
11	BocHN NH	3,890 ± 560	69.7 ± 12.7	7140 ± 2960	75.5 ± 0.3%
12	$NH-(CH_2)_3NHBoc$	344 ± 16	38.6 ± 11.5	20,600 ± 1100	77.3 ± 0.3%
13	$NH-(CH_2)_5NHBoc$	963 ± 139	44.7 ± 9.9	>10,000	68.6 ± 0.9%
14	$NH-(CH_2CH_2O)_2-(CH_2)_2NHBoc$	1580 ± 100	17.8 ± 6.7	>10,000	74.0 ± 0.8%
15	–N N–CH_2Ph	978 ± 146	20.6 ± 14.5	>30,000	71.9 ± 0.7%
16	–N N–CH_2-3Cl-Ph	1510 ± 500	51.8 ± 23.0	>30,000	52.7 ± 1.2%
17	–N N–CH_2-4F-Ph	655 ± 100	52.3 ± 32.3	>10,000	71.3 ± 1.9%
18	–N N–CH_2-4Cl-Ph	220 ± 88	102 ± 108	>30,000	66.8 ± 6.0%
19	–N N–CH_2-4Br-Ph	86.7 ± 22.6	27.3 ± 18.0	>10,000	49.8 ± 0.8%
20	$NH-(CH_2CH_2O)_2-(CH_2)_2NH_3^+$	769 ± 308	11.5 ± 2.2	>10,000	59.2 ± 2.6%
21	–N N–C(=O)–CH_2-4Br-Ph	1,010 ± 150	86.2 ± 41.4	>30,000	3100 ± 1100
22	–N N–C(=O)–$(CH_2)_3CH_3$	10.8 ± 5.3%	124 ± 50	>100,000	56.2 ± 8.1%
23	–N N–C(=O)–CH_2Ph	3510 ± 220	94.8 ± 40.7	>100,000	64.5 ± 1.8%
24	–N N–C(=O)–$(CH_2)_2$–C(=O)–OCH_3	19.4 ± 2.5%	66.2 ± 10.4	>100,000	37.2 ± 6.6%
25	–N N–C(=O)–$CHCl_2$	34.6 ± 1.5%	282 ± 164	>100,000	33.6 ± 0.7%
26	–N N–C(=O)–4-NO_2-Ph	35.5 ± 7.4%	212 ± 49	>100,000	50.9 ± 6.9%
27	–N N–C(=O)–Ph	27.7 ± 3.3%	348 ± 76	>100,000	22.6 ± 1.7%
28	–N N–C(=O)–α.naphthyl	4.9 ± 0.8%	7680 ± 2190	>100,000	31.1 ± 8.4%
29	–N N–C(=O)–CH_2-4Cl-Ph	991 ± 226	39.1 ± 13.9	>100,000	1260 ± 490
38	-	10.7 ± 1.5%	38,200 ±14,600	>100,000	17.7 ± 3.6%
30	$NH-(CH_2)_2NH_3^+$	35.8 ± 4.9%	567 ± 43	>100,000	30.8 ± 3.7%
31	$+H_3N$ NH	1350 ± 70	16.9 ± 2.3	10,700 ± 3,700	72.8 ± 0.4%
32	$NH-(CH_2)_3NH_3^+$	44.3 ± 1.6%	270 ± 9	>30,000	40.5 ± 0.2%
33	$NH-(CH_2)_5NH_3^+$	2,950 ± 260	90.1 ± 15.9	>10,000	49.9 ± 3.5%
34	–N N–C(=O)–CH-Ph_2	7470 ± 6820	92.9 ± 24.7	>100,000	40.6 ± 22.2%
35	–N N–C(=O)–$C(CH_3)_2$	38.7 ± 4.8%	58.4 ± 18.9	>100,000	32.3 ± 3.37%
36	–N N–C(=O)–CH_2-$C(CH_3)_3$	53.1 ± 4.7%	11.1 ± 6.3	>100,000	41.9 ± 8.3%
39	OPh	26.2 ± 5.5%	1000 ± 110	>10,000	32.3 ± 9.7%
40	OH	3110 ± 970	201 ± 61	>10,000	43.9 ± 6.0%
41	NH_2	1410 ± 80	160 ± 42	11,100 ± 3,900	36.4 ± 0.2%
42	OH	34.4 ± 9.2%	1750 ± 390	>100,000	75.9 ± 1.2%
43	NH_2	1800 ± 150	44.1 ± 13.6	7060 ± 2935	67.2 ± 3.3%

[a] Displacement of specific [^{3}H]DPCPX binding at the hA_1AR expressed in HEK-293 cells.
[b] Displacement of specific [^{3}H]ZM241385 binding at hA_{2A}AR expressed in HEK-293 cells. Data are expressed as K_i (SEM in nM (n = 3-6).
[c] Measurement of adenylyl cyclase activity in CHO cells stably transfected with recombinant hA_{2B}AR, expressed as IC_{50} (nM).
[d] Displacement of specific [^{125}I]I-AB-MECA binding at hA_3 receptors expressed in CHO cells. Data are expressed as K_i (SEM in nM (n = 3-6).

Table 3.2: Structures and binding profile of synthesized triazolo-triazine compounds **7-43**.

observed at the $hA_{2B}AR$; in fact all the analogues were inactive or poorly active (e.g., compounds **11**, **31**, **41**, **43**) in the functional assay. Nevertheless, the binding profile of this class of compounds at the $hA_{2A}AR$ demonstrated affinity in the nanomolar range with different degrees of selectivity versus the hA_1AR subtype.

Insertion at the C^5 position of amino or mono-Boc-diamino functionality (compounds **7**, **8**, **10-14**) led to compounds with good affinity at the $hA_{2A}AR$ (K_i range 18-70 nM) with variable selectivity versus the A_1AR. In particular, the presence of a pyrrolidine (**8**) at the 5 position favored affinity at the $A_{2A}AR$ (K_i = 59.1 nM) but poor selectivity (33-fold) versus the A_1 subtype, while introduction of Boc-piperidine (**7**) or Boc-ethylendiamine (**10**) improved both affinity and selectivity at the $A_{2A}AR$ (e.g compound **7**, K_i hA_{2A} = 21 nM, A_1/A_{2A} = 257). Interestingly, elongation of the diamino chain at the C^5 position to 3 or 5 carbon atoms (compounds **12**, **13**) led to derivatives which still retained good affinity at the $hA_{2A}AR$ but less selectivity versus the A_1 subtype (e.g., compound **13**, K_i hA_{2A} = 44.7nM, A_1/A_{2A} = 21.5), while longer chains such as a Boc-triethylenoxydiamino moiety (**14**) gave good results both in terms of affinity and selectivity (K_i hA_{2A} = 17.8 nM, A_1/A_{2A} = 89).

Trifluoroacetate salt derivatives (**9**, **30-33**) were in general less potent than the corresponding Boc derivatives (e.g., compound **7**, K_i hA_{2A} = 21 nM, A_1/A_{2A} = 257 versus compound **9**, K_i hA_{2A} = 153 nM, A_1/A_{2A} = 65). An exception occurred when long or bulky chains were present at the C^5 position. In fact, compounds **20** and **31** were more potent at the $hA_{2A}AR$ than the corresponding Boc derivatives (e.g., compound **31**, K_i hA_{2A} = 16.9 nM, A_1/A_{2A} = 79; compound **11**: K_i hA_{2A} = 69.7 nM, A_1/A_{2A} = 56), but most importantly both compounds were readily water-soluble up to 10 mM. In particular, compound **20**, which displayed an affinity at the $hA_{2A}AR$ of 11.5 nM and good selectivity versus A_1, was the most potent compound of this series. Despite this relevant improvement of the water solubility other pharmacokinetics properties, such as cell permeation or metabolic stability, are collecting in our laboratories before setting up any further in vivo testing.

Interestingly, double substitution with diamino functions at the C^5 and N^7 positions led to completely inactive compounds at all four AR subtypes, both as protected (**37**) or deprotected (**38**) forms.

An altered binding profile was observed for the piperazine derivatives alkylated or acylated at the piperazine secondary amine. In particular, in the N-benzyl series (**15-19**) good affinity at the $hA_{2A}AR$ was retained, but also an increased affinity at the hA_1 was observed with a consequent reduction of selectivity, independently of the type of substitution on the phenyl ring.

A more complex profile was observed when an acyl group was present on the piperazine secondary amine. In particular, when a benzoyl group was introduced on the piperazine nitrogen (**26**, **27**) a significant reduction of affinity at the $hA_{2A}AR$ (K_i range 212-348 nM) was observed with a sub-

sequent reduction of selectivity (35-48 fold). If the phenyl ring was replaced with a more bulky substituent such as a naphthyl nucleus (compound **28**), a complete loss of affinity at all four hARs was observed.

If the aroyl group was replaced with an aryl acetyl moiety, significant differences could be observed in the binding profile. In particular, introduction of a phenylacetyl (**23**) or a 4-substituted-phenylacetyl group (**21**, **29**) at the piperazine secondary amine led to compounds that still retained good affinity at the $hA_{2A}AR$ in the range of 40-95 nM with poor selectivity versus A_1 (12-37 fold). In contrast, introduction of a bulky substituent such as a diphenylacetyl moiety (**34**) provided a compound with a quite good affinity at the $hA_{2A}AR$ (K_i hA_{2A} = 93 nM). Importantly, the selectivity versus the hA_1 subtype (A_1/A_{2A} = 80) was high, which was exactly the opposite observed for the nearly inactive bulky aroyl derivative **28**.

A quite different profile could be observed when the piperazine secondary amine was acylated with alkyl groups. In particular, introduction of a small group (**25**) or unbranched chains (**22**, **24**) led to compounds which proved to be quite potent (K_i range 66-280 nM) at the $hA_{2A}AR$. Branched chains such as tert-butylcarbonyl (**35**) and 3,3-dimethylbutanoyl (**36**) increased the affinity at the $hA_{2A}AR$ and significantly increased selectivity versus the hA_1 subtype. In particular, derivative **36** showed high affinity at the $hA_{2A}AR$ (11.1 nM) and 900-fold selectivity versus the hA_1 subtype.

The derivatives substituted both at the C^5 and N^7 positions with small groups (**39**-**43**) showed in general weak affinity at the $hA_{2A}AR$ and low levels of selectivity. Moreover, the diamino compound **41** and the corresponding 5-hydroxy derivative **40** showed hA_{2A} affinity in the high nanomolar range (K_i range 160-200 nM), but the levels of selectivity versus the hA_1AR were very low, ranging from 2 to 12. When a benzoyl group was present at the N^7 position, the presence at the C^5 position of a hydroxy (**42**) or phenoxy (**39**) moiety greatly reduced activity at the four ARs, with affinity at the hA_{2A} subtype in the micromolar range. In contrast, when an amino group was present at the C^5 position, affinity at the $hA_{2A}AR$ (K_i hA_{2A} = 44.1 nM) was recovered with good levels of selectivity versus other receptor subtypes.

In order to rationalize the observed binding data, molecular docking simulations were performed for all the newly synthesized triazolo-triazines at both the crystallographic structure of $hA_{2A}AR$ and the hA_3AR model. Additionally, in order to analyze the possible ligand-receptor recognition mechanism in a more quantitative manner, we calculated the individual electrostatic and hydrophobic contributions to the interaction energy of each receptor residue involved in the binding with ligands. Using the calculated electrostatic and hydrophobic contributions values, color maps of electrostatic and hydrophobic interactions *per residue* were constructed.

The first important consideration is that almost all the selected poses at the $hA_{2A}AR$ of these new analogues showed some common features, as highlighted by the calculated electrostatic and hydrophobic contributions to

the interaction energy collected in Figure 3.11. In particular, all ligands made contacts mainly with residues belonging to TM2, TM3, TM6, TM7, and EL2.

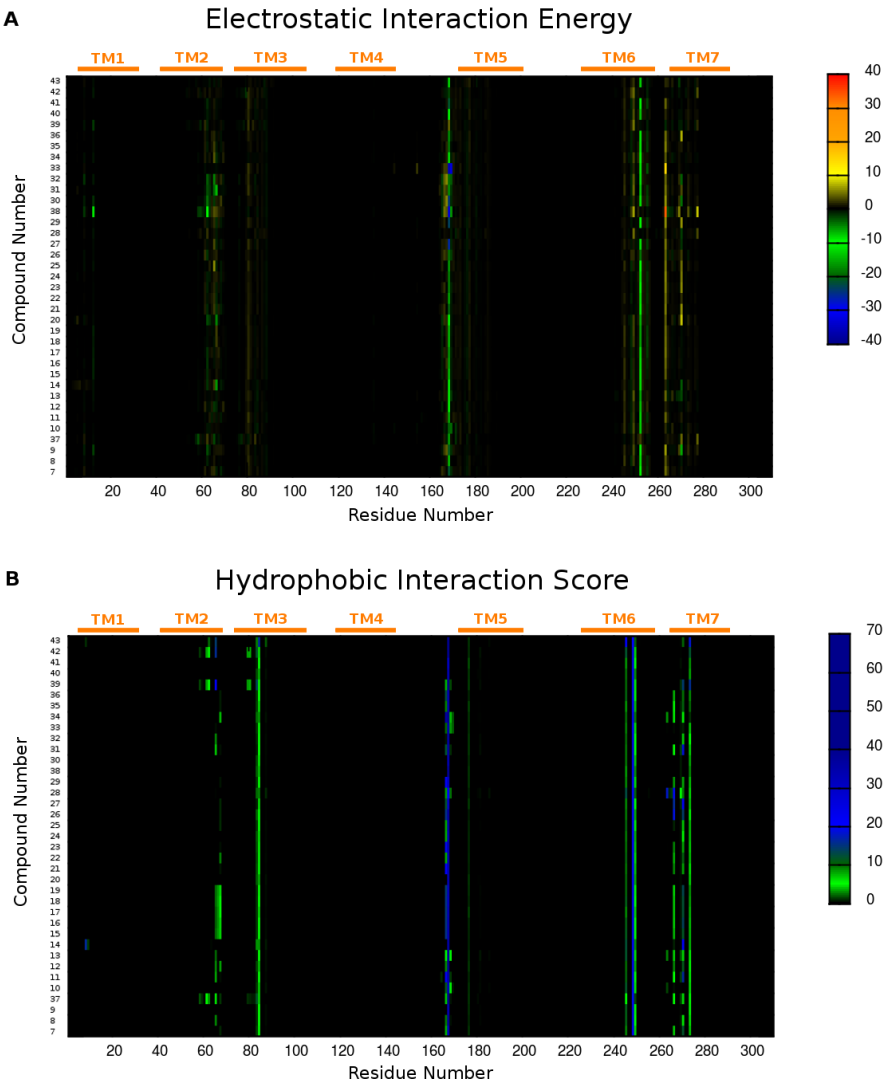

Figure 3.11: (A) *Per residue* electrostatic interaction energy map and (B) *per residue* hydrophobic interaction score map. The maps are calculated for a selected pose of each compound (**7**-**43**) inside the $hA_{2A}AR$ binding site. Electrostatic energy values are expressed in kcal/mol, while hydrophobic scores are expressed in arbitrary hydrophobic units (the higher the value, the stronger the interaction).

The *per residue* electrostatic interaction energy map (Figure 3.11, panel A) showed two bands with negative energy (colored in green) corresponding to Glu169 in EL2 and Asn253 in TM6, indicating that these two residues were responsible for the main electrostatic interactions with all the tested compounds, with a few exceptions. On the other hand, the map of the *per residue* hydrophobic interaction score (Figure 3.11, panel B) highlighted several residues involved in hydrophobic contacts with ligands, including Leu85 in TM3, Phe168 in EL2, Trp246, Leu249, His250 in TM6 and Tyr271, Ile274 in TM7. Therefore, the analysis of these maps gave important preliminary data concerning similarity and differences in the binding modes at the $hA_{2A}AR$ of these new compounds; this information was then confirmed by a detailed investigation of the docking poses as reported below.

Docking of 7-amino derivatives (Compounds **7**-**36**, **40**, and **41**):

From the docking simulation analysis, all the new derivatives with free amino group at the 7 position, with the exception of compound **28**, were seen to share a similar binding pose in the TM region of the $hA_{2A}AR$. For these compounds, ligand-recognition occurred in the upper region of the TM bundle, and the triazolo-triazine nucleus was surrounded by TMs 3, 5, 6, 7 with the 2-furyl ring located deep in the binding cavity.

Considering Figure 3.12, it is evident that the binding poses of these ligands were very similar to the crystallographic pose of ZM241385 bound to the $hA_{2A}AR$. [44] In fact, the triazolo-triazine cores were completely superposable, while the only slight difference was in the orientation of the substituents at the 5-position. Moreover, all the crucial interactions established by ZM241385 with amino acid residues of the hA_{2A} AR binding site were also found for all these new 7-amino derivatives.

The analysis in Figure 3.13 (panel A) showing the hypothetical binding pose of compound **36** (K_i hA_{2A} = 11.1 nM) at the $hA_{2A}AR$ helps to clarify this point. It appeared that the bicyclic triazolo-triazine core was anchored within the binding cleft through an aromatic stacking interaction with Phe168 (EL2) and a H-bonding interaction with Asn253 (6.55). Moreover, the exocyclic amino group at the 7 position of the bicyclic core interacted with two polar residues, Asn253 (6.55) and Glu169 (EL2), forming two H-bonds. Interestingly, the important role in ligand binding of these two residues was previously revealed by site-directed mutagenesis studies. [87, 88] The 4-(3,3-dimethylbutanoyl)-piperazinyl chain of the ligand was directed toward the more solvent-exposed extracellular region (EL2 and EL3) and interacted, through a H-bond, with Tyr271 (7.36). Moreover, the furan ring was located deep within the ligand binding cavity and formed hydrophobic interactions with the highly conserved Trp246 (6.48), an important residue in receptor activation. Finally, compound **36** also formed hydrophobic interactions with many residues of the binding site including Val84 (3.32),Leu85 (3.33), Met177 (5.38), Leu249 (6.51), and Ile274 (7.39).

Analyzing the *per residue* electrostatic contributions to the whole inter-

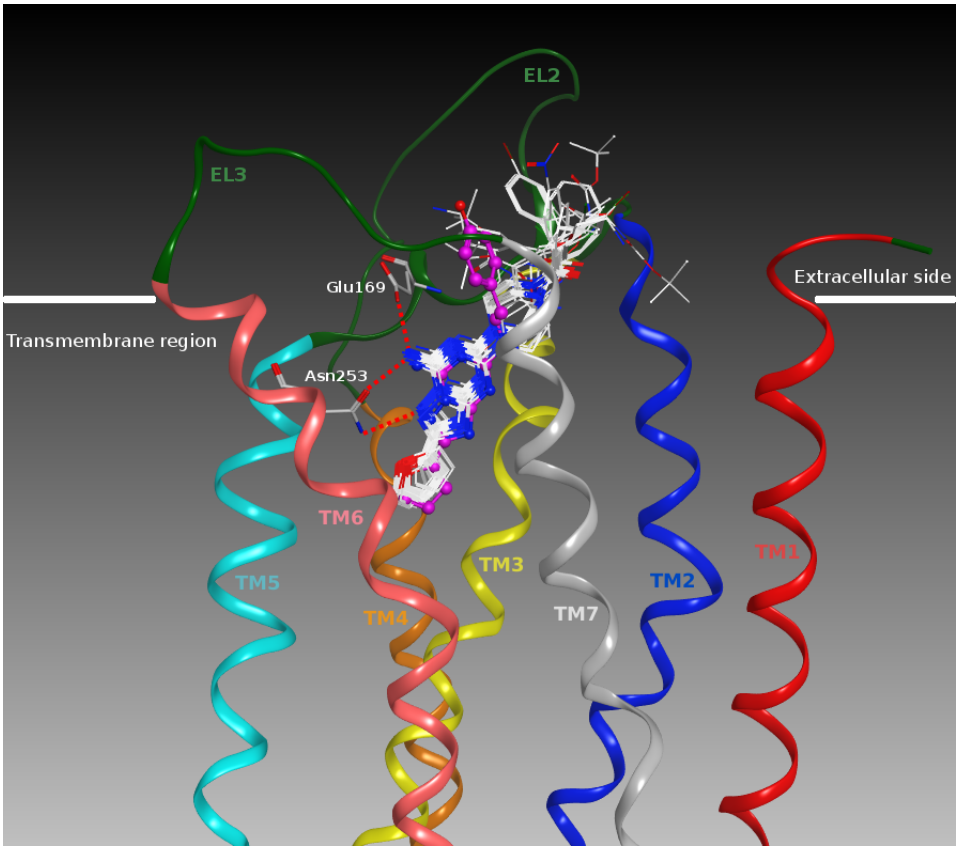

Figure 3.12: Structure superimposition of the crystallographic pose of ZM241385 (in magenta) and of the docking poses of all the 7-amino derivatives (in white) inside the $hA_{2A}AR$ binding site. Side chains of some amino acids important for ligand recognition and H-bonding interactions are highlighted. Hydrogen atoms are not displayed.

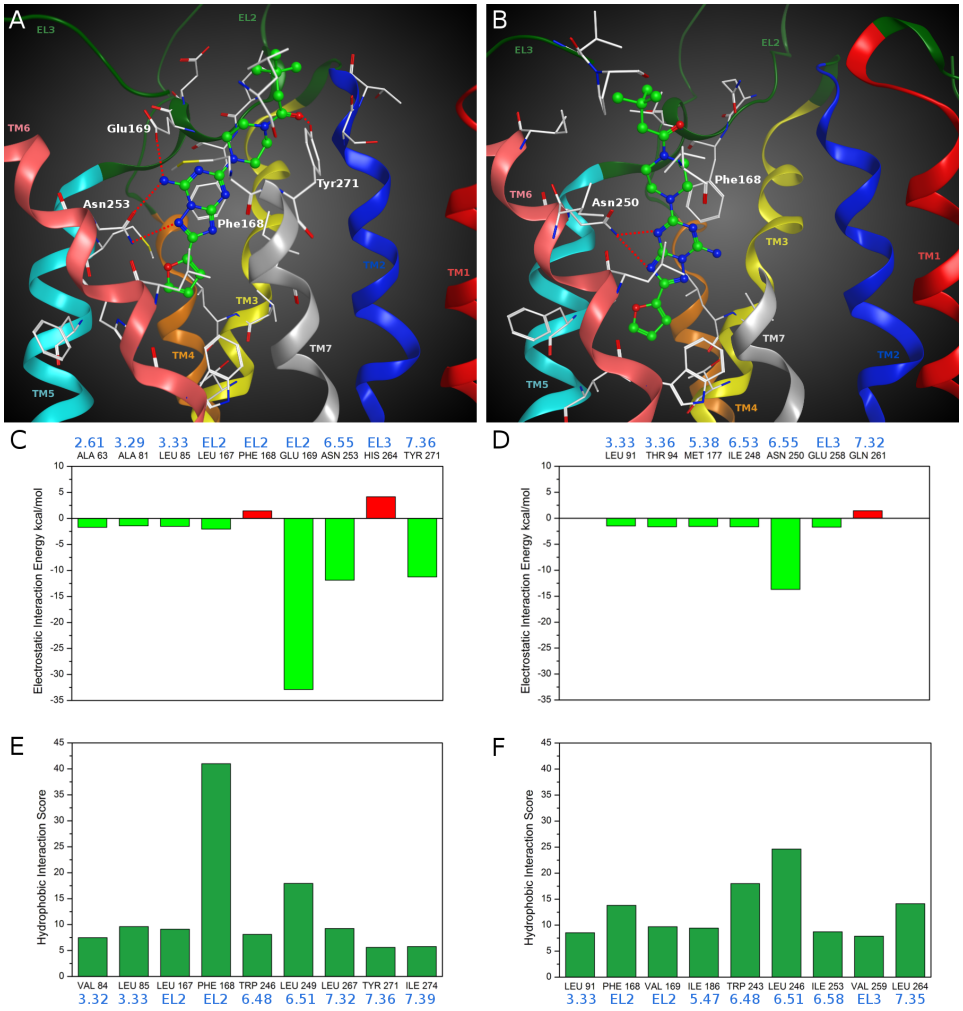

Figure 3.13: Hypothetical binding modes of compound **36** obtained after docking simulations: (A) inside the $hA_{2A}AR$ binding site; (B) inside the hA_3AR binding site. Poses are viewed from the membrane side facing TM6, TM7, and TM1. The view of TM7 is partially omitted. Side chains of some amino acids important for ligand recognition and H-bonding interactions are highlighted. Hydrogen atoms are not displayed. Electrostatic interaction energy (in kcal/mol) between the ligand and each single amino acid involved in ligand recognition observed from the hypothetical binding modes of compound **36** inside (C) $hA_{2A}AR$ and (D) hA_3AR binding sites. Hydrophobic interaction scores (in arbitrary hydrophobic units) between the ligand and each single amino acid involved in ligand recognition observed from the hypothetical binding modes of compound **36** inside (E) $hA_{2A}AR$ and (F) hA_3AR binding sites.

action energy for the compound **36**-hA_{2A}AR complex (Figure 3.13, panel C), the three main stabilizing factors were found to be related to Glu169 (EL2), Asn253 (6.55), and Tyr271 (7.36), due to the H-bonding interactions with the ligand above described; whereas, as shown in Figure 3.13 (panel E), the hydrophobic interaction scores pattern showed two strong stabilizing contributions corresponding to the interactions of the bicyclic core with Phe168 (EL2) and Leu249 (6.51).

Therefore, as exemplified by the binding pose of compound **36**, all the newly synthesized 7-amino derivatives strongly interacted with the hA_{2A}AR in a manner similar to the crystallographic pose of ZM241385. Moreover, these compounds, thanks to their different substituents at the 5 position, could variously interact with residues of the upper region of the receptor binding cavity, particularly in EL2 and EL3. Considering that the substituents at the 5 position were exposed to the highly plastic EL region and to solvent, it was difficult to define a clear SAR at the 5 position for this series.

On the other hand, the docking pose of compound **36** at the hA_3AR was located in the same region of the TM bundle as at the hA_{2A}AR, but the orientation of the ligand was different (Figure 3.13, panel B). In this case, the ligand formed only two H-bonds with Asn250 (6.55) and lost the aromatic interaction with Phe168 (EL2). The patterns of electrostatic and hydrophobic contribution to the energy of hA_3AR-ligand complexes (Figure 3.13, panels D and F) showed weaker *per residue* contributions compared to the ones at the hA_{2A}AR. Moreover, the residues present at the binding pocket entrance in the two AR subtypes possess very different features, which could affect both the orientation of the ligand while approaching the binding pocket and its accommodation into the final TM binding cleft, as already proposed for other compounds. [61] Therefore, both the lack of very strong interactions with the residues of the hA_3AR and the differences at the binding site entrance are consistent with a lack of hA_3 affinity observed for the 7-amino derivative.

Among the 7-amino derivatives, only compound **28** (K_i hA_{2A}=7680 nM) showed a different docking pose at the hA_{2A}AR (Figure 3.14). This ligand, probably due to the hindrance of the bulky and rigid R-naphthyl group, was not able to occupy the same position as the other 7-amino derivatives and consequently lost important H-bonding interactions with two critical residues of the hA_{2A}AR binding site, such as Glu169 (EL2) and Asn253 (6.55). In fact, in this docking pose the ligand formed only one H-bond with Tyr271 (7.36). This finding explained why compound **28** showed lower hA_{2A}AR affinity compared to the other 7-amino derivatives.

Docking of 7-(alkyl/acyl)amino derivatives (Compounds **37**-**39**, **42** and **43**):

With the exception of compound **43**, all the 7-(alkyl/acyl)amino derivatives showed low affinity for the hA_{2A}AR (micromolar range).

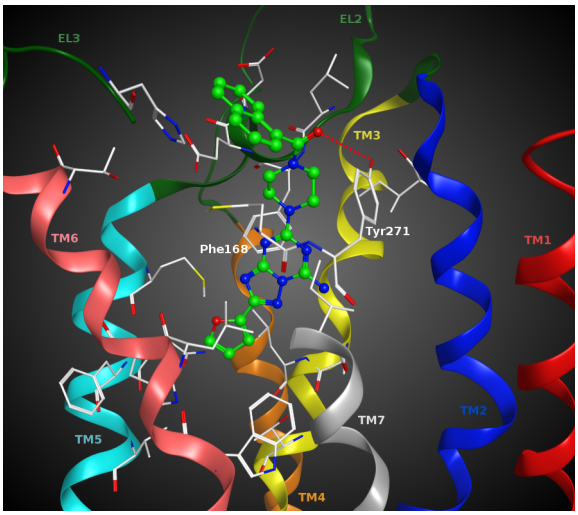

Figure 3.14: Hypothetical binding mode of compound **28** obtained after docking simulations inside the $hA_{2A}AR$ binding site. The pose is viewed from the membrane side facing TM6, TM7 and TM1. The view of TM7 is partially omitted. Side chains of some amino acids important for ligand recognition and H-bonding interactions are highlighted. Hydrogen atoms are not displayed.

Docking studies revealed that compounds **37-39** and **42** possessed a different binding mode at the $hA_{2A}AR$ compared to the 7-amino derivatives (Figure 3.15). In fact, the presence of an (alkyl/acyl)amino group at the 7 position prevented these compounds from forming a H-bonding network with Asn253 (6.55) and Glu169 (EL2), already seen to be critical for the binding of ZM241385 at this receptor subtype. This fact led these compounds to assume a different orientation inside the binding cavity of the receptor, although ligand recognition occurred in the same upper region of the TM bundle, and the triazolo-triazine nucleus was surrounded by TMs 3, 5, 6, 7 with the 2-furyl ring directed toward the inner part of the binding cavity. Therefore, their binding mode showed only a weak H-bond with Glu169 (EL2) and a stacking interaction with Phe168 (EL2). These findings were in agreement with the experimental data showing micromolar K_i values for these compounds.

In contrast to the 7-(alkyl/acyl)amino derivatives above described, compound **43** (K_i hA_{2A} = 44.1 nM), due to the presence of a free amino group at C^5, showed a characteristic mode of binding at the $hA_{2A}AR$ (Figure 3.16). The triazolo-triazine nucleus was oriented parallel to the membrane plane, and the 2-furyl ring was directed toward TM2, while the substituent at the 7 position was located in the inner part of the binding cavity. Compound **43** formed three H-bonding interactions, two with Asn253 (6.55) and one with

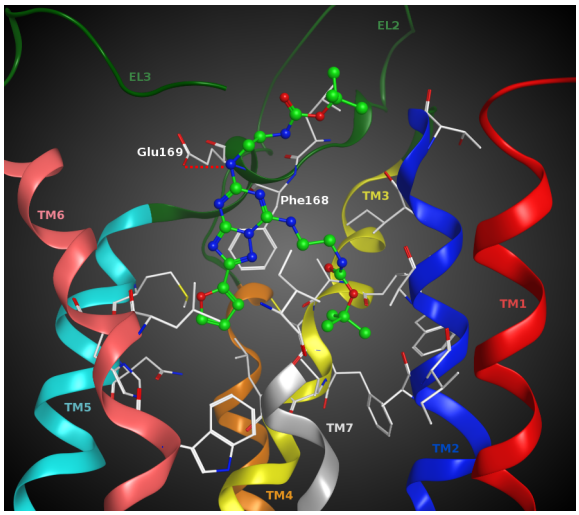

Figure 3.15: Hypothetical binding mode of compound **37** obtained after docking simulations inside the $hA_{2A}AR$ binding site. The pose is viewed from the membrane side facing TM6, TM7 and TM1. The view of TM7 is partially omitted. Side chains of some amino acids important for ligand recognition and H-bonding interactions are highlighted. Hydrogen atoms are not displayed.

Glu169 (EL2), and a π-π stacking interaction with Phe168 (EL2). Therefore, the presence of a H-bonding network with the residues of the $hA_{2A}AR$, similar to the one seen for the 7-amino derivatives, seemed to explain why compound **43**, among the 7-(alkyl/acyl)amino derivatives, is the only one that showed affinity at the $hA_{2A}AR$ in the nanomolar range.

In conclusion, we have identified new 1,2,4-triazolo[1,5-*a*]-1,3,5-triazine derivatives related to ZM241385, as promising $hA_{2A}AR$ antagonists with improved water solubility.

Molecular modeling results highlighted that all the newly synthesized 1,2,4-triazolo[1,5-*a*]-1,3,5-triazine derivatives with free amino group at the 7 position are characterized by a common binding mode very similar to the crystallographic one of ZM241385 bound to the $hA_{2A}AR$. From the docking simulations analysis, the presence of a free amino group seemed to be critical for the hA_{2A} affinity by allowing the ligands to participate in a H-bonding network with two critical residues of the binding site, Asn253 (6.55) and Glu169 (EL2). Another interaction found to be important for the hA_{2A} affinity of this series was the aromatic stacking between the triazole ring and Phe168 (EL2). On the contrary, substitution at the 7 position was detrimental for the affinity at the $hA_{2A}AR$, as confirmed also by the orientation of the 7-(alkyl/acyl)amino derivatives inside the binding cavity that led to the loss of the stabilizing hydrogen bonding network.

Among the most potent and selective novel compounds were a long-chain ether-containing amine congener **20** and its urethane-protected derivative **14**. N-Alkylated and N-acylated piperidine derivatives also displayed high affinity at the human A_{2A}AR, including an N-benzyl antagonist **19** and an N-3,3-dimethylbutanoyl derivative **36** that was roughly 900-fold selective versus both human A_1 and A_3ARs. Notably, compound **20** (K_i hA_{2A} = 11.5 nM) and a 5-(aminomethyl)cyclohexylmethyl-amino derivative **31** (K_i hA_{2A} = 16.9 nM) were readily water-soluble up to 10 mM, thus overcoming a common limitation of other bicyclic and tricyclic AR antagonists.

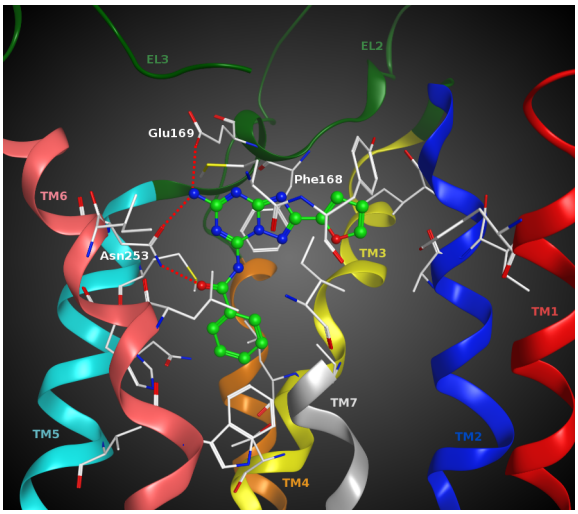

Figure 3.16: Hypothetical binding mode of compound **43** obtained after docking simulations inside the hA_{2A}AR binding site. The pose is viewed from the membrane side facing TM6, TM7 and TM1. The view of TM7 is partially omitted. Side chains of some amino acids important for ligand recognition and H-bonding interactions are highlighted. Hydrogen atoms are not displayed.

Thus, we have probed points of substitution for attachment of solubilizing groups to enhance the aqueous solubility of this class of triazolo-triazines, which are characterized by poor physicochemical properties. At the same time, potent interactions with the A_{2A}AR and, in some cases, receptor subtype selectivity have been maintained. We have used the A_{2A}AR X-ray structure to propose a structural basis for the activity and selectivity of this class of analogues and to direct the synthetic design strategy to provide access to solvent-exposed regions. In general, the strategy of grafting a terminal polar tail, which increases the polar surface area, can have a detrimental effect on bioavailability and ion channel activity. Therefore, it will be necessary to evaluate these molecules in further pharmacological testing to see if they will be useful for in vivo studies.

3.4 Pyrazolo-triazolo-pyrimidine derivatives

3.4.1 Overcome the metabolic instability

Among the several diverse structures that have demonstrated affinity at the hA_3 adenosine receptor, very interesting results have been obtained with the exploration of the pyrazolo-triazolo-pyrimidine (PTP) nucleus (**2**) (Figure 3.17). [89, 90] The PTP tricylic nucleus resembles the triazolo-quinoline core of non-selective antagonist CGS15943 (**1**), [91] except for the phenyl ring being replaced by a pyrazole, which has resulted in an increase of selectivity against other receptor subtypes. [92]

Further exploitation of substituents, mainly at positions N^8 and N^5 of such structure, [92, 82] has given rise to highly potent and moderately selective hA_3 antagonists. In particular, the combination of a methyl group at N^8 and a 4-pyridyl carbamoyl chain at N^5 has led to the most potent hA_3 antagonist ever synthesized. [93]

Conversely, substitution at position C^2 of the PTP tricyclic system has not been deeply explored, being essentially limited to the introduction of a furyl group. The furan ring has been considered as an essential structural requirement for the binding of antagonists at all the adenosine receptor subtypes, while its removal from the tricyclic system has been associated with an irreversible loss of affinity and selectivity, regardless of the receptor under investigation.

Baraldi and co-workers [94] have found that the substitution of the furan ring in PTPs with phenyl or alkoxyphenyl rings led to a loss of affinity at A_{2A}, A_{2B}, and A_3 receptors, while the A_1 subtype in some cases displayed a high nanomolar binding profile. Similarly, the functionalization of the furan ring with polar substituents resulted in completely inactive derivatives, clearly indicating that an unsubstituted furan ring at the C^2 position played a fundamental role in ligand-receptor recognition.

Notably, in most cases, substitution at the pyrazole ring occurred at the N^7 rather than at the N^8 position; hence, these compounds might not reflect the same binding profile as their N^8 analogues. This observation has triggered our interest to further investigate the effect of concurrent substitution of alkyl groups at N^8 position and a different moiety (other than furan ring) at the C^2 position of PTPs on the affinity at hA_3 receptor and selectivity over other adenosine receptor subtypes.

Interestingly, several reported hA_3 antagonists bearing tricyclic scaffolds (which are also structural resemblance of CGS15943 (**1**), including triazolo-quinoxalinones (**3**), [95, 96] pyrazolo-quinolines (**4**), [97] triazolo-pyrazinones (**5**), [98] and triazolo-benzotriazinones (**6**) [99] (Figure 3.17)), comprise a substituted phenyl moiety at the position equivalent to that of furan ring in PTP derivatives. From the structure-affinity relationship (SAR) studies of these derivatives, the presence of the phenyl ring seemed crucial to maintain

good affinity at hA_3 receptor.

In light of the beneficial effect of this phenyl ring toward the hA_3 affinity, the substitution of the C^2-furyl ring with an aryl group is therefore deemed feasible for the design and synthesis of new series of PTPs.

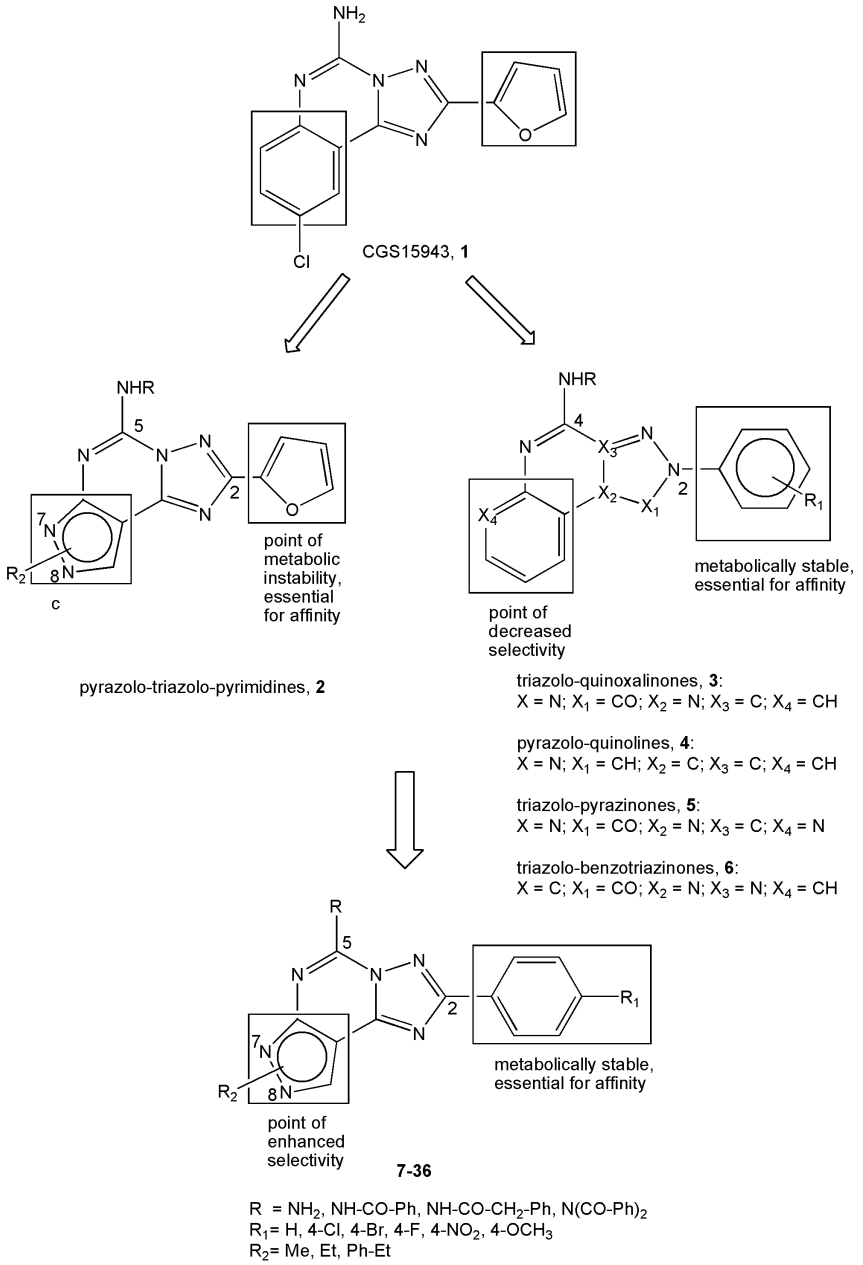

Figure 3.17: Rationale for the design of 2-(*para*-substituted)phenyl-pyrazolo-triazolo-pyrimidine derivatives

Moreover, from the pharmacokinetic aspect, several studies reported that drugs containing a furan in their chemical structure (e.g., prazosin and frusemide) were subjected to a metabolic cleavage of the furyl ring by the cytochrome P450 enzymes in the liver, resulting in remarkable hepatotoxicity in treated mice. [100, 101, 102] Some of these intermediate metabolites, for example epoxide groups and γ-keto-α,β-unsaturated aldehydes, were shown to be reactive and able to form adducts with cellular proteins or DNA, therefore causing unpredictable effects. Although these reactive metabolites can be detoxified by several enzymes in the body, this still poses some threat of toxicity and should be regarded as a safety issue.

On the other hand, metabolites derived from biotransformation of the phenyl ring through oxidation by CYP450 enzymes are expected to be relatively less reactive than those found in the metabolism of furan ring. Furthermore, the typical oxidation targeted at the *para*-position of the phenyl ring can be bypassed through the synthesis of *para*-substituted derivatives, leading to improvement of bioavailability of the new bioactive compounds.

Therefore, on the basis of potential structural and metabolic benefits of the C^2-aryl group in PTP derivatives, a novel structure-affinity relationship evaluation was conducted through the rational design and synthesis of a new series of pyrazolo-triazolo-pyrimidines bearing a (*para*-substituted)-phenyl ring at C^2, while maintaining either methyl or phenyl-ethyl groups at N^8 and a free amino, phenylacetamide or (bis-)benzamide at the N^5 position (compounds **7-36**).

The new series of 2-(*para*-substituted)phenyl-pyrazolo[4,3-*e*]1,2,4-triazolo-[1,5-*c*]-pyrimidines was successfully synthesized and characterized. Table 3.4 summarizes the receptor binding affinities of compounds **7-36** determined at the human A_1, A_{2A}, and A_3 receptors. Moreover, compounds were tested by measuring adenylyl cyclase activity in CHO cells which express the A_{2B} receptors and resulted to be completely inactive at this receptor subtype (K_i $>$ 10000 nM).

We introduced very little modifications in the pyrazole ring in order to focus our investigation on the exploitation at position C^2. In fact, only two compounds (compounds **13** and **17**, bearing a substituent at N^7 instead of N^8 were strategically included in the library to confirm the necessity to have a small alkyl group at N^8 for an optimal interaction with the hA_3 receptor subtype. For the rest of the derivatives, we fixed the methyl (compounds **7-12**), ethyl (compound **14**), and phenylethyl (compounds **15**, **16**, **18-20**) groups at N^8, with concurrent introduction of different moieties at positions C^2 and N^5 (compounds **21-36**).

The binding assays results showed that the new series of 2-aryl-pyrazolo-triazolo-pyrimidines presented good affinity at hA_3 receptors, as indicated by low nanomolar range of K_i values, and considerably improved selectivity toward the other AR subtypes (Table 3.4).

C^2 Position: To examine the impact of the furan ring substitution with

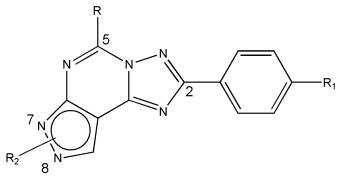

7-36

Compd	R	R_1	R_2	hA_1 (K_i nM)[a]	hA_{2A} (K_i nM)[b]	hA_3 (K_i nM)[c]
7	NH_2	H	N^8-CH_3	339 (319-359)	121 (100-147)	75 (63.1-90.4)
8	NH_2	F	N^8-CH_3	1,010 (815-1,240)	355 (307-409)	31.4 (26.9-36.6)
9	NH_2	Cl	N^8-CH_3	4,860 (3,360-7,010)	2,020 (1,060-3,840)	72.4 (71.3-73.6)
10	NH_2	Br	N^8-CH_3	2890 (2,230-3,730)	1500 (1,370-1,640)	38.6 (35.9-41.5)
11	NH_2	OCH_3	N^8-CH_3	9730 (7,740-12,200)	1,190 (1,050-1,340)	16.7 (9.80-28.3)
12	NH_2	NO_2	N^8-CH_3	>300,000	9,650 (5,490-16,900)	655 (563-763)
13	NH_2	Cl	N^7-CH_2-CH_3	121 (94.9-154)	83.8 (42.3-166)	565 (518-615)
14	NH_2	Cl	N^8-CH_2-CH_3	1,570 (1,350-1,820)	843 (566-1,260)	68.7 (52.9-89.3)
15	NH_2	H	N^8-CH_2-CH_2-Ph	74.8 (51.9-108)	196 (121-317)	76.7 (59.5-99.0)
16	NH_2	F	N^8-CH_2-CH_2-Ph	39.1 (31.9-47.9)	127 (106-151)	50.6 (32.9-78.0)
17	NH_2	Cl	N^7-CH_2-CH_2-Ph	> 100,000	5,970 (4,090-8,720)	> 30,000
18	NH_2	Cl	N^8-CH_2-CH_2-Ph	204 (159-262)	2,180 (1400-3,410)	79.7 (67.9-93.6)
19	NH_2	Br	N^8- CH_2-CH_2-Ph	498 (327-758)	>30,000	221 (152-320)
20	NH_2	OCH_3	N^8-CH_2-CH_2-Ph	289 (232-359)	1,400 (895-2,210)	25 (17.5-35.6)
21	NH-COPh	H	N^8-CH_3	622 (498-779)	324 (265-396)	5 (2.93-5.56)
22	NH-COPh	F	N^8-CH_3	2,530 (1,550-4,120)	>100,000	3.43 (1.97-5.98)
23	NH-COPh	Cl	N^8-CH_3	>30,000	>100,000	2.82 (2.24-3.56)
24	NH-COPh	Br	N^8-CH_3	>30,000	>100,000	5.24 (4.16-6.60)
25	NH-COPh	OCH_3	N^8-CH_3	>30,000	>100,000	2.1 (1.37-3.24)
26	NH-COPh	NO_2	N^8-CH_3	>30,000	>100,000	56.4 (43.5-73.0)
27	N(CO-Ph)$_2$	OCH_3	N^8-CH_3	> 10,000	> 10,000	6.88 (3.94-12.0)
28	N(CO-Ph)$_2$	Cl	N^8-CH_3	> 10,000	> 10,000	6.94 (4.58-10.5)
29	NH-COPh	H	N^8-CH_2-CH_2-Ph	313 (209-468)	963 (749-1,240)	23.9 (20.3-28.1)
30	NH-COPh	Br	N^8-CH_2-CH_2-Ph	270 (191-382)	>100,000	153 (120-195)
31	NH-$COCH_2$Ph	H	N^8-CH_3	562 (446-706)	778 (554-1,090)	0.108 (0.089-0.131)
32	NH-$COCH_2$Ph	F	N^8-CH_3	2,290 (1,780-2,930)	2,540 (1,590-4,060)	0.201 (0.175-0.230)
33	NH-$COCH_2$Ph	Cl	N^8-CH_3	4,850 (3,680-6,400)	8,320 (6,180-11,200)	0.248 (0.211-0.292)
34	NH-$COCH_2$Ph	Br	N^8-CH_3	24,400 (13,900-42,900)	>100,000	0.345 (0.313-0.381)
35	NH-$COCH_2$Ph	OCH_3	N^8-CH_3	>30,000	>100,000	0.241 (0.214-0.272)
36	NH-$COCH_2$Ph	NO_2	N^8-CH_3	23,200 (9,620-55,700)	23,900 (15,300-37,500)	0.624 (0.529-0.735)

[a] Displacement of specific [^{3}H]-CCPA binding at human A_1 receptors expressed in CHO cells, (n = 3-6).
[b] Displacement of specific [^{3}H]-NECA binding at human A_{2A} receptors expressed in CHO cells, (n = 3-6).
[c] Displacement of specific [^{3}H]-NECA binding at human A_3 receptors expressed in CHO cells, (n = 3-6). Data are expressed as geometric means, with 95% confidence limits.

Table 3.4: Binding affinity (K_i) at the four human adenosine receptors of the new 2-aryl-pyrazolo-triazolo-pyrimidines.

a phenyl ring at C^2 position toward the pharmacological profile, we compared the binding assays results of some previously reported compounds bearing the 2-furyl (e.g., compounds **90** and **91**) (Table 3.5) [103, 92] and of new compounds bearing the 2-aryl (e.g., compounds **7** and **31**).

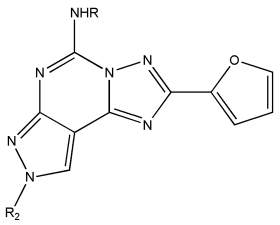

90, 91

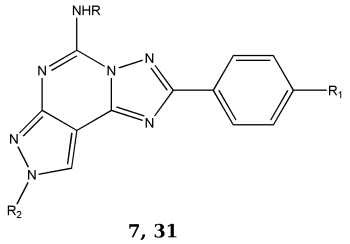

7, 31

Compd	**R**	**R_1**	**R_2**	**hA_3 (K_i nM)**	**hA_1/hA_3**	**hA_{2A}/hA_3**
90[a]	H		CH_3	300	0.33	0.009
7	H	H	CH_3	75	4.52	1.61
91[a]	Ph-CH_2CO		CH_3	0.81	867	522
31	Ph-CH_2CO	H	CH_3	0.108	5204	7204

[a] Data taken from references [92] and [103].

Table 3.5: Binding affinity (K_i) at hA_3 receptor and selectivity against hA_1 and hA_{2A} receptors for some 2-aryl and 2-furyl pyrazolo-triazolo-pyrimidines (compounds **90**, **91** and **7**, **31**).

It was observed that the bioisosteric replacement of existing furan ring with a phenyl ring resulted in a 3-7-fold increase in affinity toward the hA_3 receptor and significant improvement in selectivity (of 2-3 order of magnitude) over other adenosine receptor subtypes, namely hA_1, hA_{2A}, and hA_{2B} receptors. In other words, compounds with a phenyl ring at 2-position have demonstrated better affinity and selectivity profiles toward hA_3 receptor as compared to the 2-furyl counterparts, indicating that the aryl group at C^2 position played a more essential role on the antagonistic activity at the hA_3 receptor.

The substituents (e.g., Cl, F, Br, OCH_3, NO_2) at the *para* position of the C^2-phenyl ring were found to modulate the affinity at hA_3AR to a certain extent. In particular, among the substituents introduced at the *para* position of phenyl ring, both the OCH_3 and F groups have exerted relatively more favorable effect on the affinity at hA_3 receptor in all the N^5-unsubstituted (e.g., compound **11**, K_i hA_3 = 16.7 nM), N^5-benzamide-substituted (e.g., compound **25**, K_i hA_3 = 2.1 nM) and N^5-phenylacetamide substituted (e.g., compound **35**, K_i hA_3 = 0.241 nM) derivatives. Interestingly, although all the compounds with a 4-bromo group in the N^8-methyl series showed good affinity at the hA_3 receptor (e.g., compound **34**, K_i hA_3 = 0.345 nM), its presence in the N^8-phenylethyl-substituted derivatives (e.g., compound **30**,

K_i hA_3=153 nM) caused the opposite effect to the affinity at hA_3 receptor. This could be possibly due to the additional steric hindrance caused by the phenylethyl group, which further limited the accommodation of relatively bulky bromo group within the binding site, resulting in detrimental effect on the hA_3 affinity.

Besides that, it was observed that some N^8-methyl-substituted compounds bearing a 2-(*para*-nitro)phenyl ring (e.g., compound **12**, K_i hA_3 = 655 nM) have acquired hA_3 affinity in relatively high nanomolar range. Similarly, compound **26** (with a 2-(*para*-nitro) phenyl ring, a methyl at N^8 and a benzamide at N^5) only demonstrated moderate affinity at hA_3 receptor (K_i hA_3 = 56.4 nM) in comparison to the other derivatives with different substituents at C^2 position (compounds **22-25**), which have shown a better hA_3 affinity profile (K_i range 2-5 nM). These observations could again be attributed to the steric constraint of the relatively bigger NO_2 group as compared to other substituents. This rendered the nitro group unable to bind firmly onto the binding cavity, thus affecting the affinity at the hA_3 receptor. Therefore, because the nitro group might not be a suitable substituent at this position, it was excluded from the subsequent series of N^8-phenylethyl derivatives.

N^5 Position: From the binding assays results, it was observed that the absence of any substituent at N^5 position (such as in compounds **7-20**) did not allow good discrimination among the adenosine receptor subtypes, except for the hA_{2B} receptor. In other words, the free amino group at N^5 not only bound to the hA_3 receptor but it also showed good interaction at both hA_1 and hA_{2A} receptors. This observation was consistent with previous SAR studies, which indicated high affinity at both hA_1 and hA_{2A} receptors in N^5-unsubstituted derivatives. [92]

In fact, further incorporation of substituents at the N^5 position (as shown in compounds **21-36**) enabled a shift of affinity toward the hA_3 subtype with a concomitant decrease of affinity at hA_1 and hA_{2A} receptors, thus improving selectivity in favor of the hA_3 subtype. This finding seemed to imply that the hA_3 binding cavity around the N^5 position was rather spacious to accommodate the extended chains, in this case the benzoyl and phenyl acetyl groups. Between these two substituents, the longer phenyl acetyl group (e.g., compound **34**, K_i hA_3 = 0.345 nM) showed relatively better binding profile than the shorter benzoyl chain (e.g., compound **24**, K_i hA_3 = 5.24 nM). Moreover, the spare H on the nitrogen atom at N^5 did not seem to be crucial because its replacement with an additional benzoyl chain (as in compounds **27**, K_i hA_3 = 6.88nM and **28**, K_i hA_3 = 6.94 nM), although less favorable than a single chain, still maintained affinity at hA_3 receptor and good selectivity (>1400) against other receptor subtypes. This finding again confirmed the postulation that the binding pocket of A_3 receptor around this N^5 position was roomy enough to accommodate the bulky and branched bis-benzamidic substituent; at A_1 and A_{2A} subtypes, there was limited space available for

such bulky groups and resulted in decrease of affinity with subsequent increase of selectivity against these two receptors.

N^8 Position: It was found that when a small alkyl group was present at N^8, the compounds (**7-12**, **21-28**, and **31-36**) showed a preference for hA_3 receptors, regardless of substitution at N^5 and C^2 positions (e.g., compounds **7** [(with a phenyl at C^2 and a free amino at N^5), K_i hA_3 = 75.0 nM] and **8** [(with a 4-fluorophenyl at C^2 and a free amino at N^5), K_i hA_3 = 31.4 nM] versus compounds **21** [(with a phenyl at C^2 and a benzamide at N^5), K_i hA_3 = 5.0 nM] and **22** [(with a 4-fluorophenyl at C^2 and a benzamide at N^5), K_i hA_3 = 3.43 nM]. This was further confirmed by the introduction of a slightly longer alkyl chain (e.g., an ethyl group in compound **14**, K_i hA_3 = 68.7 nM), which still showed hA_3 antagonism and moderate selectivity. Notably, when the same substituent was shifted from position N^8 to N^7 (as in compounds **13**, K_i hA_3 = 565 nM and **17**, K_i hA_3 > 30000 nM), the affinity at hA_3 receptors dropped to at least 8 times, with the resulting binding affinity profile inclined toward hA_{2A} receptors. This observation was substantiated by the results previously reported on N^7-substituted PTPs as potent hA_{2A} antagonists. [104]

Conversely, when a group bigger than ethyl was introduced at N^8 (e.g., phenylethyl group in compounds **15**, **16**, **18-20**, and **29**, **30**), a decrease of affinity at hA_3 receptor was observed. In derivatives with free amino group at N^5 position, the substitution of the methyl group (e.g., compound **11**, K_i hA_3 = 16.7 nM) to the long and bulky phenylethyl group (e.g., compound **20**, K_i hA_3 = 25.0 nM) only showed a slight decrease of the hA_3 affinity. When a substituent was introduced at the N^5 position (e.g., compound **29**, K_i hA_3 = 23.9 nM), the presence of the phenylethyl group resulted in a great decrease of hA_3 affinity in comparison to its N^8-methyl counterpart (compound **21**, K_i hA_3 = 5.0 nM). Apparently, an inverse relationship appeared between the binding affinity values at hA_3 receptor and the molecular volume (MV) of the substituent at position N^8: the higher the MV, the lower the affinity toward the hA_3 receptor. [92]

On the whole, these results confirmed the importance of the contemporary introduction, in the PTP system, of (a) small substituents (e.g., CH3) at the N^8 position to maintain affinity and selectivity at hA_3AR, (b) a longer chain such as a phenylacetyl group at the N^5 position to confer higher affinity and a better selectivity especially toward hA_1 and hA_{2A} receptors, (c) a 2-(*para*-substituted) phenyl ring at C^2 to improve affinity and selectivity profile at hA_3 receptors in relative to the 2-furyl counterparts and protect from enzyme deactivation with subsequent higher plasma bioavailability.

Among the newly synthesized PTP derivatives, compound **31**, with a phenyl at C^2, a methyl group at N^8, and a phenylacetamidic chain at N^5, showed the best hA_3 affinity profile (K_i hA_3 = 0.108 nM) and good selectivity against the other adenosine receptors (hA_1/hA_3 = 5200; hA_{2A}/hA_3 = 7200).

A receptor-driven molecular modeling investigation has been performed

in order to rationalize the results obtained from the pharmacological evaluation. For that purpose, we performed molecular docking simulations on both the crystallographic structure of hA_{2A} and the recently published hA_3 receptor model. All the newly synthesized 2-aryl-PTP derivatives were docked into the orthosteric TMs binding cavities of both adenosine receptors. In addition, docking studies were also performed on the two previously reported PTPs bearing a furan ring at C^2 (compounds **90** and **91** in Table 3.5), [103, 92] with the aim of comparing the possible differences in binding mode between the 2-aryl and 2-furyl derivatives.

N^5-unsubstituted derivatives:

From the docking simulation analysis, almost all the new derivatives with free amino group at N^5 (compounds **7**-**20**) were seen to share a similar binding pose in the TM region of the hA_3AR. The ligand recognition occurred in the upper region of the TM bundle, and the PTP scaffold was surrounded by TMs 3, 5, 6, and 7 with the 2-aryl ring oriented toward TM2.

Figure 3.18, panel B, shows the hypothetical binding pose of compound **7**. This compound was anchored, inside the binding cleft, by two stabilizing hydrogen-bonding interactions with the side chain of Asn250 (6.55), which is highly conserved among all AR subtypes and found to be important for ligand binding at the hA_3AR. [71] It also formed an aromatic π-π stacking interaction with Phe168 (EL2), while the methyl group at N^8 was in proximity with the highly conserved Trp243 (6.48), an important residue in receptor activation and antagonist recognition. [71] It was also found to form hydrophobic interactions with many residues of the binding site including Ala69 (2.61), Val72 (2.64), Thr87 (3.29), Leu90 (3.32), Leu91 (3.33), Phe168 (EL2), Trp243 (6.48), Leu246 (6.51), Leu264 (7.35), Tyr265 (7.36), and Ile268 (7.39).

On the other hand, by comparing the binding mode of the 2-furyl counterpart (compound **90** in Table 3.5) at the hA_3 receptor (Figure 3.18, panel D), we observed a slight different binding orientation as compared to compound **7**. In fact, this compound was found to be oriented almost parallel to the membrane plane, and it formed only one H-bond with Asn250 (6.55) with concurrent loss of the π-π stacking interaction with Phe168 (EL2).

Through the analysis of *per residue* electrostatic contributions to the whole interaction energy, we found that Asn250 (6.55) showed a very negative electrostatic interaction energy in the compound **7**-hA_3AR complex due to the two stabilizing H-bonding interactions with the ligand. Conversely, for the compound **90**-hA_3AR complex, the same residue showed only a weak stabilizing electrostatic interaction. Therefore, the loss of one H-bond with Asn250 (6.55) and the π-π stacking interaction with Phe168 (EL2) could be the reason to account for the observation that the 2-furyl derivative possessed lower affinity toward the hA_3 receptor as compared to the 2-aryl derivative (compound **7**, K_i hA_3 = 75nM; compound **90**, K_i hA_3 = 300nM).

As regards the compounds with bulkier substituents at N^8, such as ethyl

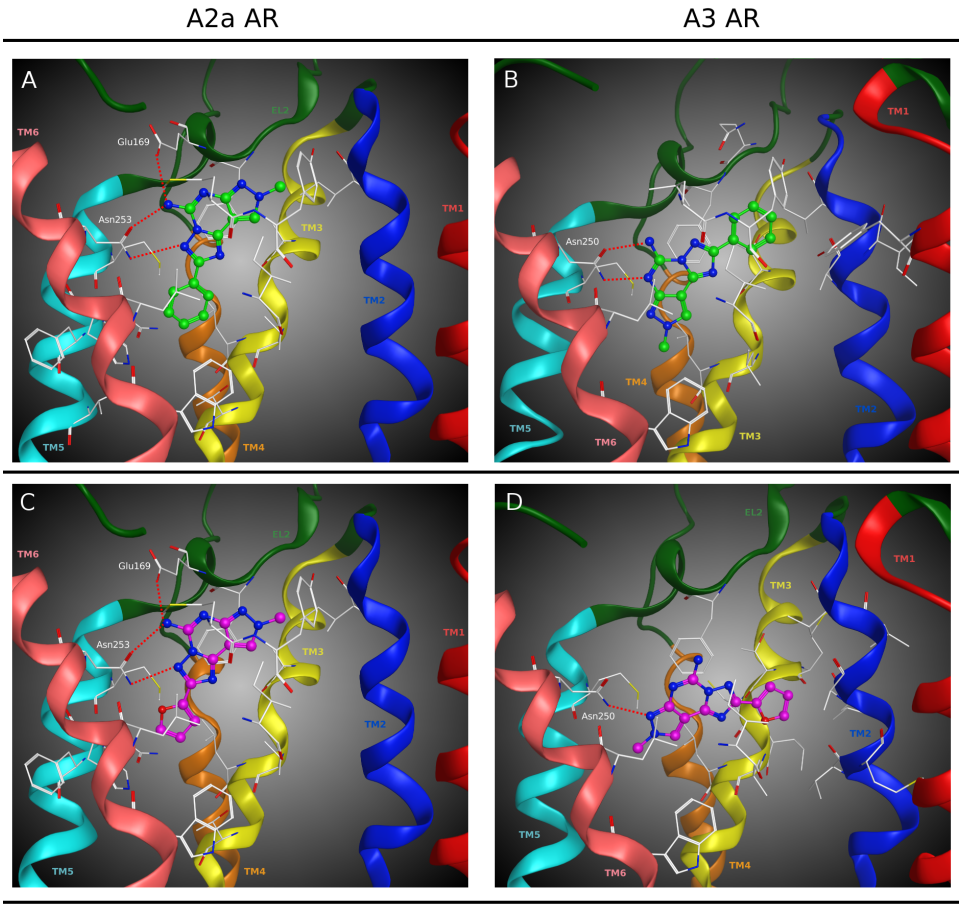

Figure 3.18: Hypothetical binding modes of N^5-unsubstituted pyrazolo-triazolo-pyrimidines obtained after docking simulations: (A) compound **7** inside the $hA_{2A}AR$ binding site; (B) compound **7** inside the hA_3AR binding site; (C) compound **90** inside the $hA_{2A}AR$ binding site; (D) compound **90** inside the hA_3AR binding site. Poses are viewed from the membrane side facing TM6, TM7, and TM1. The view of TM7 is voluntarily omitted. Side chains of some amino acids important for ligand recognition and H-bonding interactions are highlighted. Hydrogen atoms are not displayed.

group (compound **14**) and phenylethyl group (compounds **15**-**16** and **18**-**20**), they showed similar binding mode at hA_3 receptor as compared to the N^8-methyl derivatives. There seemed to be enough space in the binding cavity to accommodate such substituents at this position. Moreover, the presence of different groups at the *para* position of the phenyl ring at C^2 (e.g., Cl, F, Br, OCH_3) was well tolerated at this receptor with the only exception for the nitro group. Both steric and/or dipolar contributions of nitro group can be responsible for the loss of activity of compound **12**.

In the context of hypothetical binding poses of compound **7** and compound **90** inside the cavity of hA_{2A} receptor (Figure 3.18, panels A and C, respectively), we noted that they were very similar to each other. In fact, at the hA_{2A} receptor, both compounds formed two H-bonds with Asn253 (6.55) and another H-bond with Glu169 (EL2), two residues that have been indicated to play an important role in ligand binding at the hA_{2A}AR. [87, 88] In addition, a π-π stacking interaction with Phe168 (EL2) and hydrophobic interactions with many residues of the binding site including Val84 (3.32), Leu85 (3.33), Thr88 (3.36), Met177 (5.38), Trp246 (6.48), Leu249 (6.51), His250 (6.52), Met270 (7.35), and Ile274 (7.39), were also observed. Two of the strongly negative electrostatic contributions to the interaction energy were found to be related to the Glu169 (EL2) and Asn253 (6.55) for both complexes; however, the contribution due to Glu169 (EL2) was of around -8 kcal/mol for the compound **7**-hA_{2A}AR complex and -14 kcal/mol for the compound **90**-hA_{2A}AR complex. This finding explained why compound **7** still possessed affinity for the hA_{2A} receptor (K_i hA_{2A} = 121 nM) but less as compared to the analogue with a 2-furyl ring (compound **90**, K_i hA_{2A} = 2.80 nM).

Besides that, the presence of substituents at the *para* position of the C^2-phenyl ring has imparted a detrimental effect toward the hA_{2A} receptor affinity. With the increase in size of the *para*-substituents, a decrease in affinity at the hA_{2A} receptor was observed, which implied the existence of steric control within this region of the binding site.

Moreover, the substituents at the *para* position of the C^2-phenyl ring could affect the approaching of ligands into the hA_{2A} receptor binding cavity and subsequently mediating some interactions with residues at the entrance of the binding site. This step could be crucial for the recognition process and so for ligand affinity at the receptor. [105] Therefore, the presence of polar residues at the entrance of the hA_{2A} receptor binding cavity, such as Glu169 (EL2) and His264 (EL3), might affect ligand orientation while approaching the binding pocket, as already proposed. [61]

As for the N^7-substituted derivative, it was found that compound **13** showed similar binding mode at both the hA_3 and hA_{2A} receptor subtypes to that of the N^8-substituted derivatives.

Figure 3.19 represents the binding modes of the N^7-substituted derivative **13** at both the hA_{2A} and hA_3 receptors. Inside the hA_{2A} receptor, compound

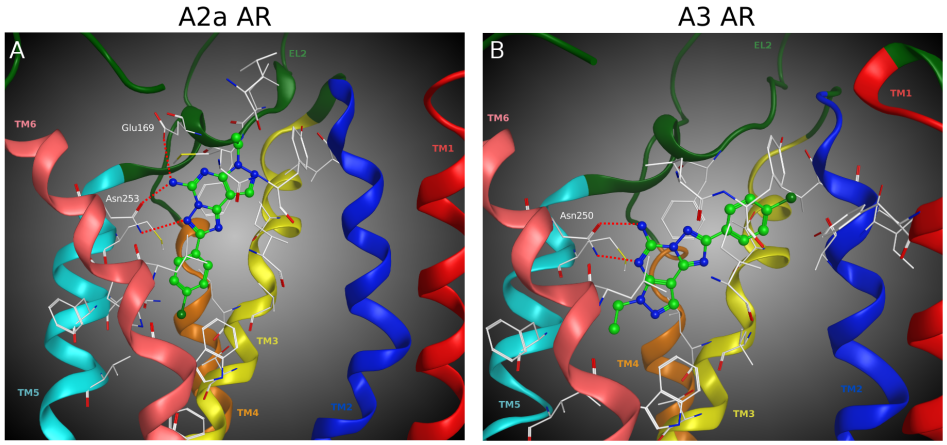

Figure 3.19: Hypothetical binding modes of compound **13** obtained after docking simulations: (A) inside the $hA_{2A}AR$ binding site and (B) inside the hA_3AR binding site. Poses are viewed from the membrane side facing TM6, TM7 and TM1. The view of TM7 is voluntarily omitted. Side chains of some amino acids important for ligand recognition and H-bonding interactions are highlighted. Hydrogen atoms are not displayed.

13 was oriented perpendicular to the membrane plane and was anchored by three stabilizing H-bonds with Asn253 (6.55) and Glu169 (EL2) side chains (Figure 3.19, panel A). As for the hA_3 receptor, it formed two H-bonding interactions with Asn250 (6.55) (Figure 3.19, panel B).

Then, for this compound, similar considerations as for the N^8-substituted derivatives could be made. At the hA_{2A} receptor, the N^7-ethyl group of compound **13** was able to interact with hydrophobic residues of the upper region of the binding cavity, including Leu167 (EL2), Leu267 (7.32), Tyr271 (7.36). At the hA_3 receptor, instead, the N^7-substituent was located deep in the binding site and oriented toward TM5 and TM6. There was only limited space just to accommodate the ethyl group at N^7, but not so for the bulkier substituents, such as the N^7-phenylethyl group in compound **17**. This suggests that the steric effect at the N^7-position might have caused the N^7-phenylethyl-substituted derivative (compound **17**) to have null affinity at the hA_3 receptor.

N^5-substituted derivatives:

As shown in Figure 3.20, the hypothetical binding modes at hA_{2A} and hA_3 receptors for the N^5-substituted derivatives with a 2-aryl ring (compounds **21**-**36**) were the same as those obtained for 2-furyl counterpart (compound **91**).

For these compounds, recognition at hA_3 receptor occurred in the upper region of the TM bundle, and the PTP scaffold was surrounded by TMs 3, 5, 6, and 7 with the 2-aryl or 2-furyl ring oriented toward TM2 and the

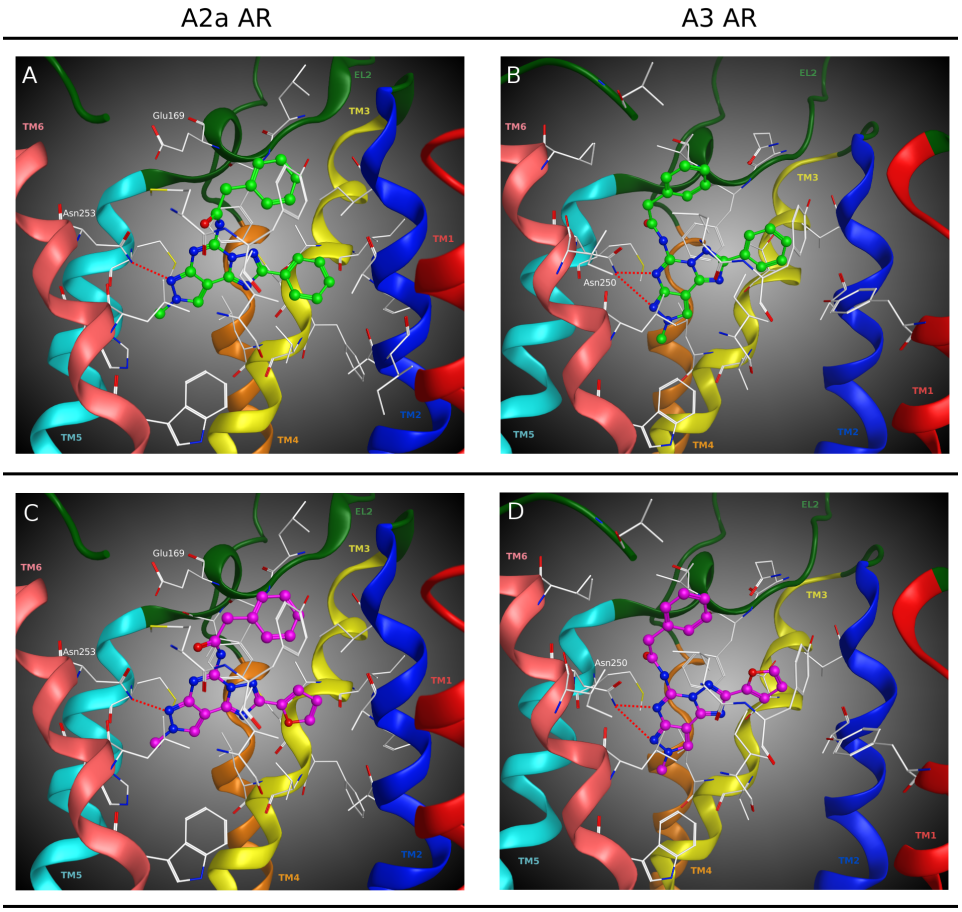

Figure 3.20: Hypothetical binding modes of the N^5-substituted derivatives obtained after docking simulations: (A) compound **31** inside the $hA_{2A}AR$ binding site; (B) compound **31** inside the hA_3AR binding site; (C) compound **91** inside the $hA_{2A}AR$ binding site; (D) compound **91** inside the hA_3AR binding site. Poses are viewed from the membrane side facing TM6, TM7, and TM1. The view of TM7 is voluntarily omitted. Side chains of some amino acids important for ligand recognition and H-bonding interactions are highlighted. Hydrogen atoms are not displayed.

substituent at N^8 located deep into the binding cavity. At the hA_3 receptor, compounds **31** and **91** formed two stabilizing H-bonding interactions with Asn250 (6.55), a π-π stacking interaction between the triazole ring and Phe168 (EL2) and hydrophobic interactions with several residues of the binding site including Ala69 (2.61), Val72 (2.64), Thr87 (3.29), Leu90 (3.32), Leu91 (3.33), Phe168 (EL2), Val169 (EL2), Trp243 (6.48), Leu246 (6.51), Ile249 (6.54), Ile253 (6.58), Val259 (EL3), Leu264 (7.35), Tyr265 (7.36), and Ile268 (7.39) (Figure 3.20, panel D).

By analyzing the calculated individual electrostatic contribution to the interaction energy of each receptor residue, it was evident that Asn250 (6.55) strongly stabilized the ligand-hA_3 receptor complexes (negative electrostatic interaction energy) due to the two hydrogen bonding interactions.

Considering the hypothetical binding pose of these compounds at the hA_{2A} receptor (Figure 3.20, panel C), it could be seen that the PTP core was rotated of about 40° compared to the binding pose of the same compounds at the hA_3 subtypes. Because of this different orientation of the molecules inside the binding cleft at the hA_{2A} receptor, both compounds **31** and **91** formed only one H-bond with Asn253 (6.55). Coherently, for these complexes, the electrostatic contributions to the interaction energy of Asn253 (6.55) were shown to be weakly stabilizing and no other amino acid with a noteworthy negative electrostatic interaction energy was identified.

In fact, it has to be pointed out that at the position 169 (EL2) of the hA_3 receptor subtype, a valine residue is present while at the corresponding position of the hA_{2A} receptor, this valine is replaced by a glutamate residue (Glu169).

It was believed that, because of this substitution at the hA_{2A} receptor, the substituent at N^5 of these derivatives were unable to occupy the same position as at the hA_3 receptor and hence, the whole molecule was shifted away from Asn253 with a simultaneous loss of a H-bond, as seen in compound **31** at the hA_{2A} binding site. This finding could be accounted for the low affinity profile at the hA_{2A}, as observed in the majority of the N^5-substituted derivatives (compounds **22-36**). In addition, due to the presence of N^5-substitutions, these derivatives could not form the H-bonding interactions with Glu169 (EL2) as observed for N^5-unsubstituted analogues. Therefore, the mutation of the valine at the position 169 with a glutamate was hypothesized to be critical for the hA_3 versus hA_{2A} selectivity profile. [61]

Moreover, at the hA_{2A} receptor, the hydrophobic side cleft delimited by TM2 and TM3 could well accommodate the 2-furyl ring of compound **91** but hardly accommodated the 2-phenyl ring of compound **31**. This steric effect could be the reason of the difference in affinity between the 2-aryl and the 2-furyl analogues at this receptor subtype (compound **31**, K_i hA_{2A} = 778 nM; compound **91**, K_i hA_{2A} = 432 nM).

For the same reason, the presence of *para*-substituents on the phenyl ring led to a drastic decrease in affinity at hA_{2A} receptor, up to complete loss of

affinity for bulkier substituents.

Conversely, the 2-phenyl and 2-furyl rings of compounds **31** and **91**, respectively, were located less deeply in the binding cavity of hA_3 receptor and hence, more space was available to accommodate them. Therefore, at the hA_3 receptor subtype, the 2-phenyl ring was preferred, and different *para*-substituents were also well tolerated.

In summary, the bioisosteric replacement of the furan ring with a phenyl ring at the C^2 position has led to the identification of a new series of 2-(*para*-substituted)phenyl-pyrazolo-triazolo-pyrimidine derivatives as hA_3 antagonists with good affinity and remarkably improved selectivity profile toward the other adenosine receptor subtypes in comparison to the 2-furyl PTP derivatives. Moreover, the substitution of 2-furyl with an aryl group in the new PTP derivatives is expected to overcome the metabolic instability due to the C^2-furan ring.

Thank to the molecular modeling studies, the experimental structure-activity relationship (SAR) findings have been rationalized by depicting the hypothetical binding mode between these newly synthesized derivatives and the specific amino acid residues within the binding site of hA_3 and hA_{2A} receptors.

In short, the rational design and synthesis of this new series of 2-(*para*-substituted)phenyl-pyrazolo-triazolo-pyrimidines has given rise to a class of potent, highly selective, and metabolically stable hA_3AR antagonists.

3.4.2 Substitutions at the C^2, N^5 and N^8 positions

Based on the observations derived from the previous study on the pyrazolo-triazolo-pyrimidine nucleus, it has been hypothesized that the combination of a (substituted)phenyl group at the C^2 position, together with substituents at the N^5 and N^8 positions deemed optimal for interaction with the hA_3AR, would effectively give rise to new potent and selective A_3AR antagonists.

In order to test our hypothesis, a new series of 2-(substituted)phenyl-pyrazolo-triazolo-pyrimidines bearing either a methyl (II) or a phenylethyl group (III) at the N^8 position, in conjunction with arylcarbamide, phenylacetamide or benzamide chains at the N^5 position was designed and synthesized (Figure 3.21).

This new series of compounds (compounds **4**, **5**, **8**–**19**, **26**, **27** and **29**–**33**) was aimed at further exploring the effect of these substituents at each position of the PTP tricyclic scaffold towards hA_3AR affinity and selectivity. Moreover, to better clarify the effect of these substituents on the binding modes of the new compounds at the hA_3AR, a molecular modeling investigation performed.

Therefore, a new series of 2-(*para*-(un)substituted)phenyl-pyrazolo[4,3-*e*]1,2,4-triazolo-[1,5-*c*]-pyrimidines was successfully synthesized and characterized. We introduced only a few modifications to the original PTP scaf-

fold, in order to focus our investigation on the combination of optimal substituents at the C^2, N^5 and N^8 positions. To that end, we selected a (substituted)phenyl group at the C^2 position and either a methyl (compounds **4**, **5** and **8**–**19**) or a phenylethyl (compounds **26**, **27** and **29**–**33**) group at N^8, with concurrent introduction of different amide moieties at position N^5.

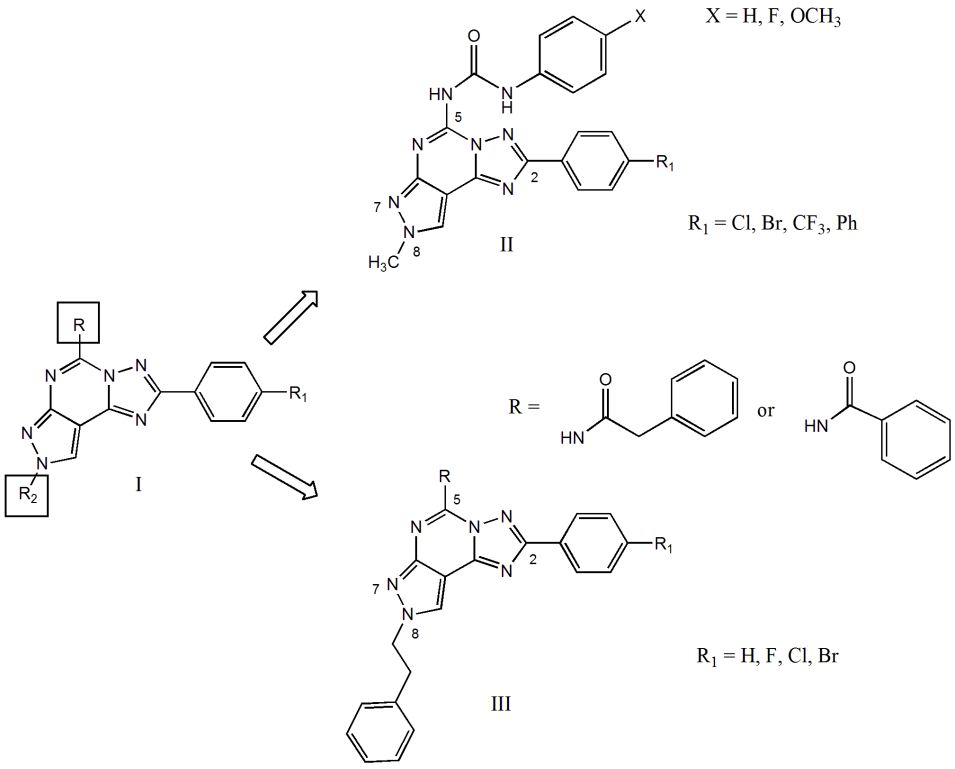

Figure 3.21: Rationale for the design of new 2-phenyl-pyrazolo-triazolo-pyrimidine derivatives.

Table 3.7 summarizes the receptor binding affinities of these compounds determined at the hA_1AR, $hA_{2A}AR$ and hA_3AR and the corresponding adenylyl cyclase activity in CHO cells that express $hA_{2B}AR$. The results showed that the new series of pyrazolo-triazolo-pyrimidines presented good affinity to hA_3AR, as indicated by K_i values in the nanomolar range and, most importantly, improved selectivities over other AR subtypes.

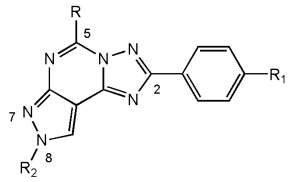

Compd	R	R_1	R_2	hA_1 (K_i nM)[a]	hA_{2A} (K_i nM)[b]	hA_{2B} (K_i nM)[c]	hA_3 (K_i nM)[d]
4	NH_2	CF_3	N^8-CH_3	>100,000	6,930 (4340-11,100)	>10,000	304 (237-391)
5	NH_2	Ph	N^8-CH_3	>100,000	>30,000	>10,000	147 (114-188)
8	NH-CO-NH-Ph	Cl	N^8-CH_3	5,550 (4050-7600)	987 (615-1580)	>10,000	1.71 (1.20-2.44)
9	NH-CO-NH-Ph	Br	N^8-CH_3	>10,000	2,360 (2160-2570)	>10,000	2.5 (1.89-3.32)
10	NH-CO-NH-Ph	CF_3	N^8-CH_3	12,900 (9180-18200)	36,000 (33,900-38,300)	>10,000	3.44 (2.34-5.05)
11	NH-CO-NH-Ph	Ph	N^8-CH_3	>30,000	>30,000	>10,000	5.9 (3.33-10.5)
12	NH-CO-NH-(4-F)Ph	Cl	N^8-CH_3	>30,000	1,060 (864-1,310)	>10,000	5.3 (4.35-6.45)
13	NH-CO-NH-(4-F)Ph	Br	N^8-CH_3	>30,000	5,930 (3,270-10,800)	>10,000	1.72 (0.91-3.26)
14	NH-CO-NH-(4-F)Ph	CF_3	N^8-CH_3	4,420 (1,700-11,500)	>30,000	>10,000	1.91 (1.01-3.59)
15	NH-CO-NH-(4-F)Ph	Ph	N^8-CH_3	>100,000	>100,000	>10,000	4.06 (3.17-5.19)
16	NH-CO-NH-(4-OCH_3)Ph	Cl	N^8-CH_3	6,490 (3,360-12,500)	1,460 (1050-2,040)	>10,000	1.33 (0.91-1.95)
17	NH-CO-NH-(4-OCH_3)Ph	Br	N^8-CH_3	>10,000	8,400 (5,220-13,500)	>10,000	1.95 (1.64-2.31)
18	NH-CO-NH-(4-OCH_3)Ph	CF_3	N^8-CH_3	>100,000	>100,000	>10,000	2.36 (1.46-3.80)
19	NH-CO-NH-(4-OCH_3)Ph	Ph	N^8-CH_3	>100,000	>100,000	>10,000	2.1 (1.41-3.14)
26	NH-COPh	F	N^8-CH_2-CH_2-Ph	395 (318-492)	4,040 (3,500-4,620)	>30,000	17.1 (14.9-19.8)
27	NH-COPh	Cl	N^8-CH_2-CH_2-Ph	221 (196-251)	19,400 (11900-31400)	>30,000	11.4 (9.94-13.0)
29	NH-COPh	OCH_3	N^8-CH_2-CH_2-Ph	831 (530-1,300)	25,200 (22,300-28,400)	>10,000	28.9 (22.0-37.9)
30	NH-$COCH_2$Ph	H	N^8-CH_2-CH_2-Ph	192 (167-220)	614 (574-656)	>30,000	3.02 (1.49-6.11)
31	NH-$COCH_2$Ph	F	N^8-CH_2-CH_2-Ph	232 (209-259)	571 (507-642)	>30,000	3.34 (3.16-3.53)
32	NH-$COCH_2$Ph	Cl	N^8-CH_2-CH_2-Ph	932 (688-1260)	3,090 (2,680-3,560)	>30,000	8.48 (4.81-14.9)
33	NH-$COCH_2$Ph	Br	N^8-CH_2-CH_2-Ph	>10,000	>10,000	>10,000	>10,000

[a] Displacement of specific [^{3}H]-CCPA binding at hA_1AR expressed in CHO cells, (n = 3–6).
[b] Displacement of specific [^{3}H]-NECA binding at hA_{2A}AR expressed in CHO cells, (n = 3–6).
[c] K_i values of the inhibition of NECA-stimulated adenylyl cyclase activity in CHO cells, (n = 3–6).
[d] Displacement of specific [^{3}H]-NECA binding at hA_3AR expressed in CHO cells, (n = 3–6). Data are expressed as geometric means, with 95% confidence limits.

Table 3.7: Binding affinity (K_i) at the four human adenosine receptors and selectivity profiles of the new 2-phenyl-pyrazolo-triazolo-pyrimidines.

N^8-Methyl derivatives:

As observed in the previous section, the bioisosteric replacement of the furan ring at the C^2 position with a phenyl ring resulted in a 3- to 8-fold increase in affinity towards hA_3AR and a significant improvement in selectivity (of 2–3 orders of magnitude) over other AR subtypes, namely hA_1AR, $hA_{2A}AR$ and $hA_{2B}AR$. In other words, compounds with a phenyl ring at the C^2 position demonstrated better affinity and selectivity profiles towards hA_3AR as compared with the 2-furyl counterparts. [76]

Nonetheless, in the present investigation we noticed a different trend of hA_3AR affinities in the new series of 2-(para-(un)substituted)phenyl-8-methyl-PTPs bearing arylcarbamoyl moieties at the N^5 position (**8**–**19**), despite the fact that these compounds still maintained good hA_3AR affinity at low nanomolar range (K_i range 1.3–5.9 nM).

It was found that the bioisosteric replacement of the existing furan ring with a phenyl ring in this group of compounds caused 7- to 37-fold decrease in affinity to hA_3AR. Notably, the selectivity over other AR subtypes of these 2-phenyl-PTP derivatives was still greatly improved in comparison with that of 2-furyl analogues.

These findings suggested that for these N^8-methyl N^5-arylcarbamides PTPs, the 2-furyl ring was more favorable than the 2-phenyl ring for hA_3AR affinity. Even so, the introduction of a phenyl ring at the C^2 position was deemed crucial to confer higher selectivity towards hA_3AR in comparison with the 2-furyl ring, while maintaining good affinity at the hA_3AR.

In addition, we also evaluated the effect of *para*-substituents on the 2-phenyl ring towards the affinity profile of hA_3AR. Based on the binding results, the substituents (e.g. Cl, Br, CF_3, Ph) at the *para*-position of the C^2-phenyl ring were found to modulate hA_3AR affinity to a certain extent.

The introduction of functional groups with relatively high molecular volume, such as a 4-trifluoromethyl (e.g. compound **4**, K_i hA_3 = 304 nM) and a 4-phenyl ring (e.g. compound **5**, K_i hA_3 = 147 nM) on the 2-phenyl ring of some N^5-unsubstituted derivatives seemed unfavorable for hA_3AR affinity, as shown by their high nanomolar K_i values. From these findings we could infer that the presence of bulky groups at the *para*-position of the C^2-phenyl ring was undesirable for the hA_3AR affinity.

In contrast, the situation improved remarkably when the same derivatives were further substituted at the N^5 position. The additional chains at N^5 (as shown in compounds **10** and **11**) enabled an increase of affinity at the hA_3AR with a concomitant decrease of binding to hA_1AR and $hA_{2A}AR$. This observation implied that the hA_3AR binding cavity around the N^5 position was spacious enough to accommodate extended chains, such as arylcarbamoyl groups (compounds **8**–**19**).

Further incorporation of *para*-substituents such as 4-fluoro (compounds **12**–**15**) and 4-methoxy (compounds **16**–**19**) groups on the phenyl ring of arylcarbamoyl moiety seemed tolerable for hA_3AR affinity giving values

in the range of 1.33–5.30 nM. Except for derivative **12**, compounds with 4-fluoro and 4-methoxy groups on the phenyl ring of arylcarbamoyl moiety generally possessed better hA_3AR affinities in comparison with the N^5-phenylcarbamoyl- substituted analogues (e.g. compound **13**, K_i hA_3 = 1.72 nM, hA_1/hA_3 >17,400; hA_{2A}/hA_3 = 3450 vs compound **9**, K_i hA_3 = 2.50 nM, hA_1/hA_3 >4000; hA_{2A}/hA_3 = 944).

Furthermore, the 4-methoxy-phenylcarbamoyl chain at the N^5 position was shown to confer good selectivity against the hA_1AR, $hA_{2A}AR$ and $hA_{2B}AR$ as well.

In general, there were no substantial differences between the electron-withdrawing (e.g. 4-fluoro in compounds **12**–**15**) and the electron-donating (e.g. 4-methoxy in compounds **16**–**19**) effects of such *para*-substituents on hA_3AR affinity, thus implying that the steric effects might be more prominent on the hA_3AR binding profiles of these new PTPs.

N^8-Phenylethyl derivatives:

As reported previously, it was found that when a small alkyl group, like a methyl, was present at the N^8 position, compounds showed a preference for hA_3AR, regardless of substitutions at the C^2 and N^5 positions (e.g. compound **9** with a 4-bromophenyl at C^2 and a phenylcarbamide at N^5, K_i hA_3 = 2.50 nM; hA_1/hA_3 >4000; hA_{2A}/hA_3 = 944).

Conversely, when a longer chain (e.g. phenylethyl group) was introduced at N^8, we observed a different trend for derivatives bearing a free or substituted amino group at the N^5 position.

As shown in the PTP series reported in the previous section, when a free amino group was present at the N^5-position, the presence of an N^8-phenylethyl group seemed to be responsible for the lower affinities and selectivities of compounds **20**–**24** for hA_3AR as compared with the N^8-methyl analogues.

On the other hand, when the same derivatives were further substituted at the N^5 position, the presence of such additional groups at N^5 seemed to be always favorable for hA_3AR affinity (e.g. compound **30**, K_i hA_3 = 3.02 nM; hA_1/hA_3 = 63.6; hA_{2A}/hA_3 = 203). However, the hA_3AR affinities and selectivities of such N^8-phenylethyl derivatives were found to be remarkably lower than those of the N^8-methyl analogues.

Between the two N^5-phenylacetyl and N^5-benzoyl moieties, the relatively flexible phenylacetyl group (e.g. compounds **31**, K_i hA_3 = 3.34 nM; hA_1/hA_3 = 69.5; hA_{2A}/hA_3 = 171 and **32**, K_i hA_3 = 8.48 nM; hA_1/hA_3 = 110; hA_{2A}/hA_3 = 364) showed relatively better binding profiles than those with the shorter benzoyl chain (e.g. compounds **26**, K_i hA_3 = 17.1 nM; hA_1/hA_3 = 23.1; hA_{2A}/hA_3 = 236 and **27**, K_i hA_3 = 11.4 nM; hA_1/hA_3 = 19.4; hA_{2A}/hA_3 = 1700). Such observations were consistent with the findings obtained for the N^8-methyl series of 2-phenyl-PTP derivatives reported in the previous section.

Moreover, it was observed that compounds with a phenyl ring at C^2

and a phenylethyl group at N^8 showed better affinity and selectivity profiles towards the hA_3AR in comparison with their 2-furyl counterparts, and this further strengthened our previous finding that the substituted-phenyl at the C^2 position indeed played a crucial role on the hA_3AR affinity and selectivity against other ARs.

In particular, among the substituents introduced at the *para*-position of the C^2-phenyl ring, both the fluoro and chloro groups exerted more favourable effects on hA_3AR affinity in the N^5-benzamide-substituted (e.g. compound **26**, K_i $hA_3 = 17.1$ nM) and N^5-phenylacetamide-substituted (e.g. compound **31**, K_i $hA_3 = 3.34$ nM) derivatives.

In order to rationalize the hA_3AR affinity profile observed for this new series of compounds, a receptor-driven molecular modeling investigation was carried out. All of the 2-(substituted)phenylpyrazolo[4,3-*e*]1,2,4-triazolo-[1,5-*c*]-pyrimidines were docked into the transmembrane binding cavity of the hA_3AR model. Additionally, for the selected binding poses, individual electrostatic and hydrophobic contributions to the whole interaction energy of each receptor residue were calculated.

N^8-Methyl derivatives:

All of the N^8-methyl-2-(substituted)phenyl-PTPs here reported showed affinities to hA_3AR in the nanomolar range. Compound **16** showed the highest affinity (K_i $hA_3 = 1.33$ nM).

The hypothetical binding mode of this compound at hA_3AR is shown in Figure 3.22: ligand-recognition occurred in the upper region of the TM bundle, and the pyrazolo-triazolo-pyrimidine scaffold was surrounded by TMs 3, 5, 6 and 7 with the phenyl ring at the C^2 position oriented towards TM2. Compound **16** was anchored by two stabilizing hydrogen-bonding interactions with the side chain of Asn250 (6.55) and an aromatic π-π stacking interaction with Phe168 (EL2). The asparagine residue 6.55, conserved among all AR subtypes, was already found to be important for ligand binding to hA_3AR. Moreover, compound **16** formed hydrophobic interactions with many residues of the hA_3AR binding site including Leu91 (3.33), Phe168 (EL2), Leu246 (6.51), Ile268 (7.39) and the highly conserved Trp243 (6.48), an important residue in receptor activation and antagonist recognition; [71] while the phenyl ring at the C^2 position interacted with Val65 (2.57), Leu68 (2.60), Ala69 (2.61), Val72 (2.64), Thr87 (3.29), Leu90 (3.32); and the phenyl ring of the phenylcarbamoyl chain at N^5 made hydrophobic contacts with Val169 (EL2), Leu264 (7.35) and Tyr265 (7.36). In addition, another H-bond was observed between the 4-methoxy group of the phenylcarbamoyl chain at N^5 and the amide group of the side chain of Gln167 (EL2).

The observed interactions were confirmed by the analysis of the calculated *per residue* electrostatic and hydrophobic contributions to the whole interaction energy for the complex between hA_3AR and compound **16**. As shown in Figure 3.23, the main electrostatic stabilizing contributions were associated with Asn250 (6.55) and Gln167 (EL2) (strong negative electrostatic

interaction energy); while the strongest hydrophobic contributions were related to Phe168 (EL2), Leu264 (6.51), Leu246 (7.35), Leu90 (3.32) and Ile268 (7.39) (high hydrophobic interaction score).

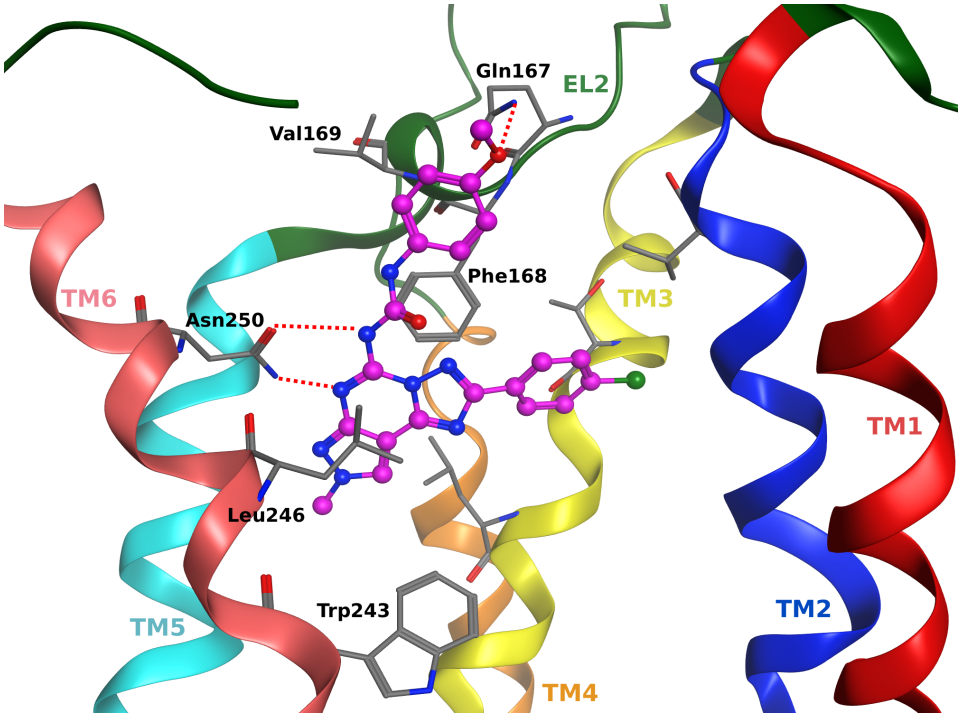

Figure 3.22: Hypothetical binding mode of the N^8-methyl derivative **16** at the hA_3AR binding site obtained after docking simulation. Pose is viewed from the membrane side facing TM6, TM7 and TM1. The view of TM7 is voluntarily omitted. Side chains of some amino acids important for ligand recognition and H-bonding interactions are highlighted. Hydrogen atoms are not displayed.

Overall, the hereby proposed binding mode of compound **16** to hA_3AR was very similar to the binding poses already described in the previous section for other PTP derivatives and presented comparable interactions with the residues of the binding site. [76]

Considering the N^5-unsubstituted-N^8-methyl-PTP derivatives, even if they showed binding modes at the hA_3AR similar to the one observed for compound **16**, they lost some stabilizing hydrophobic interactions with Val169 (EL2), Leu264 (7.35) and Tyr265 (7.36) and this could explain the lower affinities at the hA_3AR of the N^5-unsubstituted derivatives as compared with the N^5-substituted analogues.

In addition, better hA_3AR selectivity profile against the other AR subtypes was also found in such N^5-substituted derivatives. This could be at-

tributed to the lack of space to accommodate bulky substituents at that position in the other AR subtypes. In particular, the weak binding of these compounds at $hA_{2A}AR$ could be due to the different orientations that they acquired inside the hA_{2A} binding cleft as compared with the one observed inside hA_3AR.

As proposed in the previous section for other PTP derivatives, [76] the presence of Glu169 (EL2) in $hA_{2A}AR$, which is mutated to Val169 (EL2) in hA_3AR, seemed to influence the binding poses of these compounds and led to the loss of good interactions with key residue Asn253 (6.55).

Among the substituents at the N^5 position, the phenylacetamide chain was more preferable than the phenylcarbamoyl chain for hA_3AR affinity, probably because of its higher flexibility that allowed better accommodation and stronger interaction in the binding cleft.

Regarding the effect of different *para*-substituents on the 2-phenyl ring towards affinity at the hA_3AR, it appeared that the lateral cleft, which accommodated the 2-phenyl ring, was not sufficiently spacious to host bulky substituents; this could account for the general decrease in hA_3AR affinity observed with the increase in molecular volume of the *para*-substituent on the 2-phenyl ring.

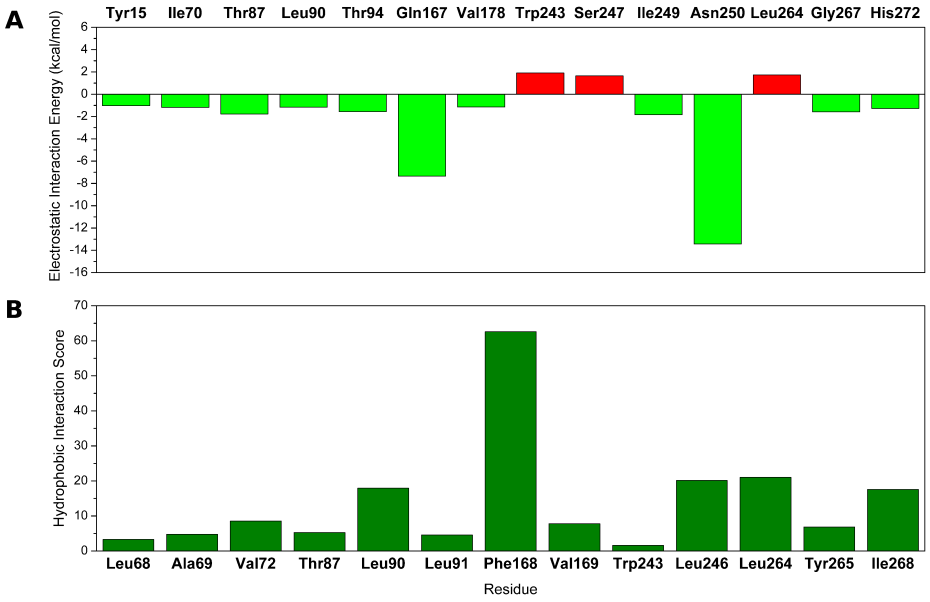

Figure 3.23: (A) Electrostatic interaction energy values (in kcal/mol) and (B) hydrophobic interaction scores (in arbitrary hydrophobic units) between the ligand and each single amino acid involved in ligand recognition calculated from the hypothetical binding mode of compound **16** inside the hA_3AR binding sites.

N^8-Phenylethyl derivatives:

The N^8-phenylethyl derivatives hereby reported, in general, presented lower affinities at the hA_3AR as compared with the N^8-methyl analogues. Among them, the most affine derivative at this receptor was compound **30** (K_i hA_3 = 3.02 nM).

Docking simulations at the hA_3AR performed for this series of compounds showed a binding mode similar to the one observed for the N^8-methyl derivatives, but with the PTP nucleus shifted up towards the entrance of the binding cavity. In fact, due to the presence of the bulkier N^8-phenylethyl chain, these compounds bound less deeply into the binding site. As a consequence, these ligands were still able to form some interactions with the key residue Asn250 (6.55), but they were weaker than those observed for the N^8-methyl derivatives. This finding seemed to explain the lower affinities of the N^8-phenylethyl derivatives at the hA_3AR as compared with the N^8-methyl analogues.

For the substituents at both the N^5 position of the PTP nucleus and the *para*-position of C^2-phenyl ring, hypotheses similar to the ones reported above for the N^8-methyl derivatives could be made.

In fact, the introduction of a benzoyl or phenylacetyl group at the N^5 position caused an increase in affinities at the hA_3AR as compared with the N^5-unsubstituted analogues, mainly due to the increase in hydrophobic interactions with residues at the entrance of the hA_3AR binding site, such as Val169 (EL2), Ile253 (6.58), Val259 (EL3), Leu264 (7.35) and Tyr265 (7.36).

On the other hand, the presence of *para*-substituents on the 2-phenyl ring in these N^8-phenylethyl derivatives was shown to be tolerable for binding at the hA_3AR, provided they were not too bulky. In fact, for these N^8-phenylethyl derivatives even the presence at this position of a relatively bulky bromo group resulted to be detrimental for the affinity at the hA_3AR, since the additional steric hindrance caused by the phenylethyl group reduced the space to accommodate bulky substituents at the *para* position of the 2-phenyl ring.

On the whole, the above-mentioned results have further defined the structure–affinity profiles at the hA_3AR for the new 2-(substituted)phenyl-PTP scaffold and emphasized the importance of (i) a longer chain such as a benzamide or phenylacetamide group at the N^5 position to confer higher affinity and better selectivity towards hA_1AR, $hA_{2A}AR$ and $hA_{2B}AR$; (ii) a small methyl group at the N^8 position in order to enhance both affinity and selectivity at the hA_3AR; (iii) a 2-(*para*-(un)substituted)phenyl ring at the C^2 position to improve affinity and selectivity profiles at the hA_3AR relative to their 2-furyl counterparts. Among the newly synthesized 2-(substituted)phenyl-PTPs, compound **16**, with a 4-chlorophenyl at C^2, a small methyl group at N^8 and a 4-methoxyphenylcarbamoyl chain at N^5, showed the best hA_3AR affinity profile (K_i hA_3 = 1.33 nM) and good selectivities against the other ARs (hA_1/hA_3 = 4880; hA_{2A}/hA_3 = 1100).

3.5 Molecular simplifications

So far, many tricyclic compounds belonging to different classes of nitrogen-containing heterocycles were developed as adenosine receptor antagonists. Besides their remarkable pharmacodynamic profile, a favorable spectrum of pharmacokinetic properties as well as the straightforwardness of their synthetic pathway have to be considered as essential requirements for any drug candidate. Indeed, structural simplification can represent a drug design strategy to shorten synthetic routes while keeping or enhancing the biological activity of the original candidate.

In particular, the rational design of various bicyclic scaffolds as simplified analogs of known tricyclic adenosine receptors antagonists is described in the following sections.

3.5.1 Pyrazolo-pyrimidinone derivatives

Among the known classes of tricyclic heteroaromatic A_3AR antagonists, the pyrazolo-[3,4-*c*]quinolin-4-one (PQ) derivatives showed good results (Figure 3.24). [97, 106] In fact, PQ derivatives showed high affinities for the hA_3 receptor (K_i range 3-30 nM) and also high hA_3 versus hA_{2A} selectivity, since they do not bind the hA_{2A} receptor. They possess quite good affinities for the hA_1AR and then scarce hA_3 versus hA_1 selectivity.

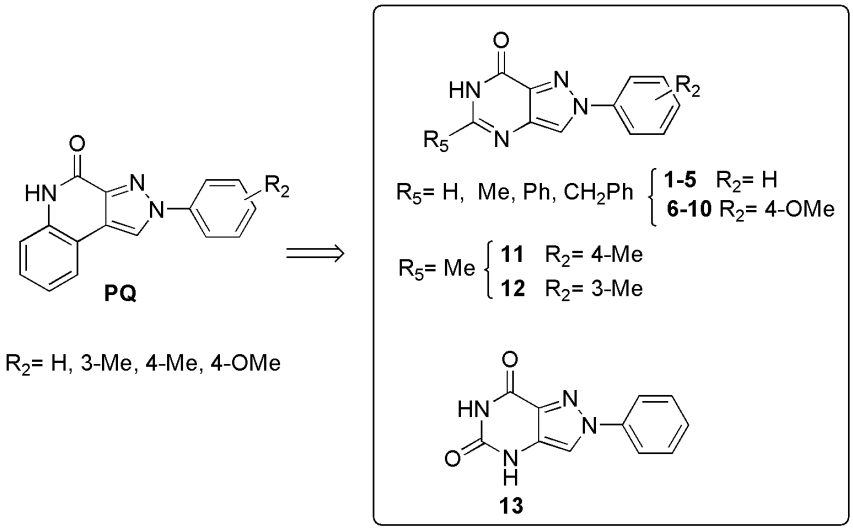

Figure 3.24: Molecular simplification approach from the pyrazolo-[3,4-*c*]quinolin-4-one to the pyrazolo[4,3-*d*]pyrimidin-7-one scaffold.

Thus, to develop a new class of compounds targeting the A_3AR, but with a better selectivity profile, we performed a molecular simplification of the PQ

structure to yield the 2-arylpyrazolo[4,3-*d*]pyrimidin-7-one derivatives **1-12** (Figure 3.24).

Substituents with different lipophilicity and steric hindrance were introduced at the 5 position of the 2-phenyl-pyrazolo-pyrimidin-7-one scaffold (R_5 = H, Me, Et, Ph, CH_2Ph) to give compounds **1-5**. Certain substituents that were profitable for hA_3AR affinity and selectivity in the PQ lead series were introduced on the 2-phenyl ring. In particular, a 4-methoxy group was appended on the 2-phenyl ring of derivatives **1-5** to afford compounds **6-10**. 3-Methyl or 4-methyl groups were also inserted on the 2-phenyl ring of the 5-methyl derivative **2** to obtain compounds **11** and **12**, respectively. Finally, an oxo function was introduced at the 5-position to give the 2-phenylpyrazolo[4,3-*d*]pyrimidin-5,7-dione **13**.

The synthesized derivatives **1-13** were tested to evaluate their binding affinity at hA_1, hA_{2A}, and hA_3 adenosine receptors. Compounds were also tested at the $hA_{2B}AR$ subtype by measuring their inhibitory effects on NECA-stimulated cAMP levels in CHO cells stably transfected with the $hA_{2B}AR$. Finally, the antagonistic potency of all the pyrazolo-pyrimidin-7-one derivatives able to bind at the hA_3AR (**1-3**, **5-8**, **10-12**) was assessed by evaluating their effect on Cl-IB-MECA-inhibited cAMP production in CHO cells, stably expressing hA_3ARs. All pharmacological data are collected in Table 3.8.

The binding results indicate that the herein reported molecular simplification of the PQ structure was successful, since it not only maintained high affinity at the hA_3AR but also increased the hA_3 selectivity. Indeed, most of the newly synthesized compounds displayed hA_3AR affinities in the low nanomolar range (K_i range 1.2-72 nM) and are totally inactive at the other three investigated ARs. Structure-affinity relationship (SAR) analysis shows that both R_2 and R_5 substituents play a key role in anchoring to the hA_3 receptor site. Both the lipophilicity and steric hindrance of the R_5 substituent are critical for hA_3 affinity.

Compound **1**, bearing a hydrogen atom at the 5-position, showed a good hA_3 affinity (K_i hA_3 = 185 nM) which was significantly enhanced when the 5-hydrogen atom was replaced by a 5-ethyl moiety (compound **3**) or, even better, by a 5-methyl group (compound **2**). The presence at the 5-position of the bulkier phenyl ring was detrimental, with derivative **4** showing a null hA_3 binding activity. Replacement of the 5-phenyl group with a 5-benzyl moiety restored the hA_3AR affinity (compound **5**). However, it was significantly lower than those of the less hindered 5-substituted derivatives **1-3**. These results indicate that the presence of a quite small lipophilic substituent at the 5-position of the pyrazolo[4,3-*d*]pyrimidin-7-one scaffold is important.

The presence of a substituent on the 2-phenyl ring (R_2) was also a crucial feature of these new hA_3AR antagonists. When a 4-methoxy group was introduced on the 2-phenyl ring of compounds **1-5**, a significant enhancement of the hA_3 affinity was obtained (compounds **6**, **8-10**). Among the

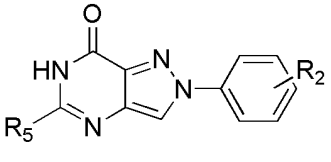

1-12

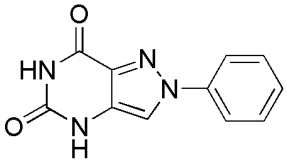

13

			Binding experiments K_i**(nM) or I(%)**			**cAMP assays** IC_{50} **(nM) or I(%)**	
	$\mathbf{R_5}$	$\mathbf{R_2}$	$\mathbf{hA_3}$[a]	$\mathbf{hA_1}$[b]	$\mathbf{hA_{2A}}$[c]	$\mathbf{hA_{2B}}$[d]	$\mathbf{hA_3}$[e]
1	H	H	185 ± 19	1%	1%	3%	725±64
2	Me	H	16 ± 2	9%	1%	2%	87±9
3	Et	H	52 ± 5	11%	6%	1%	245±23
4	Ph	H	10%	22%	10%	4%	
5	Ph-CH_2	H	900 ± 95	11%	1%	4%	>1000
6	H	4-OMe	54 ± 6	2%	1%	3%	270±26
7	Me	4-OMe	1.2 ± 0.1	5%	1%	2%	5.2±0.5
8	Et	4-OMe	14 ± 2	1%	1%	5%	63±7
9	Ph	4-OMe	16%	1%	1%	5%	
10	Ph-CH_2	4-OMe	250 ± 27	10%	1%	4%	850±76
11	Me	4-Me	10 ± 1	1%	1%	4%	46±5
12	Me	3-Me	72 ± 8	4%	1%	2%	354±33
13			12%	4%	5%	2%	

[a] Displacement of specific [^{125}I]AB-MECA binding to hA_3 CHO cells, where K_i values are mean values ± SEM of four separate assays each performed in duplicate. Percentage of inhibition in [^{125}I]AB-MECA competition binding assays to hA_3 CHO cells at 1 μM tested compounds.

[b] Percentage of inhibition in [^{3}H]DPCPX competition binding assays to hA_1 CHO cells at 1 μM tested compounds.

[c] Percentage of inhibition in [^{3}H]ZM241385 competition binding assays to hA_{2A} CHO cells at 1 μM tested compounds.

[d] Percentage of inhibition on cAMP experiments in hA_{2B}CHO cells, stimulated by 200 nM NECA, at 1 μM examined compounds.

[e] IC_{50} values are expressed as mean values ± SEM of four separate cAMP experiments in hA_3 CHO cells, inhibited by 100 nM Cl-IB-MECA.

Table 3.8: Binding Affinity (K_i) at hA_1AR, hA_{2A}AR, and hA_3AR and potency (IC_{50}) at hA_{2B}AR and hA_3AR of 2-arylpyrazolo[4,3-*d*]pyrimidin-7-one derivatives.

2-(4-methoxyphenyl) derivatives **6-10**, the 5-methylsubstituted compound **7** emerged as the most active (K_i hA_3 = 1.2 nM), confirming that the best substituent for the 5-position was the methyl group.

Thus, taking **2** as the lead derivative, we tested two further substituents on the 2-phenyl ring because in the triciclic PQ series they afforded the highest hA_3AR affinities, i.e., the 4-Me and 3-Me groups (compounds **11** and **12**). Both compounds **11** and **12** show high hA_3 affinity, in particular the 2-(4-methylphenyl)-substituted compound **11** (K_i hA_3 = 10 nM), but the 4-methoxy substituted derivative **7** remains the best in terms of hA_3 affinity.

Finally, introduction of an oxo function at the 5 position of the pyrazolo[4,3-*d*]pyrimidin-7-one nucleus exerted a deleterious effect, with compound **13** displaying null affinity at the hA_3AR.

All the new derivatives **1-3**, **5-8**, **10-12** were antagonists at the hA_3AR. They show inhibitory effects on Cl-IB-MECA-inhibited cAMP production, and their potencies are coherent with their hA_3 affinity values.

Molecular docking studies of the new 2-arylpyrazolo[4,3-*d*]-pyrimidin-7-one derivatives **1-13** were carried out on both hA_3 and hA_{2A} adenosine receptors to identify the hypothetical binding modes and to rationalize the observed structure-activity relationship.

From the docking simulation analysis, almost all the derivatives were seen to share a similar binding pose in the TM region of the hA_3AR. Ligand recognition occured in the upper region of the TM bundle, and the pyrazolo[4,3-*d*]pyrimidin-7-one scaffold was surrounded by TMs 3, 5, 6, 7 with the 2-phenyl ring pointing toward EL2 and the substituent at the 5 position (R_5) oriented toward the intracellular environment.

Figure 3.25 (panel C on the left) shows the hypothetical binding mode of compound **7**, which possesses the highest hA_3 affinity among all the newly synthesized derivatives (K_i hA_3 = 1.2 nM). This compound was anchored, inside the binding cleft, by two stabilizing hydrogen-bonding interactions with the amide moiety of Asn250 (6.55) side chain. The two hydrogen bonds involved the carbonyl group at the 7-position and one of the N atoms of the pyrazole ring, respectively. The asparagine residue 6.55, conserved among all AR subtypes, was already found to be important for ligand binding at both the hA_3 and hA_{2A}ARs. [87, 71] Compound **7** also formed hydrophobic interactions with many residues of the binding cleft including Leu90 (3.32), Leu91 (3.33), Phe168 (EL2), Val169 (EL2), Met177 (5.38), Trp243 (6.48), Leu246 (6.51), Leu264 (7.35), Tyr265 (7.36), Ile268 (7.39). In particular, the 2-phenyl ring formed an aromatic π-π stacking interaction with Phe168 (EL2), while the pyrazolo[4,3-*d*]pyrimidin-7-one core interacted with the highly conserved Trp243 (6.48), an important residue in receptor activation and in antagonist binding. [71]

The 2-arylpyrazolo[4,3-*d*]pyrimidin-7-one derivatives bearing non-bulky moieties at the 5-position, such as 5-hydrogen atom (compounds **1** and **6**),

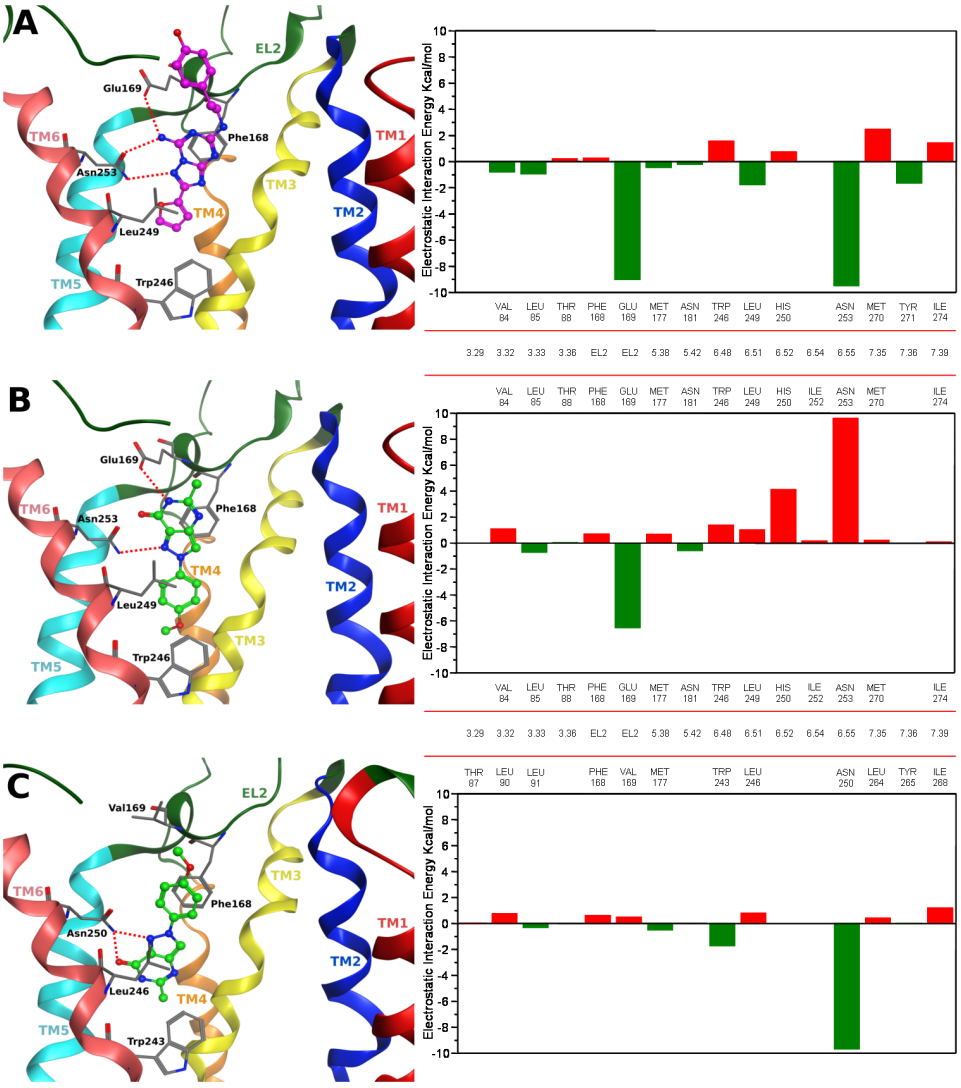

Figure 3.25: (A) Crystallographic binding mode of ZM241385 inside the hA_{2A} receptor (PDB ID: 3EML) and hypothetical binding mode of compound **7** obtained after docking simulations (B) inside the $hA_{2A}AR$ binding site and (C) inside the hA_3AR binding site. Side chains of some amino acids important for ligand recognition and H-bonding interactions are highlighted. The view of TM7 is voluntarily omitted and hydrogen atoms are not displayed. Beside each pose, the graph displays the electrostatic interaction energy (in kcal/mol) between the ligand and each single amino acid involved in ligand recognition.

5-methyl group (compounds **2**, **11**, and **12**), and 5-ethyl group (compounds **3** and **8**), showed a similar binding mode compared to compound **7**. In fact, for all these derivatives, the pyrazolo[4,3-*d*]pyrimidin-7-one core was perfectly aligned inside the TM region of the hA_3 receptor. In particular, the two hydrogen bonds with Asn250 (6.55), the aromatic stacking interaction with Phe168 (EL2), and the hydrophobic interaction with Trp243 (6.48) were conserved.

In contrast, binding poses of compounds bearing bulkier substituents, including 5-phenyl and 5-benzyl groups (compounds **4**, **5**, **9**, and **10**), were quite different. The 2-phenyl ring of these compounds was directed toward the intracellular environment rather than toward EL2, while the substituent at the 5 position pointed toward TM2. Because of this different orientation of the molecule inside the binding cleft, these derivatives lost one of the two H-bonding interactions with Asn250 (6.55) and the π-π stacking interaction between Phe168 (EL2) and the 2-phenyl ring (data not shown). The lack of these important interactions seemed to be the reason why derivatives with bulky R_5 groups showed low or null hA_3AR affinities.

Compound **13** (bearing an oxo function at the 5-position) showed a completely different docking pose inside the hA_3 binding pocket, compared to all the other derivatives, and its orientation was almost parallel to the membrane plane. Even though this molecule formed two H-bonding interactions with Asn250 (6.55), it was too far to interact with Trp243 (6.48), and so it lost the interaction with this important residue (data not shown).

With regard to the presence of a substituent on the 2-phenyl ring (R_2), it emerged that small groups (methyl and methoxy) enhanced the hA_3 affinity even though they did not seem to be involved in particular interactions with residues of the binding pocket. Nevertheless, these substituents, because of their electron-donating properties, could reinforce the π-π stacking interaction of the 2-phenyl ring with the receptor. In addition, the methyl and methoxy groups increased the topological complementarity of these compounds with the TM binding cavity.

As shown in Figure 3.25 (panel B on the left), the hypothetical binding pose of compound **7**, obtained after molecular docking to the crystal structure of the hA_{2A} receptor, was quite different compared to the pose of the same compound at the hA_3 subtype (Figure 3.25, panel C on the left), although ligand recognition occured in the same region of the TM bundle. In particular, the 2-phenyl ring pointed toward the intracellular environment and the substituent at the 5 position was oriented toward EL2. The molecule formed two H-bonds, with Asn253 (6.55) and Glu169 (EL2), and an aromatic interaction with Phe168 (EL2).

All the newly synthesized derivatives **1-13** showed this same binding mode inside the hA_{2A} receptor pocket. Although the predicted binding affinities were lower with respect to those estimated for the corresponding binding to the hA_3 receptor (around 3-9 kcal/mol), this only partially justified the

absence of A_{2A} binding observed experimentally.

From the analysis of the *per residue* electrostatic contributions to the interaction energy, one of the most critical residues affecting the affinity at ARs seemed to be the asparagine 6.55 (Asn253 in hA_{2A} and Asn250 in hA_3). In particular, Asn253 is responsible for two stabilizing interactions with ZM241385 into human A_{2A}AR (Figure 3.25, panels A). This is confirmed by the electrostatic contribution of around -10 kcal/mol to the whole interaction energy. Considering the binding poses of compound **7**, the electrostatic contribution of this asparagine residue to the interaction energy was completely different between hA_{2A} and hA_3 receptors (see Figure 3.25, panels B and C on the right, respectively). Asn250 (6.55) strongly stabilized the ligand-hA_3 receptor complex (negative electrostatic interaction energy) because of the two hydrogen bonding interactions, while Asn253 (6.55) destabilized the ligand-hA_{2A} receptor complex (positive electrostatic interaction energy). This detrimental contribution to the stability of the complex was due to the electrostatic repulsion between the oxo moiety of the pyrazolo[4,3-*d*]pyrimidin-7-one nucleus and the carbonyl group of Asn253 side chain. This could considerably reduce the permanence of the 2-arylpyrazolo[4,3-*d*]pyrimidin-7-one analogues in the TM binding pocket and explain the null affinity of these new derivatives for the hA_{2A}AR.

Moreover, comparing the docking pose of compound **7** at the hA_{2A} receptor with the crystallographic pose of the antagonist ZM241385, it can be noted that the bicyclic core of the pyrazolo[4,3-*d*]pyrimidin-7-one derivative was almost aligned with the bicyclic region of ZM241385. Nevertheless, the exocyclic amino group (H-bond donor) of ZM241385 is replaced with a carbonyl group (H-bond acceptor) in compound **7**, and this could lead to the substantially different affinities at the hA_{2A} receptor. The values of the electrostatic contributions to the binding energies were also coherent with this recognition scenario.

Therefore, as previously seen as well, it appeared that two critical residues in determining the binding affinity of antagonists at the hA_{2A}AR were Glu169 (EL20) and Asn253 (6.55). Moreover, once again, the mutation Glu/Val at position 169 of hA_{2A} and hA_3 receptors seemed to be important in determining the selectivity profiles of ARs antagonists since this difference could influence not only the binding mode but also the entrance of ligands into the TM region of these receptors as already described in section 3.1.

3.5.2 Phthalazinone derivatives

Another tricyclic scaffold that gave interesting results in the ARs antagonists field was the 2-aryl-1,2,4-triazolo[4,3-*a*]quinoxalin-1-one (TQX) nucleus. [107, 95, 96] In previous studies, was reported that the TQX core can be simplified into easily synthesizable 4-carboxamido-quinazoline (QZ) derivatives endowed with high affinity and selectivity toward hA_3AR. [108]

Many other bicyclic heteroaromatic systems, containing those structural features essential to guarantee an efficient ligand-receptor recognition, have been taken into consideration as a possible core skeleton for the design of novel hA_3AR antagonists. Among them, our attention has been caught by the phthalazin-1(2H)-one (PHTZ) ring system that has not yet been considered as a suitable scaffold to obtain AR antagonists. The interest for this new series of PHTZ analogues was driven by the structure similarity between the phthalazin-1(2H)-one skeleton and both TQX and QZ scaffolds extensively investigated in previously reported studies (Figure 3.26). [107, 95, 96, 108] Particular attention was focused on position 4 of the phthalazine ring system, where differently substituted amido and ureido moieties were introduced (compounds **2-20**, Table 3.9). In contrast, the 2-phenyl-substituent was held constant.

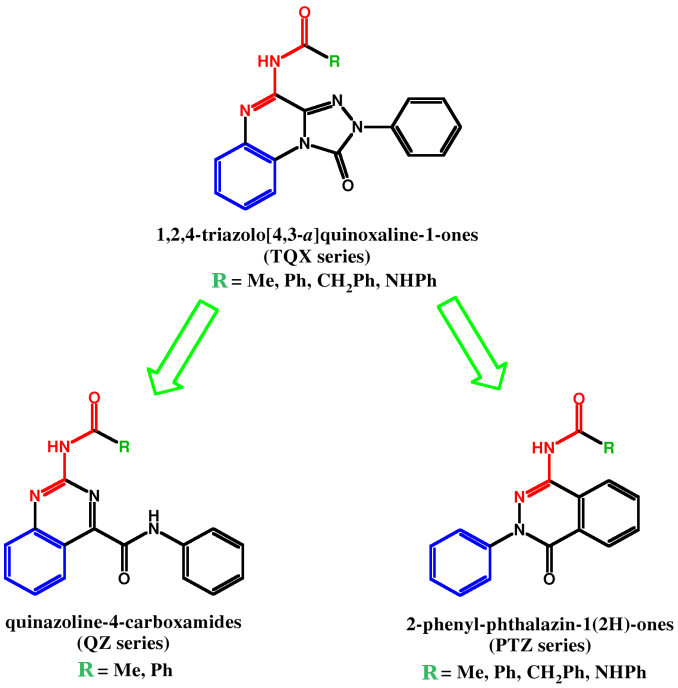

Figure 3.26: Simplification approach: from the TQX series to the QZ series and to the herein reported 2-phenylphthalazin-1(2H)-one derivatives (PHTZ series). Colors identify important conserved groups in different series.

The newly synthesized 4-substituted-phthalazinone derivatives **2-20** and the parent **1** (Table 3.9) were tested for their ability to displace radioligands from hA_1AR, $hA_{2A}AR$ and hA_3AR to determine their affinity and selectivity profiles. Moreover, the potencies (IC_{50}) of some selected compounds (**12-14**, **18**, and **19**) at the $hA_{2B}AR$ and the hA_3AR were determined (Table 3.10). The binding data of derivatives **1-20** are shown in Ta-

ble 3.9 together with those of **A** (1,2-dihydro-2-phenyl-4-phenylureido-1,2,4-triazolo[4,3-*a*]quinoxalin-1-one) [95] and **B** (2-benzoylaminoquinazoline-4-carboxyanilide), [108] selected as reference compounds of the TQX and QZ series, respectively.

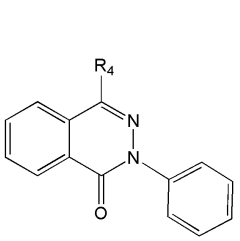

1-20

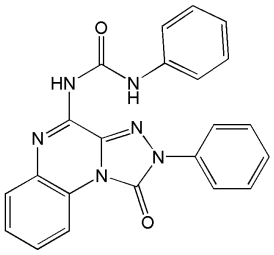

A

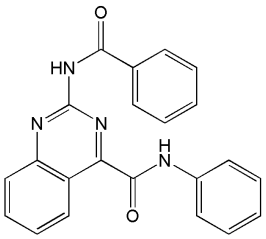

B

Compd	**R**$_4$	K_i (nM)[a] or I % hA$_3$[b]	hA$_1$[c]	hA$_{2A}$[d]
1	NH_2	8%	24%	45%
2	$NHCOCH_3$	0%	52%	14%
3	$N(COCH_3)_2$	0%	47%	10%
4	$NHCOC_6H_5$	1100 ± 100	44%	35%
5	$NHCOC_6H_4$-4Cl	17%	26%	17%
6	$NHCOC_6H_4$-4OCH_3	10%	0%	17%
7	NHCO(furan-2-yl)	8%	23%	41%
8	$NHCOCH_2C_6H_5$	28%	23%	4%
9	$NHCONHC_6H_5$	178.4 ± 17	44%	42%
10	$NHCONHC_6H_4$-4Cl	13%	10%	9%
11	$NHCONHC_6H_4$-2Cl	49%	0%	3%
12	$NHCONHC_6H_4$-4OCH_3	60.6 ± 6.2	4%	51%
13	$NHCONHC_6H_4$-3OCH_3	9.75 ± 0.25	45%	28%
14	$NHCONHC_6H_4$-2OCH_3	8.9 ± 1	0%	17%
15	$NHCONHC_6H_4$-4CH_3	45%	29%	0%
16	$NHCONHC_6H_4$-2CH_3	22%	20%	28%
17	$NHCONHC_6H_3$-2,4OCH_3	33%	29%	33%
18	$NHCONHC_6H_3$-2,5OCH_3	0.776 ± 0.037	0%	19%
19	$NHCONHCH_2C_6H_5$	29.6 ± 3	20%	23%
20	$NHCONHCH_2C_6H_4$-2OCH_3	274.2 ± 26	28%	28%
A[e]	-	276 ± 21	50.8 ± 4.2[f]	2300 ± 291[f]
B[g]	-	182 ± 10	7%	10%

[a] The K_i values are means ± SEMs of four separate assays, each performed in triplicate.
[b] Displacement of specific [^{125}I]AB-MECA binding at hA$_3$ receptors expressed in CHO cells or percentage of inhibition (I%) of specific binding at 1 μM.
[c] Displacement of specific [^{3}H]DPCPX at hA$_1$ receptors expressed in CHO cells or percentage of inhibition (I%) of specific binding at 10 μM concentration.
[d] Displacement of specific [^{3}H]NECA binding at hA$_{2A}$ receptors expressed in CHO cells or percentage of inhibition (I%) of specific binding at 10 μM concentration.
[e] Ref [95].
[f] Displacement of specific [^{3}H]CHA and [^{3}H]CGS21680 binding at A$_1$ and A$_{2A}$ receptors, respectively, in bovine brain membranes.
[g] Ref [108].

Table 3.9: Binding affinity (K_i) at hA$_3$, hA$_1$, and hA$_{2A}$ ARs of 4-substituted-2-phenylphtalazin-1(2H)-one derivatives **1-20** and of reference compounds **A** and **B**, of the TQX and QZ series.

Compd	cAMP assays IC_{50} (nM) or I%	
	hA_{2B}[a]	hA_3[b]
12	0%	28 ± 3
13	57%	18 ± 2
14	16%	17 ± 1.6
18	0%	8.25 ± 0.6
19	34%	1.15 ± 0.02

[a] Percentage of inhibition on cAMP experiments in hA_{2B} CHO cells stimulated by 100 nM NECA at different examined compound concentrations (1 nM to 10 μM).

[b] IC_{50} values represent the means ± SEMs of three separate experiments in hA_3 CHO cells, inhibited by 100 nM NECA at different examined compound concentrations (1 nM to 10 μM).

Table 3.10: Potencies (IC_{50}) at hA_{2B}AR and hA_3AR of some selected 4-substituted-2-phenylphtalazin-1(2H)-one derivatives.

Examining the binding results reported in Table 3.9, it appears that we have identified some new potent and selective adenosine hA_3 receptor antagonists belonging to the 2-phenylphtalazin-1(2H)-one series. In particular, it has to be noted that compounds **12-14**, **18**, and **19** bearing a methoxyphenyl- or a benzyl-substituted ureido moiety at position 4 are those endowed with high affinity and also selectivity toward the hA_3 receptor, as they are on the whole unable to bind at all the others ARs. These preliminary results indicate that the 2-phenylphthalazin-1(2H)-one moiety is a versatile tool for the design of new potent and selective hA_3AR antagonists. However, it is rather evident that clear and robust SARs can be difficult to obtain.

To start in, the binding affinity at the hA_3 receptor of the 4-amino-2-phenylphtalazin-1(2H)-one **1** (I hA_3 = 8%) was very discouraging, in particular because it was not in line with that of the 4-amino-2-phenyl-1,2,4-triazolo[4,3-a]quinoxalin-1-one (K_i hA_3 = 490 nM) [95] or 2-aminoquinazoline-4-carboxyanilide (K_i hA_3 = 350 nM) [108] belonging to the reference TQX and QZ series, respectively.

Despite this unfavorable starting point and on the basis of the SARs derived from both TQX and QZ hA_3AR antagonists, a series of 4-amido- (**2-8**) and 4-ureido-derivatives (**9-20**) were synthesized starting from the 4-amino intermediate **1**. All of the 4-amido compounds, including alkyl- (**2** and **3**), aryl- (**4-7**), and also arylalkyl-substituted (**8**), were inactive with the only exception being the 4-phenylamido derivative **4** that showed a K_i value of 1100 nM at the hA_3AR.

Very interestingly, replacement of the phenylamido- (**4**) with the phenylureido moiety (**9**) at the 4 position provided an appreciable increase of

receptor affinity. In fact, the 4-phenylureido derivative **9** was about 6-fold more active (K_i hA_3 = 178.4 nM) than its amido analogue **4**. As previously described for other ureido-related hA_3AR antagonists, [109] the urea moiety contributes to the observed large differences among the hA_3 binding affinities of these derivatives. Thus, the presence of a second NH group able to reinforce the hydrogen bond network within the putative transmembrane binding cavity appears to be primarily responsible for the ameliorating effect of the receptor-antagonist recognition.

Starting from the encouraging hA_3 binding data of the 4-phenylureido compound **9**, we decided to explore the role of a substituted phenyl ring at the level of the 4-ureido moiety by introducing groups with different electronic and lipophilic properties at position *ortho*, *meta*, or *para*. Insertion of the electron-withdrawing and lipophilic chloro atom at position *para* or *ortho* produced, respectively, a total loss (compound **10**) or a dramatic reduction (compound **11**) of receptor affinity at the hA_3 subtype. The strong electron-donating methoxy group was then introduced on the targeted 4-phenylureidomoiety leading to the *para*-substituted compound **12**, which was shown to be highly potent at the adenosine hA_3 receptor subtype (K_i hA_3 = 60.6 nM). Next, the *para*-methoxy substituent of **12** was moved to position *meta* and *ortho* to evaluate whether this shift could further optimize the anchoring at the hA_3 receptor site. This modification led, respectively, to compounds **13** and **14**, which are two of the most potent and selective hA_3AR antagonists belonging to the new 2-phenylphthalazin-1(2H)-one series here reported.

Accordingly, we evaluated the effect on hA_3AR affinity of introduction of another methoxy group on the 4-substituent of **14** by synthesizing the 2,4-dimethoxy and 2,5- dimethoxyphenyl-substituted compounds **17** and **18**, respectively. The second methoxy substituent introduced at the 5 position of the phenyl ring of **14** contributes positively to hA_3AR affinity, which showed an 11-fold increase (compare **18** to **14**). In fact, the (2,5-dimethoxyphenylureido)-phthalazin-1(2H)-ones **18** is the most potent hA_3AR antagonist among this series, with a K_i value of 0.776 nM and at least 10000-fold selectivity over hA_1 and hA_{2A} receptors. Unexpectedly, the 2,4-dimethoxy-substitued compound **17** as well as the 4-(4-methylphenyl)- and 4-(2-methylphenyl)-ureido derivatives **15** and **16** did not show any appreciable binding affinity toward the hA_3AR.

Introduction of a benzyl-ureido moiety at the 4 position of the phthalazin-1(2H)-one scaffold led to compound **19**, which revealed to be 6-fold more active than the homologue **9** at the hA_3AR (K_i hA_3 = 29.6 nM). Finally, the highly profitable methoxy group was introduced at the *ortho* position on the benzylic group of **19**, yielding compound **20** that unexpectedly showed a 9-fold decreased hA_3 affinity.

Among the new PHTZ series, compounds **12**-**14**, **18**, and **19** possessed the highest hA_3 affinity and selectivity versus both hA_1 and hA_{2A} recep-

tors. To determine also their hA_3 versus hA_{2B} selectivity, we tested these derivatives in cAMP assays, which evidenced low or null hA_{2B} affinity, being in general ineffective in inhibiting NECA-stimulated cAMP levels in hA_{2B} CHO cells. Furthermore, the effect of compounds **12-14**, **18**, and **19** in limiting the NECA-inhibited cAMP accumulation in hA_3 CHO cells was determined. Coherently with their high hA_3 affinity, all of the selected PHTZ derivatives proved to be very potent in this test, showing an antagonistic behavior (Table 3.10).

Trying to explain the observed structure-affinity relationship and the selectivity profile of these new 2-phenylphthalazin-1(2H)-one derivatives, a receptor-driven molecular modeling investigation was performed.

Since the new 2-phenylphthalazin-1(2H)-one derivatives reported in this section were conceived as simplified analogues of previously synthesized 1,2,4-triazolo[4,3-*a*]quinoxaline-1-one compounds (TQX series), [107, 95, 96] molecular docking studies were performed on all of the PHTZ derivatives (compounds **1-20**) and on the TQX derivative **A**, taken as reference. Moreover, docking simulations were also performed on compound **B**, a quinazoline-4-carboxamide derivative (QZ series) previously reported. [108]

Therefore, all of the selected compounds were docked into the TM binding site of the hA_3AR three-dimensional model, to identify their hypothetical binding modes at this receptor and to analyze possible analogies among the different series. In addition, docking simulations at the hA_{2A}AR crystal structure were carried out to explain the hA_3 versus hA_{2A} selectivity profile of all of these derivatives.

Analysis of the docking results revealed that all of the studied compounds (**1-20**, **A**, and **B**) share a binding pose that is somehow similar in the TM region of the hA_3AR. In fact, at this receptor, ligand recognition occured in the upper region of the TM bundle, and the tricyclic or bicyclic scaffold of the ligands was surrounded by TMs 3, 5, 6, and 7.

Figure 3.27 panel A shows the hypothetical binding mode of the reference TQX derivative **A** (K_i hA_3 = 276 nM). This compound was anchored, inside the binding cleft, by three stabilizing hydrogen-bonding interactions with the side chain of Asn250 (6.55). These three hydrogen bonds involved the N^5 atom of the TQX nucleus and the two NH groups of the 4-ureidic moiety, respectively. The asparagine residue 6.55, conserved among all of the AR subtypes, was already found, through mutagenesis studies, [87, 71] to be important for ligand binding at both the hA_3 and the hA_{2A}ARs. Compound **A** also formed hydrophobic interactions with many residues of the binding cleft including Ala69 (2.61), Val72 (2.64), Leu90 (3.32), Leu91 (3.33), Phe168 (EL2), Val169 (EL2), Met177 (5.38), Trp243 (6.48), Leu246 (6.51), Ile249 (6.54), Ile253 (6.58), Val259 (EL3), Leu264 (7.35), Tyr265 (7.36), and Ile268 (7.39). In particular, the planar tricyclic core of the ligand strongly interacted with Phe168 (EL2) and with the highly conserved Trp243 (6.48), an important residue for receptor activation and antagonist binding. [71]

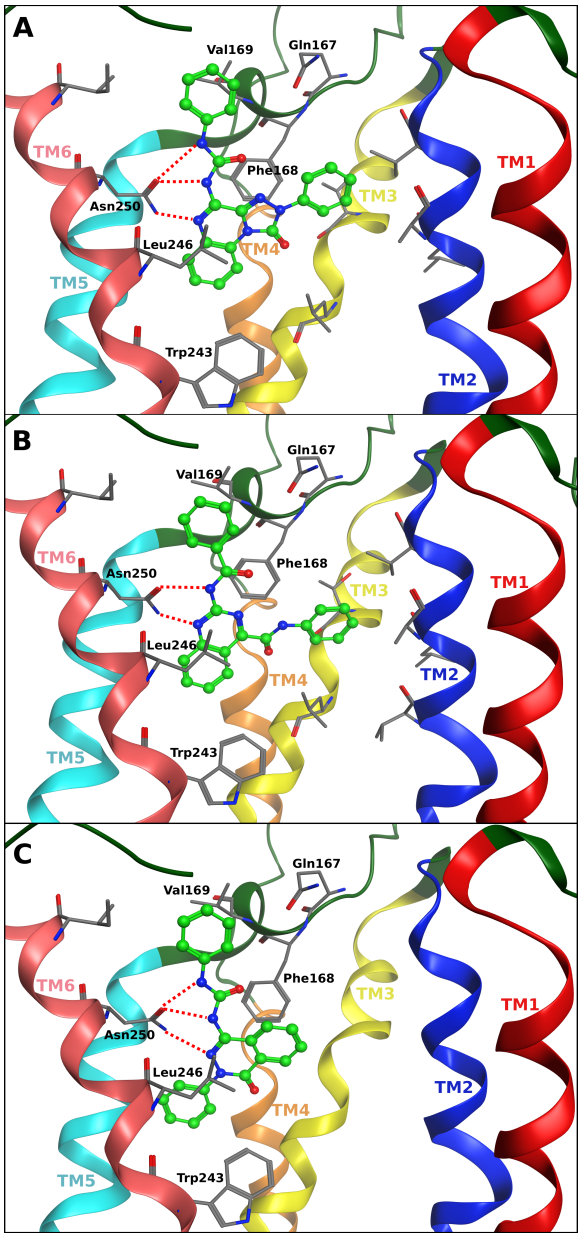

Figure 3.27: Hypothetical binding modes obtained after docking simulations inside the hA_3AR binding site of (A) compound **A**, (B) compound **B**, and (C) compound **9**. Poses are viewed from the membrane side facing TM6, TM7, and TM1. The view of TM7 is voluntarily omitted. Side chains of some amino acids important for ligand recognition and H-bonding interactions are highlighted. Hydrogen atoms are not displayed.

As shown in Figure 3.27 panel B, the hypothetical binding pose of the QZ derivative **B** (K_i hA_3 = 182 nM), obtained after molecular docking into the three-dimensional model of the hA_3AR, was very similar to that of compound **A** (Figure 3.27 panel A). In fact, ligand recognition occured in the same region of the TM bundle. In particular, the appended phenyl ring on the 4-carboxyamide moiety of **B** was oriented toward TM2, such as the 2-phenyl ring of the TQX derivative **A**, and the 2-benzoylamino group of **B** pointed toward the extracellular loop region, such as the 4-phenylureido moiety of compound **A**. Moreover, compound **B** formed two H-bonds with Asn250 (6.55) and a strong hydrophobic interaction with Phe168 (EL2).

It is worth noting that in compound **B** the formation of an intramolecular H-bond between the nitrogen at the 3-position of the quinazoline system and the NH of the amide moiety at the 4-position leads to the stabilization of a conformer, which simulates a planar tricycle with similar steric properties to the original TQX analogue (compound **A**). The planarity of the QZ derivative, due to this intramolecular H-bond, seemed to increase complementarity with the hA_3 receptor; the key role of this intramolecular H-bond was already analyzed in previous docking studies of the QZ derivatives carried out on the rhodopsin-based homology model of hA_3AR. [108]

The hypothetical binding mode, at the hA_3AR, of one of the herein reported 2-phenyl-phthalazin-1(2H)-ones (compound **9**, K_i hA_3 = 178.4 nM) is displayed in Figure 3.27 panel C. Molecular docking simulations showed that the new compound **9** was efficiently accommodated into the TM binding cavity with the 4-phenylureido substituent directed toward the extracellular loop region. Interestingly, compound **9** maintained all of the crucial interactions already seen for the TQX and QZ derivatives and also a similar binding pose. This ligand formed three hydrogen-bonding interactions with the Asn250 (6.55) side chain, involving the N3 atom of the PHTZ nucleus and the two NH groups of the ureidic moiety, respectively. In addition, the phthalazinone scaffold formed a π-π stacking interaction with Phe168 (EL2). Other hydrophobic interactions were established with several residues of the binding cavity, such as Ala69 (2.61), Leu90 (3.32), Leu91 (3.33), Val169 (EL2), Met177 (5.38), Phe182 (5.43), Ile186 (5.47), Trp243 (6.48), Leu246 (6.51), Ile249 (6.54), Ile253 (6.58), Val259 (EL3), Leu264 (7.35), and Ile268 (7.39). The described docking pose of compound **9** reflects more or less the hypothetical binding mode of all of the analyzed 2-phenylphthalazin-1(2H)-one derivatives (compounds **1**-**20**).

In addition, electrostatic and hydrophobic interaction contributions between compounds **9**, **A**, and **B** and each amino acid involved in ligand recognition (Figures 3.28 and 3.29, respectively) were calculated from the hypothetical binding modes at the hA_3AR displayed in Figure 3.27. Analysis of these data confirmed the hypothesis of an analogous binding mode at the hA_3AR for the TQX, QZ, and PHTZ derivatives here reported.

As shown in Figure 3.28, it is clear that, from the electrostatic point of

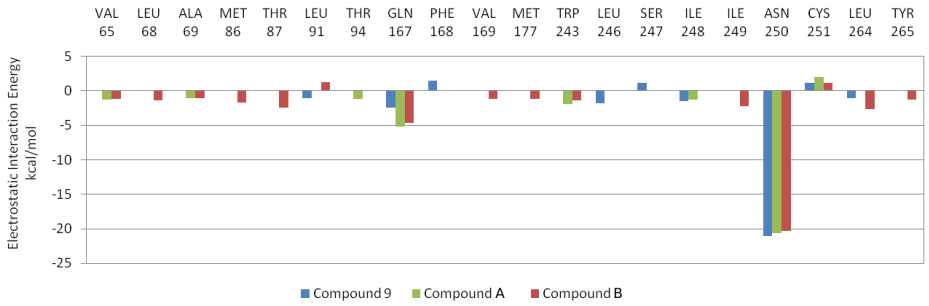

Figure 3.28: Electrostatic interaction energy (in kcal/mol) between compounds **9**, **A**, and **B** and each single amino acid involved in ligand recognition calculated from the hypothetical binding modes inside the hA_3AR.

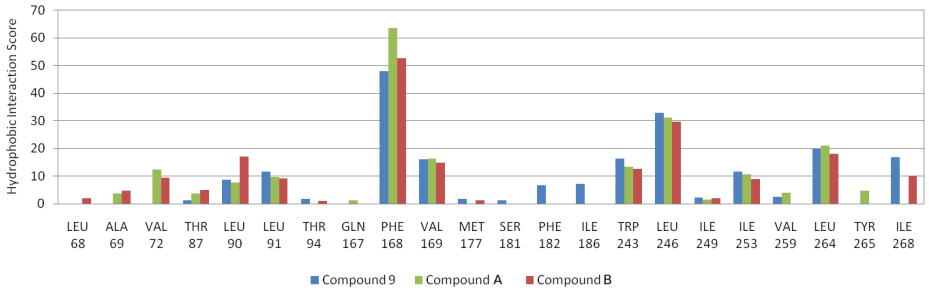

Figure 3.29: Hydrophobic interaction score (in arbitrary hydrophobic unit) between compounds **9**, **A**, and **B** and each single amino acid involved in ligand recognition calculated from the hypothetical binding modes inside the hA_3AR.

view, one of the most critical residues affecting the affinity at the hA_3AR seemed to be Asn250 (6.55) that is responsible for the stabilizing H-bonding interactions with all of the three ligands. This was supported by the Asn250 electrostatic contribution of around -20 kcal/mol to the whole interaction energy of the three ligand-receptor complexes. Moreover, no significant detrimental electrostatic contributions (positive electrostatic interaction energy) were observed for these complexes.

The hydrophobic interactions mapped in Figure 3.29 show a similar pattern for all of the three ligand-receptor complexes. In particular, the most important hydrophobic contribution was mediated by Phe168 (EL2), conserved among all ARs, which strongly interacted with the bicyclic/tricyclic core of the ligands. In addition, the ligand scaffold was involved in hydrophobic contacts with Leu90 (3.32), Leu91 (3.33), Trp243 (6.48), Leu246 (6.51), and Ile268 (7.39), while the phenyl ring appended on the ureido/ amido moiety interacted with Val169 (EL2), Ile253 (6.58), and Leu264 (7.35).

Some aspects of the SAR of this phthalazinone series were very difficult to rationalize. Surprisingly, some substituents, such as phenylamido and benzylamido, that positively affected the affinity in other series of hA_3AR antagonists, showed, in contrast, discouraging results in these new compounds. The proposed binding mode seems to partially explain why compounds bearing a 4-ureido substituent possessed higher affinity at the hA_3AR than the 4-amido analogues. In fact, the increased affinities of the 4-ureido-derivatives could be due to the formation of an additional H-bonding interaction with the Asn250 (6.55) carbonyl group.

With regard to the substituents on the phenyl ring appended on the 4-ureido moiety, the binding data showed that both of their features, electron-donating or electron-withdrawing, and their position played a crucial role in modulating the affinity at the hA_3AR. Considering the proposed binding mode at this receptor subtype, it is clear that such substituents were located near the extracellular loop region and could possibly interact with residues belonging to EL2 and EL3. Because of the difficult characterization and the high plasticity of the loop region, it is hard to accurately predict particular interactions with this part of the ligand and therefore to explain the observed effects of these substituents. Some amino acids possibly involved in interactions with the substituted phenyl ring are Gln167 (EL2), Val169 (EL2), Met174 (5.35), Ile253 (6.58), Val259 (EL3), and Leu264 (7.35).

Further studies are in progress in our laboratory to better define the extracellular loops conformation that could be responsible for the interaction with the substituents at the 4-position of these ligands.

As far as the $hA_{2A}AR$ is concerned, docking simulations performed for compounds **1-20** revealed no good binding poses at this receptor subtype, as highlighted by the docking pose of compound **9** at the $hA_{2A}AR$ displayed in Figure 3.30, panel A. In fact, at the $hA_{2A}AR$, compound **9** resulted to be turned of 180° as compared to the docking pose of the same compound in-

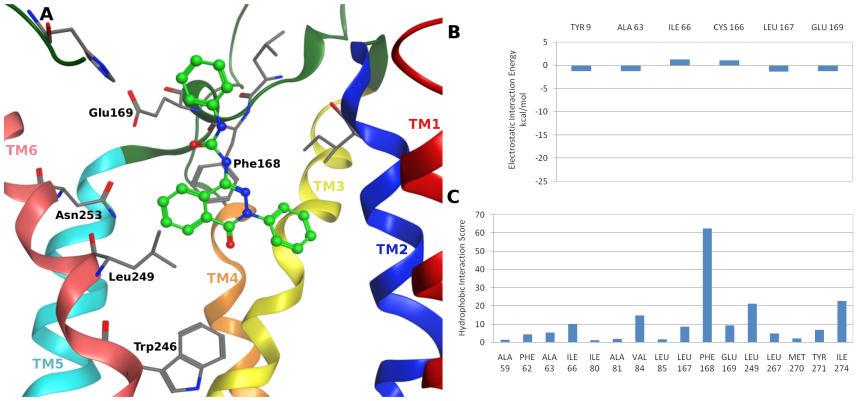

Figure 3.30: (A) Hypothetical binding mode obtained after docking simulation inside the $hA_{2A}AR$ binding site of compound **9**. The pose is viewed from the membrane side facing TM1, TM6, and TM7. The view of TM7 is voluntarily omitted. Hydrogen atoms are not displayed. (B) Electrostatic interaction energy (in kcal/mol) between compound **9** and each single amino acid involved in ligand recognition calculated from the hypothetical binding mode inside the $hA_{2A}AR$. (C) Hydrophobic interaction score (in arbitrary hydrophobic unit) between compound **9** and each amino acid involved in ligand recognition calculated from the hypothetical binding mode inside the $hA_{2A}AR$.

side the hA_3AR binding site, probably due to the presence of Glu169 (EL2) and of the steric hindrance of the substituent at the 4 position. As a consequence of this flipped orientation, compound **9** was not able to strongly interact with the critical residues Asn253 (6.55) or Glu169 (EL2) through H-bonds as instead previously noticed for the crystallographic binding pose of ZM241385 at the $hA_{2A}AR$ [44] and found in other docked compounds possessing antagonist activity at the $hA_{2A}AR$. [76]

Indeed, analyzing the *per residue* electrostatic and hydrophobic contributions for the docking pose of compound **9** inside the $hA_{2A}AR$ (Figure 3.30, panels B and C, respectively), it is evident the lack of any strong electrostatic interaction with residues of the binding site and the presence of only few strong hydrophobic interactions, such as the one with Phe168. This finding can explain the low or null affinity at the $A_{2A}AR$ subtype of all of the PHTZ compounds (**1-20**) here reported.

In conclusion, molecular docking studies of the newly synthesized 2-phenylphthalazin-1(2H)-ones, performed at the hA_3AR, revealed for these compounds a binding mode similar to that of the previously reported TQX and QZ derivatives, as was expected from the simplification approach. These three classes of hA_3AR antagonists showed analogous interactions with the binding cavity of the receptor as confirmed by the analysis of the electrostatic

and hydrophobic contributions to the interaction energy. Therefore, the analysis on all the three (TQX, QZ, and PHTZ) series led to the identification of converging ligand-receptor binding requirements, which were considered as essential features for profitable hA_3 receptor-antagonist recognition; further studies are in progress to better clarify these structural requirements and to develop new PHTZ derivatives with higher hA_3AR affinity.

3.5.3 Triazolo-pyrimidine and styril-furan derivatives

Another interesting bicyclic scaffold for the development of ARs antagonists is the 1,2,4-triazolo[1,5-*c*]pyrimidine nucleus that was investigated as a molecular simplification of the pyrazolo-triazolo-pyrimidine (PTP) nucleus and as a deaza analogues of triazolo-triazine core. In fact, a new class of compounds based on the triazolo-pyrimidine nucleus has been synthesized, including derivatives bearing different substituents at the 5 and 8 positions, to analyze their binding profile at the four human AR.

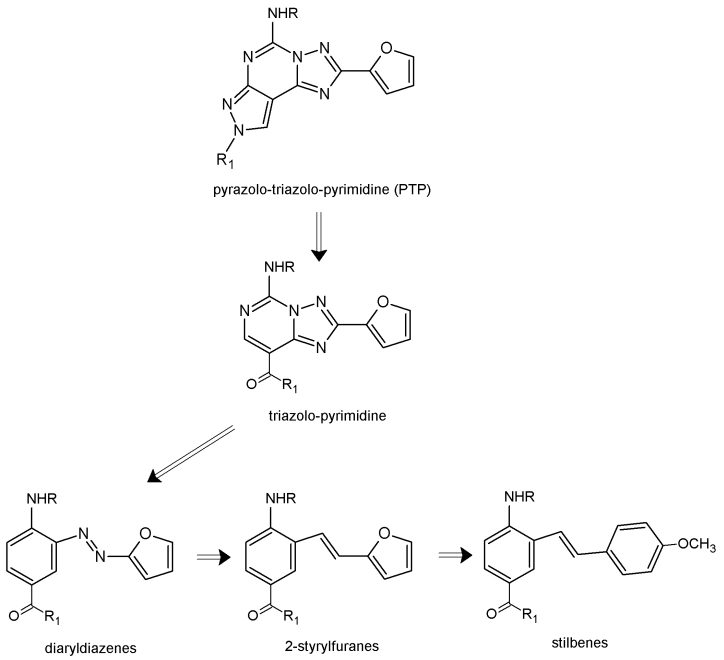

Figure 3.31: Rational for the design of stilbene and 2-styryl-furan derivatives.

In particular, arylcarbamoyl or arylacetyl moieties, which gave good results in the pyrazolo-triazolo-pyrimidine family were introduced at the N^5 position, while various amides and esters were present at the 8 position. This series did not display very good affinities at the A_3AR, but an urea or a phenylacetamide group at the 5 position favoured the binding at the $A_{2A}AR$.

Subsequently, with the intent of further simplify the triazolo-pyrimidine nucleus, we proposed other classes of compounds as potential adenosine receptors antagonists, such as the diaryl-diazenes, 2-styryl-furanes and stilbenes (see Figure 3.31). We started with the synthesis of few 2-styryl-furan derivatives and with the bioisosteric replacement of the furan ring with a *para*-methoxy phenyl ring to obtain some stilbene derivatives, as a preliminary study on this kind of very simplified molecules.

Docking studies at the hA_3AR and $hA_{2A}AR$ were performed for all of these new derivatives to confirm that these molecules are able to interact with those residues of the binding sites that several studies demonstrated to be critical for the binding of antagonists.

The affinity of all the synthesized compounds at the hA_1AR, $hA_{2A}AR$ and hA_3AR was determined using radioligands displacement tests; while their potency at the $hA_{2B}AR$ was evaluated determining the inhibition of NECA-stimulated adenylyl cyclase activity. Pharmacological data for some selected triazolo-pyrimidine, 2-styryl-furan and stilbene compounds are collected in Table 3.11 (complete data not shown, manuscript in preparation).

The synthesized triazolo-pyrimidine compounds showed affinities at the hA_3AR and/or $hA_{2A}AR$ ranging from high nanomolar to nanomolar concentrations, with different degree of selectivity versus the other receptor subtypes. The presence of a free amino group at the 5 position (compounds **5**-**7**) led to quite good interesting affinity versus the $hA_{2A}AR$. This finding is in agreement with the previously reported considerations obtained for $hA_{2A}AR$ antagonists, where the presence of a free amino group was important to bind two critical residues of the binding site. In particular combination of a free amino function at the 5 position and a ethoxycarbonyl moiety at the 8 position led to a derivative **7** which resulted to be potent and quite selective for the $hA_{2A}AR$. (K_i hA_{2A} = 3.32 nM). Instead, simultaneous introduction at the 8 position of a methyl carboxamido (**5**) or β-phenethylcarboxamido (**6**) groups produced a reduction of the affinity (3-5 fold) at the $hA_{2A}AR$ with a drastic reduction of selectivity as a consequence. On the other hand, when a dimethoxybenzyl groups is present at the N^5 position (**1**-**4**) a decent affinity at the hA_3AR was observed but the selectivity versus the other receptor subtypes was poor.

Concerning the 2-styryl-furan and stilbene series (compounds **8**-**13**), in general, at the $hA_{2A}AR$ and hA_3AR the furan ring was preferred to the 4-methoxy-phenyl moiety. As expected, the presence of a free amino group in the furan series (compound **11**, K_i hA_{2A} = 587 nM) gave best results in terms of affinity and selectivity for the hA_{2A} subtype. Surprisingly, an opposite behavior was observed in the anisole series, where affinity improved with the size of substituent at the 5 position. Concerning the hA_3AR the best compound was the 4-methylamino derivative (compound **12**) of the furan series that displays K_i of 973 nM at this subtype and selectivity of 10 and 3.5 times at the hA_1 and hA_{2A} ARs, respectively.

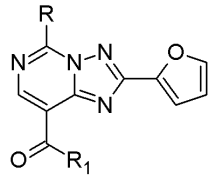

1-7

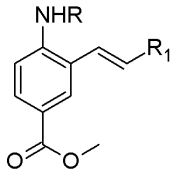

8-13

Compd	R	R_1	hA_1 (K_i nM)a	hA_{2A} (K_i nM)b	hA_{2B} (K_i nM)c	hA_3 (K_i nM)d
1	$NHCH_2Ph$-3,4OCH_3	OEt	315 (203-489)	116 (44.3-305)	13,300 (7,950-22,200)	38.7 (28.2-53.1)
2	$NHCH_2Ph$-3,4OCH_3	OH	958 (731-1,260)	5,320 (3,680-7,700)	> 30,000	159 (121-208)
3	$NHCH_2Ph$-3,4OCH_3	$NHCH_3$	428 (271-677)	25.8 (20.2-32.8)	2,490 (1,730-3,580)	282 (182-435)
4	$NHCH_2Ph$-3,4OCH_3	$NHCH_2CH_2Ph$	385 (291-511)	65.2 (43.9-96.9)	> 30,000	87.7 (71.7-107)
5	NH_2	$NHCH_3$	135 (104-174)	15 (10.6-21.3)	2,030 (1,470-2,796)	609 (459-808)
6	NH_2	$NHCH_2CH_2Ph$	57.1 (38.1-85.5)	11.1 (8.46-14.5)	5,320 (4,230-6,700)	140 (60.9-322)
7	NH_2	OEt	185 (92.5-371)	3.32 (2.03-5.42)	1,110 (683-1,810)	238 (144-395)
8	H	Ph-4-OCH_3	> 100,000	> 100,000	> 30,000	14,700 (11,400-19,000)
9	Me	Ph-4-OCH_3	> 30,000	16,200 (13,800-18,900)	> 30,000	3,500 (2,460-4,980)
10	Et	Ph-4-OCH_3	> 100,000	13,700 (11,000-16,900)	> 30,000	3,340 (2,800-3,990)
11	H	2-furyl	3,530 (2,380-5,230)	587 (441-781)	> 30,000	10,700 (7,980-14,300)
12	Me	2-furyl	10,400 (7,930-13,800)	3,430 (2,470-4,770)	> 30,000	973 (697-1,360)
13	Et	2-furyl	8,190 (5,230-12,800)	5,710 (3,690-8,840)	> 30,000	4,040 (3,300-4,940)

[a] Displacement of specific [^{3}H]-CCPA binding at human A_1 receptors expressed in CHO cells, (n = 3-6).
[b] Displacement of specific [^{3}H]-NECA binding at human A_{2A} receptors expressed in CHO cells.
[c] K_i values of the inhibition of NECA-stimulated adenylyl cyclase activity in CHO cells expressing hA_{2B} receptors.
[d] Displacement of specific [^{3}H]-NECA binding at human A_3 receptors expressed in CHO cells. Data are expressed as geometric means, with 95% confidence limits.

Table 3.11: Binding affinity (K_i) at the four human adenosine receptors of some new triazolo-pyrimidine, 2-styryl-furan and stilbene derivatives.

Molecular docking studies performed at the $hA_{2A}AR$ and hA_3AR helped to rationalize the collected binding results for these simplified compounds. In particular, it is interesting to compare the binding modes at the $hA_{2A}AR$ of compounds **5** and **11** displayed in Figures 3.32 and 3.33, respectively.

Considering Figure 3.32, it is evident that the binding pose of compound **5** (K_i hA_{2A} = 15 nM) was very similar to the crystallographic pose of ZM241385 bound to the $hA_{2A}AR$, [44] and the crucial interactions established by ZM241385 with amino acid residues of the $hA_{2A}AR$ binding site were also found for this new triazolo-pyrimidine derivative.

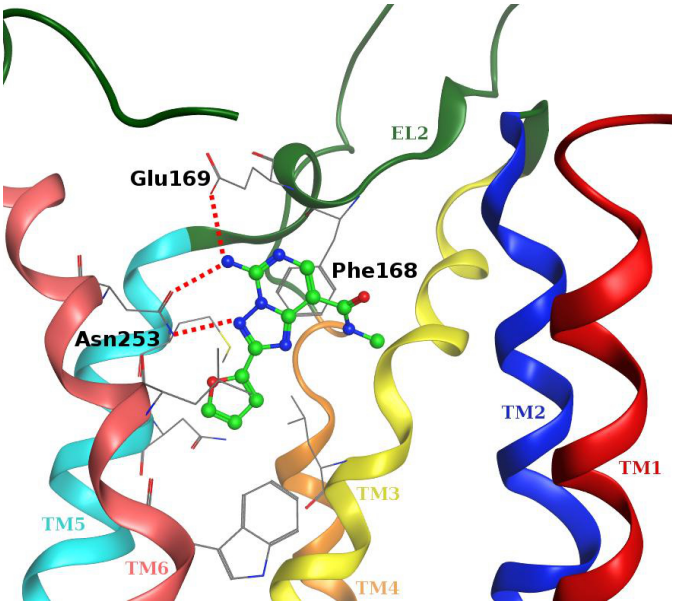

Figure 3.32: Hypothetical binding mode obtained after docking simulations of triazolo-pyrimidine compound **5** inside the $hA_{2A}AR$ binding site. Poses are viewed from the membrane side facing TM6, TM7 and TM1. The view of TM7 is voluntarily omitted. Side chains of some amino acids important for ligand recognition and H-bonding interactions are highlighted. Hydrogen atoms are not displayed.

In fact, it appeared that the bicyclic triazolo-pyrimidine core was anchored within the binding cleft through an aromatic stacking interaction with Phe168 (EL2) and a H-bonding interaction with Asn253 (6.55). Moreover, the exocyclic amino group at the 5 position of the bicyclic core interacted with Asn253 (6.55) and Glu169 (EL2), forming two H-bonds. The furan ring was located deep inside the binding cavity, in a position similar to the one of the furan ring of ZM241385, and formed hydrophobic interactions with the highly conserved Trp246 (6.48), Leu249 (6.51) and Leu85 (3.33). The substituent at the 8 position was located in a small lateral cleft but did not form strong interactions with residues of $hA_{2A}AR$.

On the other hand, docking pose of compound **11** (K_i hA_{2A} = 587 nM) inside the $hA_{2A}AR$ (Figure 3.33) showed a quite comparable binding mode. In particular, the phenyl ring of this derivative formed a strong aromatic stacking interaction with Phe168 (EL2); the furan ring was deeply located inside the binding cavity close to Trp246 (6.48); the methyl ester group was positioned in a small side cleft; and the free amino group formed two hydrogen bonds with Asn253 (6.55) and Glu169 (EL2). Therefore, some of the crucial interactions with the $hA_{2A}AR$ binding site observed for ZM241385 and compound **5** were conserved for this 2-styryl-furan derivative. However, this compound was missing one of the anchoring point constituted by an additional H-bond with Asn253 (6.55).

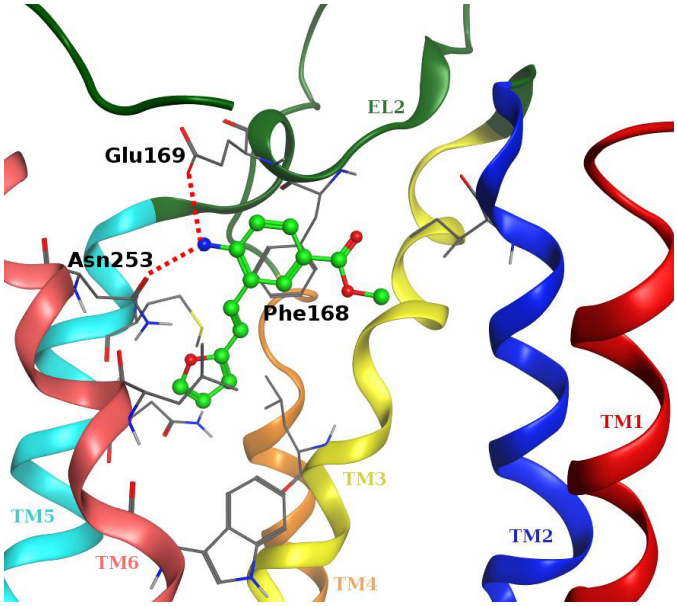

Figure 3.33: Hypothetical binding mode obtained after docking simulations of 2-styryl-furan compound **11** inside the $hA_{2A}AR$ binding site. Poses are viewed from the membrane side facing TM6, TM7 and TM1. The view of TM7 is voluntarily omitted. Side chains of some amino acids important for ligand recognition and H-bonding interactions are highlighted.

These observations, seemed to explain the affinity in the high nanomolar range of compound **11** in comparison with the low nanomolar range of the analogue triazolo-pyrimidine derivative **5**.

Therefore, even though 2-styryl-furan and stilbene derivatives did not display high affinity at the four adenosine receptors, results of this preliminary study are encouraging. In particular, compounds **11** and **12** showed affinity in the submicromolar range versus $hA_{2A}AR$ and hA_3AR respectively and could represent a starting point to more deep investigations on these derivatives. Further studies are in progress in our laboratory to define a

more complete structure-affinity relationship for these new series of very simplified compounds as adenosine receptors antagonists.

3.6 Fluorescent derivatives

Assays to characterize adenosine receptors in tissues and to evaluate binding affinity of newly synthesized compounds as ARs ligands are often dependent on the use of high affinity radioligands. [110] Fluorescent agonists and antagonists of GPCRs have been studied as molecular probes for binding experiments. [111, 112, 113]

Recently, several 4,4-difluoro-4-bora-3a,4a-diaza-s-indacene (BODIPY) derivatives have been reported as fluorescent ligands of the ARs, including the A_3AR, [114] and used to study receptor complexes. However, these fluorescent tracers are relatively nonselective within the AR family.

Receptor-selective fluorescent ligands are used increasingly as tools for the study of receptor physiology and pathophysiology at the cellular and even the subcellular level. [112] Furthermore, they are being increasingly investigated as tools in drug discovery research. [113] In both cases, techniques employing receptor-selective fluorescent ligands have proved to be complementary to, and in several cases even superior to, the traditional radioligand-based techniques. Increasing costs and public concerns associated with radioactive isotope handling and disposal are also making the use of fluorescent ligands more attractive in research and diagnostics.

The fluorophore-conjugated tricyclic derivative MRS5346 was recently introduced as a versatile ligand for fluorescence polarization (FP) studies of the A_{2A}AR. [115] This ligand was selective for that AR subtype and was not suitable for measurements of the A_3AR.

Therefore, the development of fluorescent ligands for the A_3 subtype is an interesting research topic in medicinal chemistry. Here, we have explored some chain-elongated derivatives of known AR antagonists, including the pyrazolo[4,3-*e*][1,2,4]triazolo[1,5-*c*]pyrimidin-5-ylamine class (pyrazolo-triazolo-pyrimidine, PTP), already reported to display A_3AR selectivity. [92] We also prepared a fluorescent derivative of the closely related triazolo[1,5-c]quinazolin-5-amine class (triazolo-quinazoline, TQ), of which the potent, but nonselective AR antagonist N-[9-chloro-2-(2-furanyl)[1,2,4]triazolo[1,5-*c*]quinazolin-5-amine (CGS15943, compound **7** in Figure 3.34) is a member. [116, 91]

These derivatives were designed with the idea of develop suitable molecular probes in flow cytometry (FCM) studies. FCM is a sensitive and reliable method for examining and counting fluorophore-tagged whole cells. It is routinely used in clinical practice (e.g. diagnosis of health disorders such as leukemia) [117] and has many applications in drug research (e.g. nucleic acid analysis), [118] but its application to quantitative receptor binding

studies has been limited. [119] However, FCM can accurately measure the mean fluorescence intensity (MFI) of fluorescent small molecules bound to a cell as well, which is directly proportional to the number of receptor-bound molecules and therefore indicative of its receptor binding affinity.

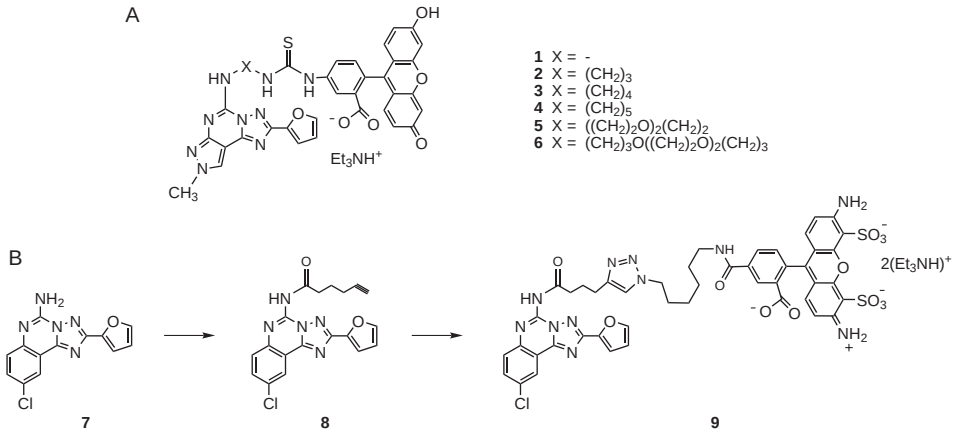

Figure 3.34: The chemical structures of fluorescent (A) PTP and (B) TQ derivatives. The route to synthesis of TQ derivative MRS5449 (compound **9**) is shown.

Therefore, known heterocyclic antagonists of the A_3AR of high affinity were derivatized through the exocyclic amine with chemically functionalized chains and conjugated to fluorophores of the fluorone class. PTP derivatives of varying chain length **1-6** (Figure 3.34) were prepared by coupling the fluorescein isothiocyanate, isomer 1 (FITC) to various chain-extended alkyl amino derivatives, in which the anchoring point was the exocyclic amine common to many structural classes of AR antagonists. FITC was used previously in a fluorescent agonist conjugate designed for binding to the A_{2A}AR. [120] Derivatives **2-4** contained homologous n-alkyl spacer chains, and **5** and **6** contained multiple ether linkages.

As an alternative to the known, generally A_3AR-selective PTP scaffold, we explored the use of the TQ scaffold. It is known that acylations at the exocyclic amine of a nonselective triazolo[1,5-*c*]quinazolin-5-amine AR antagonist, CGS15943, provide varying degrees of A_3AR selectivity. [91] Therefore, to obtain MRS5449 (compound **9**) we used an alternate coupling approach of click chemistry [121] to label the TQ scaffold with a more photostable analogue of fluorescein, i.e. the fluorophore Alexa Fluor-488, as was used in previous FP study of the A_{2A}AR. [115] The Alexa Fluor-488 dye used to label the TQ derivative is a substitution product of fluorescein, as used in the PTP derivatives. Its spectral properties are nearly identical to those of fluorescein, over which it has many advantages. Its photostability and brightness are much greater and relatively pH-insensitive. These properties

and its relatively high Stokes shift allow it to be a suitable dye for FCM experiments.

The binding affinity of these derivatives at three subtypes of hARs was determined using standard radioligand binding methods, and showed promising results for some of them (data not shown, manuscript in preparation). Moreover, functional assays of cyclic AMP accumulation in CHO cells expressing the A_3AR and FCM experiments were performed.

We performed molecular modeling studies with the aim to identify the binding modes of the newly synthesized fluorescent derivatives at the hA_3AR homology model.

Due to the conformational complexity of the ligands, we applied a two-step approach consisting of molecular docking of the ligand scaffolds followed by conformational searching of fluorophore-chain fragments inside the hA_3AR binding site.

In the first step, molecular docking simulations were performed using both PTP and TQ scaffolds derivatized only through their exocyclic amines with a C4-alkyl chain (i.e. n-butyl for PTP and n-butanoyl for TQ) and without including the corresponding fluorophores. The electrostatic and hydrophobic contributions to the interaction energy of each receptor residue involved in the binding with these fragments were then calculated.

Binding poses at the hA_3AR of these PTP and TQ simplified analogs, along with their *per residue* electrostatic and hydrophobic contributions graphs are reported in Figures 3.35, 3.36 and 3.37, respectively.

Interestingly, analysis of top-scoring docking poses revealed that PTP and TQ scaffolds possessed a similar binding mode in the TM region of the hA_3AR. Ligands recognition occurred in the upper region of the TM bundle, and the tricyclic nuclei were surrounded by TMs 3, 5, 6, and 7 with the furyl rings directed toward TM2. Moreover, PTP and TQ scaffolds showed similar crucial interactions with residues of the binding site, such as two hydrogen bonds with Asn250 (6.55) and an aromatic π-π stacking interaction with Phe168 (EL2).

These observed similar interaction patterns were confirmed by the analysis of calculated electrostatic and hydrophobic contributions to the interaction energy of each receptor residue involved in the binding with these fragments. Comparison of these contributions for the two binding poses pointed out high similarities with only slight differences. In fact, favorable electrostatic contributions to the binding energy were stronger for the PTP fragment binding pose, while favorable hydrophobic contributions to the binding energy were stronger for the TQ fragment binding pose (see Figures 3.36 and 3.37).

Starting from the top-scoring pose of each of the PTP and TQ simplified analogs, the corresponding complete ligands linked to the corresponding fluorophores were constructed by elongating the C4-alkyl spacer in the direction of the extracellular environment. Afterwards, an exhaustive con-

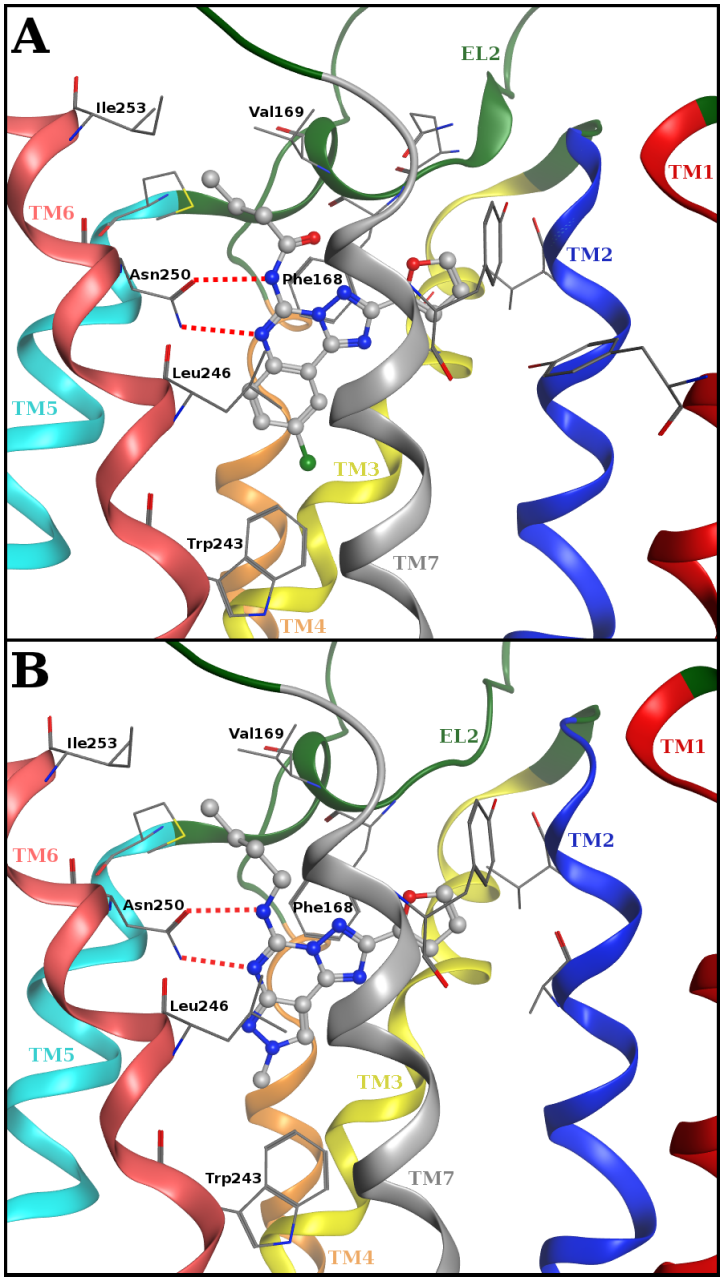

Figure 3.35: Hypothetical binding modes obtained after docking simulations inside the hA_3AR binding site of (A) a molecular fragment of MRS5449 (TQ scaffold and part of the chain) and (B) a molecular fragment of compound **3** (PTP scaffold and chain). Poses are viewed from the membrane side facing TM6, TM7 and TM1. Side chains of some amino acids important for ligand recognition and H-bonding interactions are highlighted. Hydrogen atoms are not displayed.

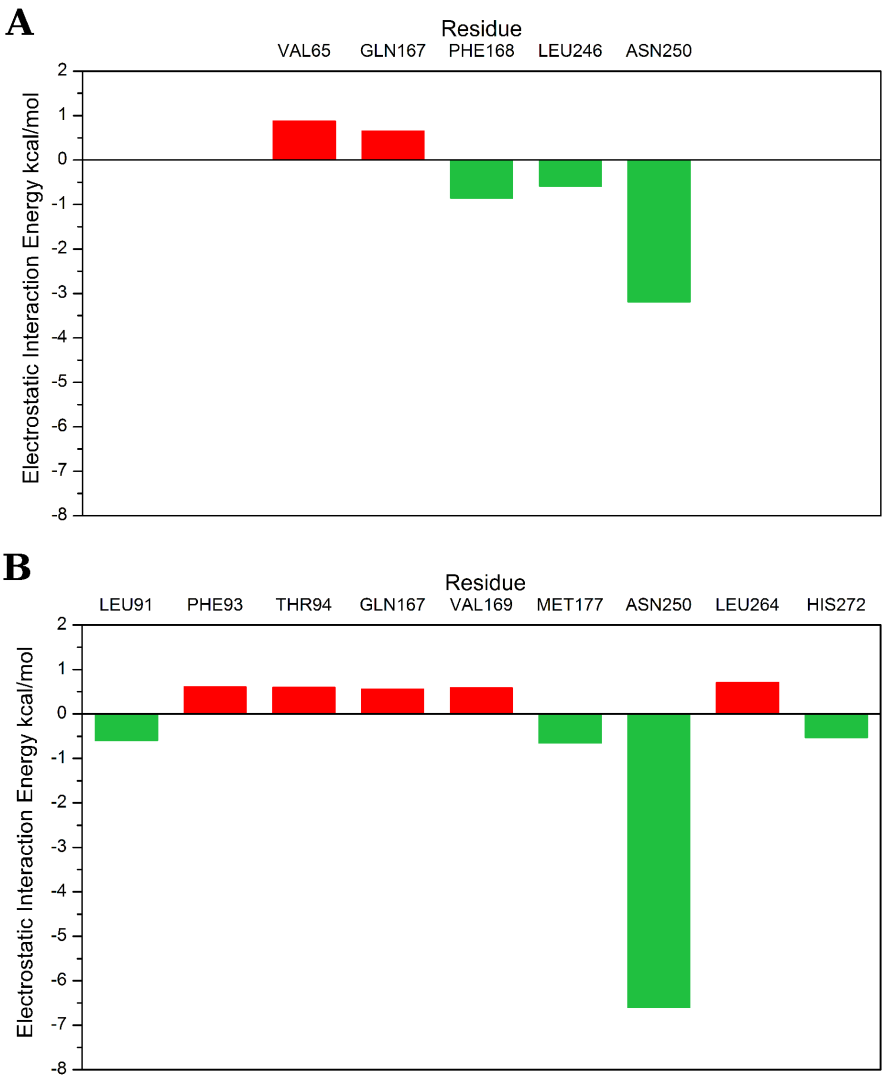

Figure 3.36: Electrostatic interaction energies (in kcal/mol) between the ligand and each single amino acid involved in ligand recognition calculated from the hypothetical binding modes, inside the hA_3AR binding site, of (A) a molecular fragment of MRS5449, compound **9** (Figure 3.35, panel A) and (B) a molecular fragment of compound **3** (Figure 3.35, panel B).

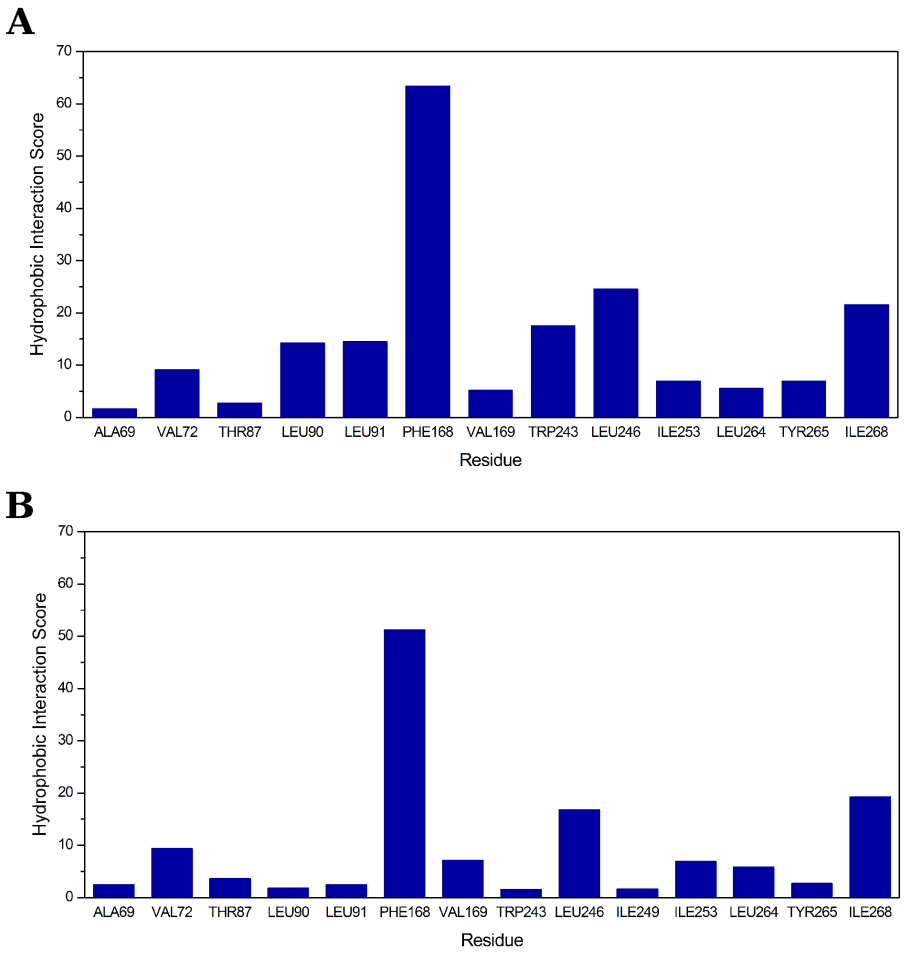

Figure 3.37: Hydrophobic interaction scores (in arbitrary hydrophobic units) between the ligand and each single amino acid involved in ligand recognition calculated from the hypothetical binding modes, inside the hA_3AR binding site, of (A) a molecular fragment of MRS5449, compound **9** (Figure 3.35, panel A) and (B) a molecular fragment of compound **3** (Figure 3.35, panel B).

formational analysis of the fluorescent ligands along with extracellular loop 2 (EL2) of the protein (starting from Asn150 to Gln167) was performed, using the LowModeMD search method implemented in MOE. [122] Structures of other extracellular loops of the hA_3AR (EL1, EL3) were kept fixed, while conformational search was performed for EL2, because it consists of a long sequence, and its conformation is consequently highly uncertain in the model.

Therefore, this procedure allowed us to explore the conformations of the fluorophore-chain fragments that have the most favorable interactions with EL2 and with the outer part of the binding site. Detailed binding conformations at the hA_3AR of MRS5449 and compound **3** obtained after LowModeMD search are reported in Figure 3.38; while, a schematic representation of these two ligand-receptor complexes, embedded in a solvated lipid bilayer simulating the cell membrane, is displayed in Figure 3.39.

Analysis of the obtained conformations showed that compound **3** was able to form only a few interactions with the residues at the entrance of the hA_3AR binding site, but was unable to interact with residues of EL2. This seemed to be due to the insufficient length of the chain departing from the exocyclic amine that precluded the fluorophore reaching and interacting with the tip of EL2.

On the contrary, the Alexa Fluor-488 fluorophore of MRS5449 (compound **9**) strongly interacted, mainly through its amino and sulfonate groups, with several residues of EL2, including His158, Arg159, Asn160, Ser165 and Gln167.

Therefore, both the increased chain length and the extra functionality on the fluorophore (i.e. amino and sulfonate groups) of MRS5449 seemed to establish a more favorable interaction of this conjugate with the hA_3AR.

As shown in Figure 3.39, the Alexa Fluor-488 fluorophore of MRS5449 was located in the outer loop area of the hA_3AR, entirely outside of the TM region. Thus, this ligand seemed to possess excellent structural features for its application as a fluorescent probe in pharmacological experiments to characterize the hA_3AR.

In summary, we have developed some fluorescent ligands, by conjugating known hA_3AR antagonists with different fluorophores. Some of these bivalent ligands can serve as receptor subtype-selective molecular probes for FCM experiments on intact cells expressing the hA_3AR. Thus, a fluorescence assay using FCM can be a useful tool in hA_3AR binding studies and for the physiological and pathophysiological characterization of hA_3AR and the pharmacological characterization of its ligands.. A similar approach can be applied to develop fluorescent ligands for other AR subtypes and other GPCRs.

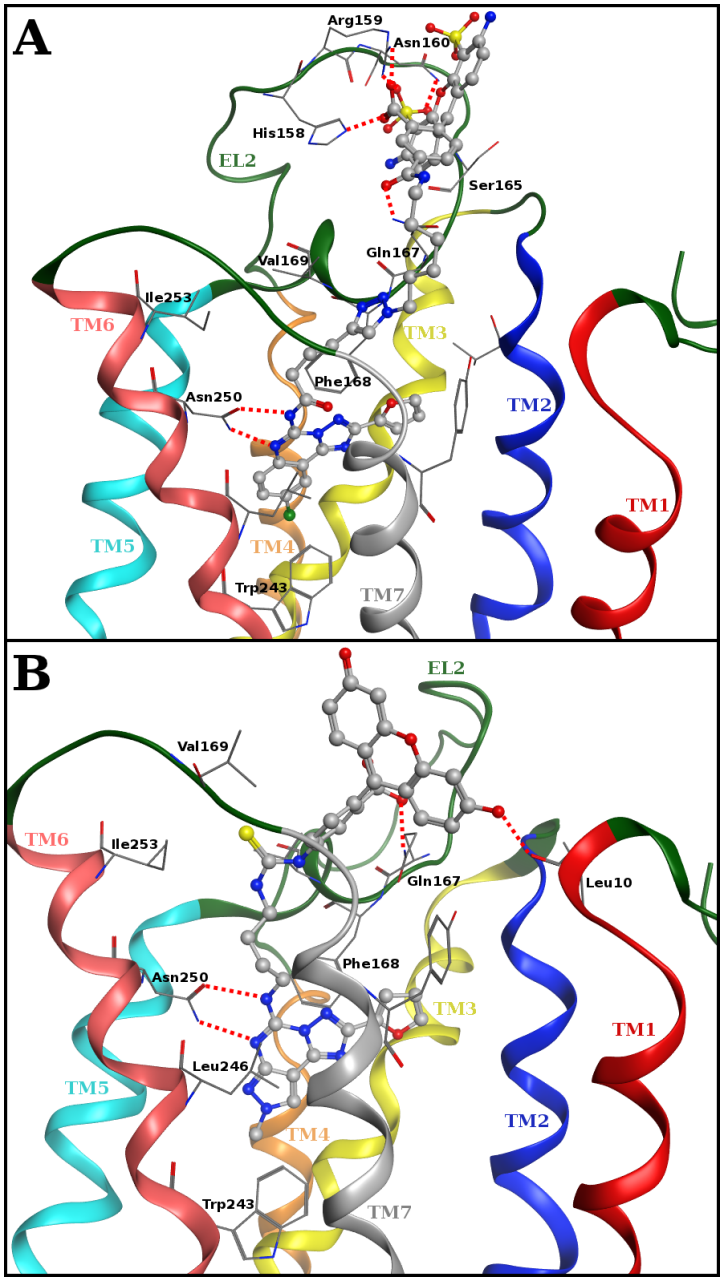

Figure 3.38: Hypothetical binding conformations at the hA_3AR, obtained after LowModeMD search, of (A) MRS5449 (compound **9**) and (B) compound **3**. Poses are viewed from the membrane side facing TM6, TM7 and TM1. Side chains of some amino acids important for ligand recognition and H-bonding interactions are highlighted. Hydrogen atoms are not displayed.

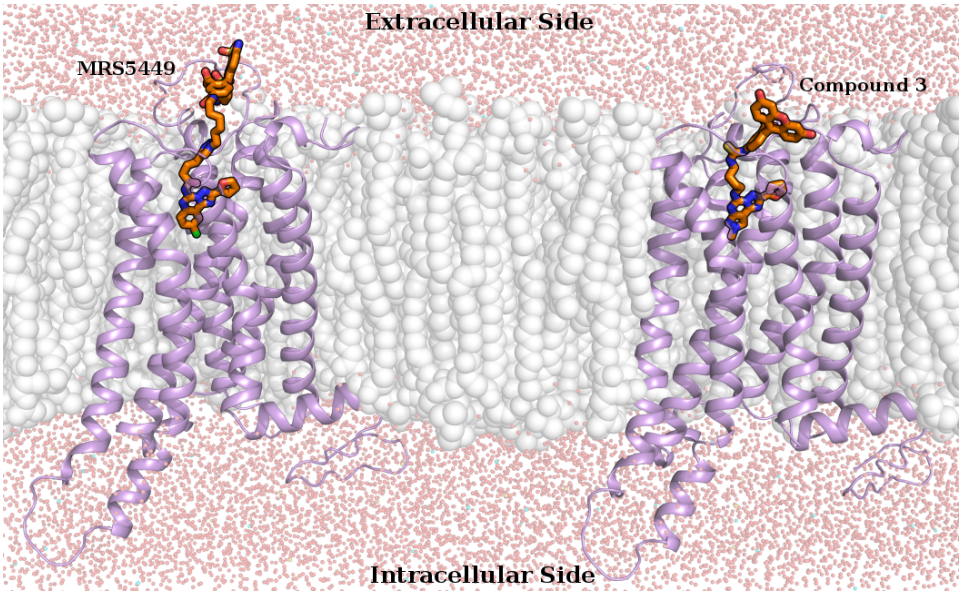

Figure 3.39: Hypothetical binding conformations at the hA_3AR model of MRS5449 (on the left) and compound **3** (on the right), obtained after molecular modeling studies. Ligand-receptor models are embedded in a solvated lipid bilayer, simulating the cell membrane, and are viewed through a cross-section of the plasma membrane.

Chapter 4

Conclusions and future perspectives

In this study a detailed investigation at the molecular level of the structure of adenosine receptors has been performed. In particular, the crystallographic structure of the $hA_{2A}AR$ has been used as starting point for the construction of a homology model of the hA_3AR. The 3D structures of these two receptor subtypes were then used to perform molecular docking simulations of ARs antagonists.

This molecular modeling approach has been integrated with the work of synthetic and pharmacological groups with the aim to experimentally validate all the information and to guide the design of new compounds as potential ARs antagonists.

The performed *in silico* analysis permitted the formulation of preliminary hypothesis on the specific roles of a few crucial amino acids in ligand entering and recognition processes. Moreover, through the interpretation of affinity and selectivity profiles of adenosine receptors antagonists, the identification of structural features important for the interaction with these receptors was possible.

These information were used to guide different ligand optimization approaches, considering both pharmacokinetic and pharmacodynamic properties. In fact, on the one hand, different substitution points on known antagonist scaffolds, such as triazolo-triazine and the pyrazolo-triazolo-pyrimidine, have been explored with the aim to modulate the affinity towards the AR subtypes and to develop more potent and selective antagonists. While, on the other hand, in order to improve the pharmacokinetic profile of potential drug candidates, modifications to overcome a point metabolic instability or to increase the solubility of some derivatives were suggested.

Another optimization strategy adopted has been the molecular simplification of known adenosine receptors antagonists to obtain more simple compounds possessing AR antagonist activity and easier synthetic preparation

routes.

Finally, the design of fluorescent ARs antagonists, useful as molecular probes in pharmacological experiments to characterize these receptors, has been performed and led to interesting results.

Further studies are in progress in our laboratory to gain a deeper knowledge of adenosine receptors structure, in particular through the use of membrane molecular dynamics simulations of ARs models and conformational analyses of the loops region and, in particular, of EL2.

On the whole, this study shows the success of an integrated approach, that include molecular modeling, synthesis and biological work, for the characterization of the adenosine receptors class of GPCRs and for the development of ARs antagonists as useful tools in medicinal chemistry.

Bibliography

[1] K. L. Pierce, R. T. Premont, and R. J. Lefkowitz, "Seven-transmembrane receptors.," *Nature reviews. Molecular cell biology*, vol. 3, pp. 639–50, Sept. 2002.

[2] R. J. Lefkowitz, "Historical review: a brief history and personal retrospective of seven-transmembrane receptors.," *Trends in pharmacological sciences*, vol. 25, pp. 413–22, Aug. 2004.

[3] K. Lounsbury, *Pharmacology: Principles and Practice. Chapter 6 - Signal Transduction and Second Messengers*. Elsevier Inc., 1 ed., 2009.

[4] T. Patel, "Single transmembrane spanning heterotrimeric G protein-coupled receptors and their signaling cascades," *Pharmacological reviews*, vol. 56, no. 3, pp. 371–385, 2004.

[5] G. Milligan, "A day in the life of a G protein-coupled receptor: the contribution to function of G protein-coupled receptor dimerization.," *British journal of pharmacology*, vol. 153 Suppl, pp. S216–29, Mar. 2008.

[6] S. Prinster, C. Hague, and R. Hall, "Heterodimerization of g protein-coupled receptors: specificity and functional significance," *Pharmacological reviews*, vol. 57, no. 3, pp. 289–298, 2005.

[7] G. Milligan, "G-protein-coupled receptor heterodimers: pharmacology, function and relevance to drug discovery.," *Drug discovery today*, vol. 11, pp. 541–9, June 2006.

[8] S. Moro, G. Spalluto, and K. a. Jacobson, "Techniques: Recent developments in computer-aided engineering of GPCR ligands using the human adenosine A3 receptor as an example.," *Trends in pharmacological sciences*, vol. 26, pp. 44–51, Jan. 2005.

[9] S. Takeda, "Identification of G protein-coupled receptor genes from the human genome sequence," *FEBS Letters*, vol. 520, pp. 97–101, June 2002.

[10] D. K. Vassilatis, J. G. Hohmann, H. Zeng, F. Li, J. E. Ranchalis, M. T. Mortrud, A. Brown, S. S. Rodriguez, J. R. Weller, A. C. Wright, J. E. Bergmann, and G. a. Gaitanaris, "The G protein-coupled receptor repertoires of human and mouse.," *Proceedings of the National Academy of Sciences of the United States of America*, vol. 100, pp. 4903–8, Apr. 2003.

[11] R. Fredriksson, M. Lagerström, L. Lundin, and H. Schiöth, "The G-protein-coupled receptors in the human genome form five main families. Phylogenetic analysis, paralogon groups, and fingerprints," *Molecular pharmacology*, vol. 63, no. 6, p. 1256, 2003.

[12] L. F. Kolakowski, "GCRDb: a G-protein-coupled receptor database.," *Receptors & channels*, vol. 2, pp. 1–7, Jan. 1994.

[13] S. Foord, T. Bonner, R. Neubig, E. Rosser, J. Pin, A. Davenport, M. Spedding, and A. Harmar, "International Union of Pharmacology. XLVI. G protein-coupled receptor list," *Pharmacological reviews*, vol. 57, no. 2, pp. 279–288, 2005.

[14] J. A. Ballesteros and H. Weinstein, "Integrated methods for the construction of three-dimensional models and computational probing of structure-function relations in G protein-coupled receptors," *Methods in neurosciences*, vol. 25, pp. 366–428, 1995.

[15] L. Arvanitakis, E. Geras-Raaka, and M. C. Gershengorn, "Constitutively signaling G-protein-coupled receptors and human disease.," *Trends in endocrinology and metabolism: TEM*, vol. 9, no. 1, pp. 27–31, 1998.

[16] B. K. Rana, T. Shiina, and P. A. Insel, "Genetic variations and polymorphisms of G protein-coupled receptors: functional and therapeutic implications.," *Annual review of pharmacology and toxicology*, vol. 41, pp. 593–624, Jan. 2001.

[17] M. D. Thompson, W. M. Burnham, and D. E. C. Cole, "The G protein-coupled receptors: Pharmacogenetics and Disease," *Critical Reviews in Clinical Laboratory Sciences*, vol. 42, pp. 311–389, Oct. 2008.

[18] B. B. Fredholm, G. Arslan, L. Halldner, B. Kull, G. Schulte, and W. Wasserman, "Structure and function of adenosine receptors and their genes," *Naunyn-Schmiedeberg's Archives of Pharmacology*, vol. 362, pp. 364–374, Oct. 2000.

[19] B. B. Fredholm, a. P. IJzerman, K. a. Jacobson, K. N. Klotz, and J. Linden, "International Union of Pharmacology. XXV. Nomenclature and classification of adenosine receptors.," *Pharmacological reviews*, vol. 53, pp. 527–52, Dec. 2001.

[20] B. B. Fredholm, "Adenosine receptors as targets for drug development.," *Drug news perspectives*, vol. 16, no. 5, pp. 283–289, 2003.

[21] K. A. Jacobson and Z.-G. Gao, "Adenosine receptors as therapeutic targets.," *Nature reviews. Drug discovery*, vol. 5, pp. 247–64, Mar. 2006.

[22] C. E. Müller and K. a. Jacobson, "Recent developments in adenosine receptor ligands and their potential as novel drugs.," *Biochimica et biophysica acta*, vol. 1808, pp. 1290–308, May 2011.

[23] S. Moro, Z.-G. Gao, K. a. Jacobson, and G. Spalluto, "Progress in the pursuit of therapeutic adenosine receptor antagonists.," *Medicinal research reviews*, vol. 26, pp. 131–59, Mar. 2006.

[24] T. J. Furlong, K. D. Pierce, L. A. Selbie, and J. Shine, "Molecular characterization of a human brain adenosine A2 receptor.," *Brain research. Molecular brain research*, vol. 15, pp. 62–6, Sept. 1992.

[25] P. A. Borea, S. Gessi, S. Bar-Yehuda, and P. Fishman, "A3 adenosine receptor: pharmacology and role in disease.," *Handbook of experimental pharmacology*, vol. 193, pp. 297–327, Jan. 2009.

[26] M. Abbracchio, R. Brambilla, S. Ceruti, H. Kim, D. Von Lubitz, K. Jacobson, and F. Cattabeni, "G protein-dependent activation of phospholipase C by adenosine A3 receptors in rat brain.," *Molecular pharmacology*, vol. 48, pp. 1038–1045, 1995.

[27] H. Ali, O. Choi, P. Fraundorfer, K. Yamada, H. Gonzaga, and M. Beaven, "Sustained activation of phospholipase D via adenosine A3 receptors is associated with enhancement of antigen-and Ca (2+)-ionophore-induced secretion in a rat mast cell line.," *Journal of Pharmacology and Experimental Therapeutics*, vol. 276, no. 2, p. 837, 1996.

[28] V. Shneyvays, D. Leshem, T. Zinman, L. K. Mamedova, K. a. Jacobson, and A. Shainberg, "Role of adenosine A1 and A3 receptors in regulation of cardiomyocyte homeostasis after mitochondrial respiratory chain injury.," *American journal of physiology. Heart and circulatory physiology*, vol. 288, pp. H2792–801, June 2005.

[29] M. Englert, U. Quitterer, and K. N. Klotz, "Effector coupling of stably transfected human A3 adenosine receptors in CHO cells.," *Biochemical pharmacology*, vol. 64, pp. 61–5, July 2002.

[30] G. Schulte, "Signalling from adenosine receptors to mitogen-activated protein kinases," *Cellular Signalling*, vol. 15, pp. 813–827, Sept. 2003.

[31] S. Gessi, S. Merighi, K. Varani, E. Leung, S. Mac Lennan, and P. A. Borea, "The A3 adenosine receptor: an enigmatic player in cell biology.," *Pharmacology & therapeutics*, vol. 117, pp. 123–40, Jan. 2008.

[32] R. Brambilla, F. Cattabeni, S. Ceruti, D. Barbieri, C. Franceschi, Y. C. Kim, K. A. Jacobson, K. N. Klotz, M. J. Lohse, and M. P. Abbracchio, "Activation of the A3 adenosine receptor affects cell cycle progression and cell growth.," *NaunynSchmiedebergs archives of pharmacology*, vol. 361, no. 3, pp. 225–234, 2000.

[33] S. Merighi, P. Mirandola, K. Varani, S. Gessi, E. Leung, P. G. Baraldi, M. A. Tabrizi, and P. A. Borea, "A glance at adenosine receptors: novel target for antitumor therapy.," *Pharmacology therapeutics*, vol. 100, no. 1, pp. 31–48, 2003.

[34] K. A. Jacobson, A. M. Klutz, D. K. Tosh, A. A. Ivanov, D. Preti, and P. G. Baraldi, "Medicinal chemistry of the A3 adenosine receptor: agonists, antagonists, and receptor engineering.," *Handbook of experimental pharmacology*, vol. 193, pp. 123–59, Jan. 2009.

[35] S. Paoletta, S. Federico, G. Spalluto, and S. Moro, "Receptor-driven identification of novel human A3 adenosine receptor antagonists as potential therapeutic agents.," *Methods in enzymology*, vol. 485, pp. 225–44, Jan. 2010.

[36] Z.-G. Gao, S.-K. Kim, T. Biadatti, W. Chen, K. Lee, D. Barak, S. G. Kim, C. R. Johnson, and K. a. Jacobson, "Structural determinants of A(3) adenosine receptor activation: nucleoside ligands at the agonist/antagonist boundary.," *Journal of medicinal chemistry*, vol. 45, pp. 4471–84, Sept. 2002.

[37] The UniProt Consortium, "Ongoing and future developments at the Universal Protein Resource.," *Nucleic acids research*, vol. 39, pp. D214–9, Jan. 2011.

[38] H. Berman, J. Westbrook, Z. Feng, G. Gilliland, T. Bhat, H. Weissig, I. Shindyalov, and P. Bourne, "The Protein Data Bank," *Nucleic Acids Research*, vol. 28, pp. 235–242, Jan. 2000.

[39] B. K. Kobilka and X. Deupi, "Conformational complexity of G-protein-coupled receptors.," *Trends in pharmacological sciences*, vol. 28, pp. 397–406, Aug. 2007.

[40] K. Palczewski, "Crystal Structure of Rhodopsin: A G Protein-Coupled Receptor," *Science*, vol. 289, pp. 739–745, Aug. 2000.

[41] D. M. Rosenbaum, V. Cherezov, M. A. Hanson, S. r. G. F. Rasmussen, F. S. Thian, T. S. Kobilka, H.-J. Choi, X.-J. Yao, W. I. Weis, R. C. Stevens, and B. K. Kobilka, "GPCR engineering yields high-resolution structural insights into beta2-adrenergic receptor function," *Science*, vol. 318, pp. 1266–1273, Nov. 2007.

[42] V. Cherezov, D. M. Rosenbaum, M. a. Hanson, S. r. G. F. Rasmussen, F. S. Thian, T. S. Kobilka, H.-J. Choi, P. Kuhn, W. I. Weis, B. K. Kobilka, and R. C. Stevens, "High-resolution crystal structure of an engineered human beta2-adrenergic G protein-coupled receptor.," *Science*, vol. 318, pp. 1258–65, Nov. 2007.

[43] T. Warne, M. J. Serrano-Vega, J. G. Baker, R. Moukhametzianov, P. C. Edwards, R. Henderson, A. G. W. Leslie, C. G. Tate, and G. F. X. Schertler, "Structure of a beta1-adrenergic G-protein-coupled receptor.," *Nature*, vol. 454, pp. 486–91, July 2008.

[44] V.-P. Jaakola, M. T. Griffith, M. a. Hanson, V. Cherezov, E. Y. T. Chien, J. R. Lane, a. P. IJzerman, and R. C. Stevens, "The 2.6 Angstrom Crystal Structure of a Human A2A Adenosine Receptor Bound to an Antagonist," *Science*, vol. 322, pp. 1211–1217, Nov. 2008.

[45] E. Y. T. Chien, W. Liu, Q. Zhao, V. Katritch, G. W. Han, M. A. Hanson, L. Shi, A. H. Newman, J. A. Javitch, V. Cherezov, and R. C. Stevens, "Structure of the human dopamine D3 receptor in complex with a D2/D3 selective antagonist.," *Science (New York, N.Y.)*, vol. 330, pp. 1091–5, Nov. 2010.

[46] B. Wu, E. Y. T. Chien, C. D. Mol, G. Fenalti, W. Liu, V. Katritch, R. Abagyan, A. Brooun, P. Wells, F. C. Bi, D. J. Hamel, P. Kuhn, T. M. Handel, V. Cherezov, and R. C. Stevens, "Structures of the CXCR4 chemokine GPCR with small-molecule and cyclic peptide antagonists.," *Science (New York, N.Y.)*, vol. 330, pp. 1066–71, Nov. 2010.

[47] T. Shimamura, M. Shiroishi, S. Weyand, H. Tsujimoto, G. Winter, V. Katritch, R. Abagyan, V. Cherezov, W. Liu, G. W. Han, T. Kobayashi, R. C. Stevens, and S. Iwata, "Structure of the human histamine H1 receptor complex with doxepin.," *Nature*, vol. 475, pp. 65–70, July 2011.

[48] F. Xu, H. Wu, V. Katritch, G. W. Han, K. a. Jacobson, Z.-G. Gao, V. Cherezov, and R. C. Stevens, "Structure of an agonist-bound human A2A adenosine receptor.," *Science (New York, N.Y.)*, vol. 332, pp. 322–7, Apr. 2011.

[49] A. S. Doré, N. Robertson, J. C. Errey, I. Ng, K. Hollenstein, B. Tehan, E. Hurrell, K. Bennett, M. Congreve, F. Magnani, C. G. Tate, M. Weir, and F. H. Marshall, "Structure of the Adenosine A(2A) Receptor in Complex with ZM241385 and the Xanthines XAC and Caffeine.," *Structure (London, England : 1993)*, vol. 4, pp. 1283–1293, Aug. 2011.

[50] G. Lebon, T. Warne, P. C. Edwards, K. Bennett, C. J. Langmead, A. G. W. Leslie, and C. G. Tate, "Agonist-bound adenosine A2A receptor structures reveal common features of GPCR activation.," *Nature*, vol. 474, pp. 521–5, June 2011.

[51] Chemical Computing Group Inc. (1010 Sherbrooke Street West Suite 910 Montreal Quebec H3A 2R7 Canada), "MOE (Molecular Operating Environment), version 2010.10."

[52] J. Stewart, "MOPAC 7."

[53] Cambridge Crystallographic Data Centre (12 Union Road Cambridge CB2 1EZ UK), "GOLD suite, version 5.1."

[54] R. Friesner, J. Banks, R. Murphy, T. Halgren, J. Klicic, T. Daniel, M. Repasky, E. Knoll, D. Shaw, M. Shelley, J. Perry, P. Francis, and P. S. Shenkin, "Glide: a new approach for rapid, accurate docking and scoring. 1. Method and assessment of docking accuracy," *Journal of medicinal chemistry*, vol. 47, pp. 1739–1749, Mar. 2004.

[55] O. Korb, T. Stützle, and T. E. Exner, "PLANTS: Application of Ant Colony Optimization to Structure-Based Drug Design," *Lecture Notes in Computer Science*, vol. 4150, pp. 247–258, 2006.

[56] W. D. Cornell, P. Cieplak, C. I. Bayly, I. R. Gould, K. M. Merz, D. M. Ferguson, D. C. Spellmeyer, T. Fox, J. W. Caldwell, and P. A. Kollman, "A Second Generation Force Field for the Simulation of Proteins, Nucleic Acids, and Organic Molecules," *Journal of the American Chemical Society*, vol. 117, pp. 5179–5197, May 1995.

[57] T. A. Halgren, "Merck molecular force field. I. Basis, form, scope, parameterization, and performance of MMFF94," *Journal of Computational Chemistry*, vol. 17, pp. 490–519, Apr. 1996.

[58] A. Leach, *Molecular Modelling: Principles and Applications*. Pearson Education EMA, second edi ed., 2001.

[59] H. Holtje, W. Sippl, D. Rognan, and G. Folkers, *Molecular Modeling: Basic Principles and Applications*. Wiley-VCH, third edit ed., 2008.

[60] P. Labute, "Protonate3D: assignment of ionization states and hydrogen coordinates to macromolecular structures.," *Proteins*, vol. 75, pp. 187–205, Apr. 2009.

[61] O. Lenzi, V. Colotta, D. Catarzi, F. Varano, D. Poli, G. Filacchioni, K. Varani, F. Vincenzi, P. A. Borea, S. Paoletta, E. Morizzo, and S. Moro, "2-Phenylpyrazolo[4,3-d]pyrimidin-7-one as a new scaffold to obtain potent and selective human A3 adenosine receptor antagonists: new insights into the receptor-antagonist recognition.," *Journal of medicinal chemistry*, vol. 52, pp. 7640–52, Dec. 2009.

[62] A. Martinelli and T. Tuccinardi, "Molecular modeling of adenosine receptors: new results and trends.," *Medicinal research reviews*, vol. 28, pp. 247–77, Mar. 2008.

[63] E. Morizzo, S. Federico, G. Spalluto, and S. Moro, "Human A3 adenosine receptor as versatile G protein-coupled receptor example to validate the receptor homology modeling technology," *Current pharmaceutical design*, vol. 15, no. 35, pp. 4069–4084, 2009.

[64] Q. Jiang, A. Van Rhee, J. Kim, S. Yehle, J. Wess, and K. Jacobson, "Hydrophilic side chains in the third and seventh transmembrane helical domains of human A2A adenosine receptors are required for ligand recognition.," *Molecular pharmacology*, vol. 50, p. 512, Sept. 1996.

[65] J. Kim, Q. Jiang, M. Glashofer, S. Yehle, J. Wess, and K. Jacobson, "Glutamate residues in the second extracellular loop of the human A2a adenosine receptor are required for ligand recognition.," *Molecular pharmacology*, vol. 49, p. 683, Apr. 1996.

[66] J. Kim, J. Wess, A. van Rhee, T. Schöneberg, and K. Jacobson, "Site-directed Mutagenesis Identifies Residues Involved in Ligand Recognition in the Human A Adenosine Receptor," *Journal of Biological Chemistry*, vol. 270, pp. 13987–13997, June 1995.

[67] V.-P. Jaakola, J. R. Lane, J. Y. Lin, V. Katritch, A. P. Ijzerman, and R. C. Stevens, "Ligand binding and subtype selectivity of the human A(2A) adenosine receptor: identification and characterization of essential amino acid residues," *The Journal of Biological Chemistry*, vol. 285, pp. 13032–13044, Apr. 2010.

[68] Z.-G. Gao, S.-K. Kim, A. S. Gross, A. Chen, J. B. Blaustein, and K. a. Jacobson, "Identification of essential residues involved in the allosteric modulation of the human A(3) adenosine receptor.," *Molecular pharmacology*, vol. 63, pp. 1021–31, May 2003.

[69] H. Duong, Z. Gao, and K. Jacobson, "Nucleoside modification and concerted mutagenesis of the human A3 adenosine receptor to probe interactions between the 2-position of adenosine analogs and Gln167 in the second extracellular loop," *Nucleosides, Nucleotides, and Nucleic Acids*, vol. 24, no. 10-12, pp. 1507–1517, 2005.

[70] A. Chen, Z. Gao, D. Barak, and B. Liang, "Constitutive activation of A3 adenosine receptors by site-directed mutagenesis," *Biochemical and*, vol. 284, pp. 596–601, June 2001.

[71] Z.-G. Gao, A. Chen, D. Barak, S.-K. Kim, C. E. Müller, and K. a. Jacobson, "Identification by site-directed mutagenesis of residues involved in ligand recognition and activation of the human A3 adenosine receptor.," *The Journal of biological chemistry*, vol. 277, pp. 19056–63, May 2002.

[72] K. a. Jacobson, Z. G. Gao, a. Chen, D. Barak, S. a. Kim, K. Lee, a. Link, P. V. Rompaey, S. van Calenbergh, and B. T. Liang, "Neoceptor concept based on molecular complementarity in GPCRs: a mutant adenosine A(3) receptor with selectively enhanced affinity for amine-modified nucleosides.," *Journal of medicinal chemistry*, vol. 44, pp. 4125–36, Nov. 2001.

[73] G. Pastorin, S. Federico, S. Paoletta, M. Corradino, F. Cateni, B. Cacciari, K. Klotz, Z. Gao, K. Jacobson, G. Spalluto, and Others, "Synthesis and pharmacological characterization of a new series of 5, 7-disubstituted-[1, 2, 4] triazolo [1, 5-a][1, 3, 5] triazine derivatives as adenosine receptor antagonists: A preliminary inspection of ligand-receptor recognition process," *Bioorganic & medicinal chemistry*, vol. 18, pp. 2524–2536, Apr. 2010.

[74] S. L. Cheong, A. V. Dolzhenko, S. Paoletta, E. P. R. Lee, S. Kachler, S. Federico, K.-N. Klotz, A. V. Dolzhenko, G. Spalluto, S. Moro, and G. Pastorin, "Does the combination of optimal substitutions at the C(2)-, N(5)- and N(8)-positions of the pyrazolo-triazolo-pyrimidine scaffold guarantee selective modulation of the human A(3) adenosine receptors?," *Bioorganic & medicinal chemistry*, vol. 19, pp. 6120–34, Oct. 2011.

[75] S. Federico, S. Paoletta, S. L. Cheong, G. Pastorin, B. Cacciari, S. Stragliotto, K. N. Klotz, J. Siegel, Z.-G. Gao, K. a. Jacobson, S. Moro, and G. Spalluto, "Synthesis and Biological Evaluation of a New Series of 1,2,4-Triazolo[1,5-a]-1,3,5-triazines as Human A(2A) Adenosine Receptor Antagonists with Improved Water Solubility.," *Journal of medicinal chemistry*, pp. 877–889, Jan. 2011.

[76] S. L. Cheong, A. A. Dolzhenko, S. Kachler, S. Paoletta, S. Federico, B. Cacciari, K.-N. Klotz, S. Moro, G. Spalluto, and G. Pastorin, "The significance of 2-furyl ring substitution with a 2-(para-substituted) aryl group in a new series of pyrazolo-triazolo-pyrimidines as potent and highly selective hA(3) adenosine receptors antagonists: new insights

into structure-affinity relationship a," *Journal of medicinal chemistry*, vol. 53, pp. 3361–75, Apr. 2010.

[77] D. Poli, D. Catarzi, V. Colotta, F. Varano, G. Filacchioni, S. Daniele, L. Trincavelli, C. Martini, S. Paoletta, and S. Moro, "The identification of the 2-phenylphthalazin-1(2H)-one scaffold as a new decorable core skeleton for the design of potent and selective human A3 adenosine receptor antagonists.," *Journal of medicinal chemistry*, vol. 54, pp. 2102–13, Apr. 2011.

[78] S. M. Poucher, J. R. Keddie, P. Singh, S. M. Stoggall, P. W. Caulkett, G. Jones, and M. G. Coll, "The in vitro pharmacology of ZM 241385, a potent, non-xanthine A2a selective adenosine receptor antagonist.," *British journal of pharmacology*, vol. 125, no. 6, pp. 1096–1102, 1998.

[79] M. De Zwart, R. C. Vollinga, M. W. Beukers, D. F. Sleegers, J. K. Von Frijtag Drabbe Künzel, M. De Groote, and A. P. IJzerman, "Potent antagonists for the human adenosine A2B receptor. Derivatives of the triazolotriazine adenosine receptor antagonist ZM241385 with high affinity," *Drug Development Research*, vol. 48, no. 3, pp. 95–103, 1999.

[80] X. D. Ji and K. A. Jacobson, "Use of the triazolotriazine [3H]ZM 241385 as a radioligand at recombinant human A2B adenosine receptors.," *Drug Design and Discovery*, vol. 16, no. 3, pp. 217–226, 1999.

[81] P. G. Baraldi, B. Cacciari, R. Romagnoli, G. Spalluto, K. N. Klotz, E. Leung, K. Varani, S. Gessi, S. Merighi, and P. A. Borea, "Pyrazolo[4,3-e]-1,2,4-triazolo[1,5-c]pyrimidine derivatives as highly potent and selective human A(3) adenosine receptor antagonists.," *Journal of medicinal chemistry*, vol. 42, pp. 4473–8, Nov. 1999.

[82] G. Pastorin, T. Da Ros, G. Spalluto, F. Deflorian, S. Moro, B. Cacciari, P. G. Baraldi, S. Gessi, K. Varani, and P. A. Borea, "Pyrazolo[4,3-e]-1,2,4-triazolo[1,5-c]pyrimidine derivatives as adenosine receptor antagonists. Influence of the N5 substituent on the affinity at the human A 3 and A 2B adenosine receptor subtypes: a molecular modeling investigation.," *Journal of medicinal chemistry*, vol. 46, pp. 4287–96, Sept. 2003.

[83] P. G. Baraldi, B. Cacciari, R. Romagnoli, G. Spalluto, A. Monopoli, E. Ongini, K. Varani, and P. A. Borea, "7-Substituted 5-amino-2-(2-furyl)pyrazolo[4,3-e]-1,2,4-triazolo[1,5-c]pyrimidines as A2A adenosine receptor antagonists: a study on the importance of modifications at the side chain on the activity and solubility.," *Journal of medicinal chemistry*, vol. 45, pp. 115–26, Jan. 2002.

[84] P. G. Baraldi, B. Cacciari, G. Spalluto, M. Bergonzoni, S. Dionisotti, E. Ongini, K. Varani, and P. A. Borea, "Design, synthesis, and biological evaluation of a second generation of pyrazolo[4,3-e]-1,2,4-triazolo[1,5-c]pyrimidines as potent and selective A2A adenosine receptor antagonists.," *Journal of medicinal chemistry*, vol. 41, pp. 2126–33, June 1998.

[85] R. A. Cunha, M. D. Constantino, and J. A. Ribeiro, "ZM241385 is an antagonist of the facilitatory responses produced by the A2A adenosine receptor agonists CGS21680 and HENECA in the rat hippocampus.," *British journal of pharmacology*, vol. 122, pp. 1279–84, Dec. 1997.

[86] E. Ongini, S. Dionisotti, S. Gessi, E. Irenius, and B. B. Fredholm, "Comparison of CGS 15943, ZM 241385 and SCH 58261 as antagonists at human adenosine receptors.," *Naunyn-Schmiedeberg's archives of pharmacology*, vol. 359, pp. 7–10, Jan. 1999.

[87] J. Kim, J. Wess, A. M. van Rhee, T. Schöneberg, and K. A. Jacobson, "Site-directed mutagenesis identifies residues involved in ligand recognition in the human A2a adenosine receptor.," *The Journal of biological chemistry*, vol. 270, pp. 13987–97, June 1995.

[88] J. Kim, Q. Jiang, M. Glashofer, S. Yehle, J. Wess, and K. A. Jacobson, "Glutamate residues in the second extracellular loop of the human A2a adenosine receptor are required for ligand recognition.," *Molecular Pharmacology*, vol. 49, no. 4, pp. 683–691, 1996.

[89] P. G. Baraldi, B. Cacciari, P. A. Borean, K. Varanin, G. Pastorin, T. Da Ros, M. A. Tabrizi, F. Fruttarolo, and G. Spalluto, "Pyrazolo-triazolo-pyrimidine derivatives as adenosine receptor antagonists: a possible template for adenosine receptor subtypes?," *Current pharmaceutical design*, vol. 8, pp. 2299–332, Jan. 2002.

[90] P. G. Baraldi, B. Cacciari, R. Romagnoli, K.-N. Klotz, G. Spalluto, K. Varani, S. Gessi, S. Merighi, and P. A. Borea, "Pyrazolo[4,3-e]1,2,4-triazolo[1,5-c]pyrimidine derivatives as adenosine receptor ligands: A starting point for searching A2B adenosine receptor antagonists," *Drug Development Research*, vol. 53, pp. 225–235, June 2001.

[91] Y. C. Kim, X. D. Ji, and K. A. Jacobson, "Derivatives of the triazoloquinazoline adenosine antagonist (CGS15943) are selective for the human A3 receptor subtype.," *Journal of medicinal chemistry*, vol. 39, pp. 4142–8, Oct. 1996.

[92] P. G. Baraldi, B. Cacciari, R. Romagnoli, G. Spalluto, S. Moro, K. N. Klotz, E. Leung, K. Varani, S. Gessi, S. Merighi, and P. A. Borea,

"Pyrazolo[4,3-e]1,2,4-triazolo[1,5-c]pyrimidine derivatives as highly potent and selective human A(3) adenosine receptor antagonists: influence of the chain at the N(8) pyrazole nitrogen.," *Journal of medicinal chemistry*, vol. 43, pp. 4768–80, Dec. 2000.

[93] A. Maconi, G. Pastorin, T. Da Ros, G. Spalluto, Z.-G. Gao, K. A. Jacobson, P. G. Baraldi, B. Cacciari, K. Varani, S. Moro, and P. A. Borea, "Synthesis, biological properties, and molecular modeling investigation of the first potent, selective, and water-soluble human A(3) adenosine receptor antagonist.," *Journal of medicinal chemistry*, vol. 45, pp. 3579–82, Aug. 2002.

[94] P. G. Baraldi, F. Fruttarolo, M. A. Tabrizi, D. Preti, R. Romagnoli, H. El-Kashef, A. Moorman, K. Varani, S. Gessi, S. Merighi, and P. A. Borea, "Design, synthesis, and biological evaluation of C9- and C2-substituted pyrazolo[4,3-e]-1,2,4-triazolo[1,5-c]pyrimidines as new A2A and A3 adenosine receptors antagonists.," *Journal of medicinal chemistry*, vol. 46, pp. 1229–41, Mar. 2003.

[95] V. Colotta, D. Catarzi, F. Varano, L. Cecchi, G. Filacchioni, C. Martini, L. Trincavelli, and A. Lucacchini, "1,2,4-Triazolo[4,3-a]quinoxalin-1-one: a versatile tool for the synthesis of potent and selective adenosine receptor antagonists.," *Journal of medicinal chemistry*, vol. 43, pp. 1158–64, Mar. 2000.

[96] O. Lenzi, V. Colotta, D. Catarzi, F. Varano, G. Filacchioni, C. Martini, L. Trincavelli, O. Ciampi, K. Varani, F. Marighetti, E. Morizzo, and S. Moro, "4-amido-2-aryl-1,2,4-triazolo[4,3-a]quinoxalin-1-ones as new potent and selective human A3 adenosine receptor antagonists. synthesis, pharmacological evaluation, and ligand-receptor modeling studies.," *Journal of medicinal chemistry*, vol. 49, pp. 3916–25, June 2006.

[97] V. Colotta, D. Catarzi, F. Varano, F. Capelli, O. Lenzi, G. Filacchioni, C. Martini, L. Trincavelli, O. Ciampi, A. M. Pugliese, F. Pedata, A. Schiesaro, E. Morizzo, and S. Moro, "New 2-arylpyrazolo[3,4-c]quinoline derivatives as potent and selective human A3 adenosine receptor antagonists. Synthesis, pharmacological evaluation, and ligand-receptor modeling studies.," *Journal of medicinal chemistry*, vol. 50, pp. 4061–74, Aug. 2007.

[98] V. Colotta, O. Lenzi, D. Catarzi, F. Varano, G. Filacchioni, C. Martini, L. Trincavelli, O. Ciampi, A. M. Pugliese, C. Traini, F. Pedata, E. Morizzo, and S. Moro, "Pyrido[2,3-e]-1,2,4-triazolo[4,3-a]pyrazin-1-one as a new scaffold to develop potent and selective human A3 adenosine receptor antagonists. Synthesis, pharmacological evaluation, and

ligand-receptor modeling studies.," *Journal of medicinal chemistry*, vol. 52, pp. 2407–19, Apr. 2009.

[99] F. Da Settimo, G. Primofiore, S. Taliani, A. M. Marini, C. La Motta, F. Simorini, S. Salerno, V. Sergianni, T. Tuccinardi, A. Martinelli, B. Cosimelli, G. Greco, E. Novellino, O. Ciampi, M. L. Trincavelli, and C. Martini, "5-amino-2-phenyl[1,2,3]triazolo[1,2-a][1,2,4]benzotriazin-1-one: a versatile scaffold to obtain potent and selective A3 adenosine receptor antagonists.," *Journal of medicinal chemistry*, vol. 50, pp. 5676–84, Nov. 2007.

[100] J. C. L. Erve, S. C. Vashishtha, W. DeMaio, and R. E. Talaat, "Metabolism of prazosin in rat, dog, and human liver microsomes and cryopreserved rat and human hepatocytes and characterization of metabolites by liquid chromatography/tandem mass spectrometry.," *Drug metabolism and disposition: the biological fate of chemicals*, vol. 35, pp. 908–16, June 2007.

[101] D. P. Williams, D. J. Antoine, P. J. Butler, R. Jones, L. Randle, A. Payne, M. Howard, I. Gardner, J. Blagg, and B. K. Park, "The metabolism and toxicity of furosemide in the Wistar rat and CD-1 mouse: a chemical and biochemical definition of the toxicophore.," *The Journal of pharmacology and experimental therapeutics*, vol. 322, pp. 1208–20, Sept. 2007.

[102] J. M. Le Fur and J. P. Labaune, "Metabolic pathway by cleavage of a furan ring.," *Xenobiotica; the fate of foreign compounds in biological systems*, vol. 15, pp. 567–77, July 1985.

[103] P. G. Baraldi, B. Cacciari, S. Moro, G. Spalluto, G. Pastorin, T. Da Ros, K.-N. Klotz, K. Varani, S. Gessi, and P. A. Borea, "Synthesis, biological activity, and molecular modeling investigation of new pyrazolo[4,3-e]-1,2,4-triazolo[1,5-c]pyrimidine derivatives as human A(3) adenosine receptor antagonists.," *Journal of medicinal chemistry*, vol. 45, pp. 770–80, Feb. 2002.

[104] P. G. Baraldi, B. Cacciari, G. Spalluto, M. J. Pineda de las Infantas y Villatoro, C. Zocchi, S. Dionisotti, and E. Ongini, "Pyrazolo[4,3-e]-1,2,4-triazolo[1,5-c]pyrimidine derivatives: potent and selective A(2A) adenosine antagonists.," *Journal of medicinal chemistry*, vol. 39, pp. 1164–71, Mar. 1996.

[105] S. Moro, C. Hoffmann, and K. a. Jacobson, "Role of the extracellular loops of G protein-coupled receptors in ligand recognition: a molecular modeling study of the human P2Y1 receptor.," *Biochemistry*, vol. 38, pp. 3498–507, Mar. 1999.

[106] V. Colotta, D. Catarzi, F. Varano, L. Cecchi, G. Filacchioni, C. Martini, L. Trincavelli, and a. Lucacchini, "Synthesis and structure-activity relationships of a new set of 2-arylpyrazolo[3,4-c]quinoline derivatives as adenosine receptor antagonists.," *Journal of medicinal chemistry*, vol. 43, pp. 3118–24, Aug. 2000.

[107] V. Colotta, D. Catarzi, F. Varano, F. R. Calabri, O. Lenzi, G. Filacchioni, C. Martini, L. Trincavelli, F. Deflorian, and S. Moro, "1,2,4-triazolo[4,3-a]quinoxalin-1-one moiety as an attractive scaffold to develop new potent and selective human A3 adenosine receptor antagonists: synthesis, pharmacological, and ligand-receptor modeling studies.," *Journal of medicinal chemistry*, vol. 47, pp. 3580–90, July 2004.

[108] E. Morizzo, F. Capelli, O. Lenzi, D. Catarzi, F. Varano, G. Filacchioni, F. Vincenzi, K. Varani, P. A. Borea, V. Colotta, and S. Moro, "Scouting human A3 adenosine receptor antagonist binding mode using a molecular simplification approach: from triazoloquinoxaline to a pyrimidine skeleton as a key study," *Journal of Medicinal Chemistry*, vol. 50, pp. 6596–6606, Dec. 2007.

[109] J. E. Van Muijlwijk-Koezen, H. Timmerman, H. Van Der Goot, W. M. Menge, J. Frijtag Von Drabbe Künzel, M. De Groote, and A. P. IJzerman, "Isoquinoline and quinazoline urea analogues as antagonists for the human adenosine A(3) receptor.," *Journal of Medicinal Chemistry*, vol. 43, no. 11, pp. 2227–2238, 2000.

[110] B. B. Fredholm, A. P. IJzerman, K. A. Jacobson, J. Linden, and C. E. Müller, "International Union of Basic and Clinical Pharmacology. LXXXI. Nomenclature and classification of adenosine receptors–an update.," *Pharmacological reviews*, vol. 63, pp. 1–34, Mar. 2011.

[111] A. Bajaj, A. Celić, F.-X. Ding, F. Naider, J. M. Becker, and M. E. Dumont, "A fluorescent alpha-factor analogue exhibits multiple steps on binding to its G protein coupled receptor in yeast.," *Biochemistry*, vol. 43, pp. 13564–78, Oct. 2004.

[112] K. Kuder and K. Kieć-Kononowicz, "Fluorescent GPCR ligands as new tools in pharmacology.," *Current medicinal chemistry*, vol. 15, pp. 2132–43, Jan. 2008.

[113] R. J. Middleton and B. Kellam, "Fluorophore-tagged GPCR ligands.," *Current opinion in chemical biology*, vol. 9, pp. 517–25, Oct. 2005.

[114] Y. Cordeaux, S. J. Briddon, S. P. H. Alexander, B. Kellam, and S. J. Hill, "Agonist-occupied A3 adenosine receptors exist within heterogeneous complexes in membrane microdomains of individual living cells.,"

The FASEB journal : official publication of the Federation of American Societies for Experimental Biology, vol. 22, pp. 850–60, Mar. 2008.

[115] M. Kecskés, T. S. Kumar, L. Yoo, Z.-G. Gao, and K. a. Jacobson, "Novel Alexa Fluor-488 labeled antagonist of the A(2A) adenosine receptor: Application to a fluorescence polarization-based receptor binding assay.," *Biochemical pharmacology*, vol. 80, pp. 506–11, Aug. 2010.

[116] G. Ghai, J. E. Francis, M. Williams, R. A. Dotson, M. F. Hopkins, D. T. Cote, F. R. Goodman, and M. B. Zimmerman, "Pharmacological characterization of CGS 15943A: a novel nonxanthine adenosine antagonist.," *The Journal of pharmacology and experimental therapeutics*, vol. 242, pp. 784–90, Sept. 1987.

[117] K. Weng, X. Xie, G. Qiu, and W. Gu, "Clinical reagents of GM-CSF and IFN-α induce the generation of functional chronic myeloid leukemia dendritic cells in vitro.," *Cytotechnology*, vol. 64, pp. 75–81, Jan. 2012.

[118] S. Oertel, M. Thiemann, K. Richter, K. J. Weber, P. E. Huber, R. L. Perez, S. Brons, M. Bischof, A. E. Kulozik, V. Ehemann, J. Debus, and C. Blattmann, "Combination of suberoylanilide hydroxamic acid with heavy ion therapy shows promising effects in infantile sarcoma cell lines.," *Radiation oncology (London, England)*, vol. 6, p. 119, Jan. 2011.

[119] P. C. Simons, M. Shi, T. Foutz, D. F. Cimino, J. Lewis, T. Buranda, W. K. Lim, R. R. Neubig, W. E. McIntire, J. Garrison, E. Prossnitz, and L. A. Sklar, "Ligand-receptor-G-protein molecular assemblies on beads for mechanistic studies and screening by flow cytometry.," *Molecular pharmacology*, vol. 64, pp. 1227–38, Nov. 2003.

[120] R. T. McCabe, P. Skolnick, and K. A. Jacobson, "2-[2-[4-[2-[2-[1,3-Dihydro-1,1-bis(4-hydroxyphenyl)-3-oxo-5-isobenzofuranthioureidyl]ethylaminocarbonyl]ethyl]phenyl] ethylamino]-5?-N-ethylcarboxamidoadenosine (FITC-APEC): A fluorescent ligand for A2a-adenosine receptors," *Journal of Fluorescence*, vol. 2, pp. 217–223, Dec. 1992.

[121] J. E. Moses and A. D. Moorhouse, "The growing applications of click chemistry.," *Chemical Society reviews*, vol. 36, pp. 1249–62, Aug. 2007.

[122] P. Labute, "LowModeMD–implicit low-mode velocity filtering applied to conformational search of macrocycles and protein loops.," *Journal of Chemical Information and Modeling*, vol. 50, no. 5, pp. 792–800, 2010.